STUDIES ON THE ELASTIC STABILITY OF BODIES

A THESIS

Presented to

The Faculty of the Division of Graduate

Studies and Research

By

Mahender Kumar Singhal

In Partial Fulfillment

of the Requirements for the Degree

Doctor of Philosophy

in the School of Aerospace Engineering

Georgia Institute of Technology

August, 1973

STUDIES ON THE ELASTIC STABILITY OF BODIES

Approved:

Wilfred H. Horton, Chairman

R. D. Barksdale

J. M. Anderson

Date approved by Chairman: 8-17-73

ACKNOWLEDGMENTS

I am deeply indebted to Professor Wilfred H. Horton for his contribution to this research. He was always available for consultation and his guidance for the successful completion of this work was invaluable. He had profound influence on this author's professional and personal thinking. I gratefully acknowledge his help and advice.

I sincerely thank Dr. J. I. Craig for his timely help with the data acquisition system.

I would also like to thank Dr. R. D. Barksdale, Dr. J. M. Anderson, Dr. R. L. Carlson and Dr. J. I. Craig for their constructive criticism and valuable suggestions for the improvement of this thesis.

This work was carried out under the sponsorship of the National Aeronautics and Space Administration (Grant No. NGL-11-002-096) and the United States Air Force (Grant No. AFOSR-68-1476). Their encouragement and support are gratefully acknowledged.

TABLE OF CONTENTS

TABLE OF CONTENTS (Continued)

LIST OF TABLES

LIST OF TABLES (Continued)

LIST OF ILLUSTRATIONS

LIST OF ILLUSTRATIONS (Continued)

NOMENCLATURE

a	constant in all rational function approximations; 1/2 of the smaller side of rectangular element (torsional constants); radius of sectorial element (torsional constants); radius of circular plate.
b	constant in all rational function approximations; 1/2 of the larger side of rectangular element (torsional constants)
$c, d, a_1, b_1, \ldots, a_2, b_2, \ldots$	constants in rational function approximations
h	thickness of the circular plate
k	stiffness constant of lateral spring (stability of columns); elastic restraining constant (instability of a circular plate).
ℓ	distance apart of inflection points under lateral load
m	mass per unit length of beam
p	internal or external pressure
q	defined in equation (15); intensity of lateral load (instability of a circular plate)
r	radial coordinate
t	thickness of plate, shell skin
w	deflection of column, beam; radial displacement of shell
w_i	imperfection in a shell body
x	nondimensional cartesian coordinate
A, B	constants
C	constant; stability function (stability of frameworks)
D	$Eh^3/\{12(1-\nu^2)\}$

E	Young's modulus
G	modulus of rigidity
I	moment of inertia of column, beam cross section
$J_0(\ ), J_1(\ )$	Bessel functions of first kind
K	K_1/K_2 for rectangular element (torsional constants); $M_t/G\theta a^4$ for sectorial element (torsional constants)
K_1	$M_t/G\theta(2a)^3 2b$ for rectangular element
K_2	$M_t/\tau_{max}(2a)^2(2b)$ for rectangular element
K_t, K_b	stress concentration factor in tension, bending
K^*	defined in equation (40)
L	length of column, beam
M_t	torque carried by the torsional element
N	lateral load on a column, beam
P	axial compression
P_c	classic critical load
P_{cr}	critical axial compression
P_{exp}	actual buckling load
P_{msw}	critical load predicted from Southwell's plot
P_{sw}	maximum load level used to get Southwell data.
Q	$\pi^2 EI/L^2$
R	radius of fillet (experimental data); radius of column end (stability of columns); radius of circular shell
S, SC	stability functions (stability of frameworks)
W	amplitude of deflection function
W_i	amplitude of imperfection

α	kL^3/EI; sectorial angle in degrees (torsional constants)
β	$\phi L/EI$ (columns and beams); nondimensional restraining constant for circular plate (instability of a circular plate)
δ	displacement
ε	% error (in all approximate formulae) = {100·(Approximate value - exact value)/exact value}
εm	maximum % error
ζ	ratio of length of rigid body to the length of column
η	intersection ratio (as shown in Table 8)
θ	angle of twist
Λ	I_1/I_2
λ	$\sqrt{(PL^2/EI)}$
μ	$[\omega^2 mL^4/EI]^{1/4}$
ν	Poisson's ratio
ξ	L/2R
$(\sigma_r)_{cr}$	critical radial stress
σ_{cr}	critical compressive stress
τ_{max}	maximum shear stress
Φ	stress function
ϕ	torsional stiffness constant associated with rotational restraint (columns and beams)
Ψ	tangential coordinate
ω	natural frequency of vibration

SUMMARY

The subject of elastic stability has been studied for many years and the various formulations have grown increasingly complex. The basic aim of this research has been the attainment of simplicity with accuracy. The particular work described in this thesis is both of experimental and analytical type.

The purpose of the experimental research undertaken was to develop a reliable yet simple nondestructive testing technique for thin cylindrical shells under axial compression. The basis of the method is the fact that the stiffness of a compression member, in a direction normal to the applied axial load, tends to zero as the critical condition is reached. This is true for columns, plates and shells. For columns, it has some quite interesting practical consequences. It is shown in this work that the plot of stiffness versus axial compression for a column is a straight line and that these lines are a family of parallel lines for different boundary conditions. The product of the critical load and the stiffness of the column under no axial load is, therefore, constant. Consequently, it enables the accurate determination of the critical load from the knowledge of the stiffness of the column ascertained by nondestructive lateral load. However, for shell bodies such a simple relation is not apparent. Nevertheless, tests made on unstiffened, stringer stiffened and stringer and ring stiffened circular shells demonstrates that even for low values of

compressive force there is significant change in wall stiffness under increasing axial load and at many points the plot of stiffness versus axial force is linear. It is shown that the point at which this decrease in stiffness is maximum is the center of the first unstable region and its intercept on the load axis accurately predicts the actual buckling load. Thus the process generates data on the relative strength of various portions of the shell body as well as defining the critical condition. Further studies made on an unstiffened elliptic shell with and without a cutout indicates that the method is pertinent to noncircular shells. The results predicted by this loss of stiffness method are extremely accurate. However, this method is not applicable for all types of shell bodies. Its inadequacy to predict accurate critical condition for a spirally stiffened shell body is demonstrated. Nonetheless, when the conditions are appropriate, unstiffened or conventionally stiffened shell bodies under axial compression, the simplicity of the procedure and the elimination of the complex instrumentation and computation system makes this technique alluring to test engineers.

The motivation behind the analytical research was to develop a systematic method for the derivation of simple, accurate but approximate formulae for the critical load, mode shape and deflection function for columns and plates with realistic boundary conditions. The unique properties of rational functions - viz the dependent variable being finite for infinite variation of the independent variable and vice versa, are used for the development of such derivations. The

critical condition to be evaluated is expressed as a rational function in terms of the end fixity parameters. The known characteristics of the structural element corresponding to the extreme and some intermediate conditions of the fixity parameters are then used to evaluate the appropriate constants in the rational function approximation. The formulae thus obtained are of high accuracy. The direct utility of these formulae to practising engineers is certain. Their value in reducing program sizes for many computer design problems is obvious and their use in parametric studies undeniable.

CHAPTER I

INTRODUCTION

The subject of the elastic stability of structures, in particular column structures, is not new. Column type devices have played an important role in civil engineering for many centuries. At first, of course, they were made from wood or stone but in more recent times metallic elements have tended to predominate. However, despite the universal role of these elements for so many years there are still some issues of concern in their use. The prime problem to be resolved centers around the conditions of end fixities which exist in realistic structures. The problem has long been recognized. However, mathematicians have primarily devoted their attention to those idealistic conditions which are described as simply supported or rigidly clamped. Simple support means the freedom to rotate but not to translate while clamped implies the freedom neither to rotate nor translate. At a practical level neither of these ideal conditions is attainable. Nevertheless, over the many years of experimental and analytical study which have followed the pioneer work of Musschenbroek (1) and Euler (2) these ideal conditions have been sought by the one and assumed by the other.

The first study in the stability of columns was made by Musschenbroek (1) in 1729. He constructed a machine specially to investigate the behavior of axially compressed columns. As the result

of his study he was able to propose an empirical formula for the compressive strength of a column. He suggested that resistances of beams compressed by forces parallel to their length, all things being equal, is in the inverse ratio of the squares of their lengths. This is, of course, substantially true. In 1744, Euler (2) made the now classic analysis of the behavior of a perfectly elastic, initially straight, centrally compressed column. Despite his great analytical achievement the practising engineers, unfortunately, still have to rely upon the experience and the empirical formulae obtained from tests on columns with practical boundary conditions.

Hodgkinson (3) in 1840 published the results of some excellent experimental work on columns. The purpose of the study was, in Hodgkinson's own words, "to supply the deficiencies of Euler's theory of the strength of pillars, if it should appear capable of being rendered practically useful; and if not, to endeavor to adapt the experiments so as to lead to useful results." These experimental data were, however, at variance with the predictions of Euler and analysts thus raised questions about the validity of Euler's theory.

Ayrton and Perry (4) in 1886 were the first to recognize that the discrepancy between practice and analysis lies in the imperfection of the test system. They realized that the hyperbolic relation between load and buckling displacement, first promulgated by Young (5) in 1807, was the crucial issue. They recast this hyperbolic relation into a linear form by choosing the variables to be the reciprocals of the load and displacement. The slope of the resultant straight line is

proportional to the reciprocal of the Euler load. They demonstrated the validity of Euler's computations for long slender columns by interpreting Hodgkinson's (3) test data on Dantzic oak and wrought iron struts. Ayrton and Perry were, however, not alone in their appreciation of the issues as their correspondance with Smith (6) clearly shows. Unfortunately, their most important contribution to the subject of column stability was ignored.

Southwell (7) in 1932, independently rediscovered this elegant idea of transforming the hyperbolic relation between load and displacement of a compressed strut to a linear form. However, he chose to plot the ratio of displacement to the load against the displacement. The Euler load is then obtained as the reciprocal of the slope of the resultant straight line.

Southwell verified his concept by interpreting the well acclaimed von Kármán's (8) test data on columns. After the publication of this work in the proceedings of the Royal Society, interest in the subject developed. Gough and Cox (9) in 1932 applied the method to the interpretation of test data on the stability of thin strips under shearing forces. In 1934 Bridget, Jerome and Vosseller (10) analyzed the data obtained from buckling tests on thin walled open sections.

Fisher (11) in 1934, investigated the subject more thoroughly and noted the effects of errors in measurement and made the important observation that the presence of lateral forces and eccentricity of loading could be considered as equivalent to geometric imperfections. It is interesting to note that while there was increasing attention

directed to the practical application of this hyperbolic relationship in a wider context than Southwell had formulated, scant attention was paid to the more general analysis which had been published by Westergaard (12) in 1922 and Fairthorne (13) in 1934.

Donnell (14) in 1938, in a classic paper on the application of Southwell's method for the analysis of buckling tests made some most important contributions.

(1) He suggested a plot of the load against the ratio of load to displacement as an alternative manner of analyzing the data. Figure 1, reproduced from reference (15), compares the Ayrton and Perry, Southwell and Donnell approaches. The advantage of Donnell's method seems to be in the direct determination of the instability load.

(2) His studies indicated that Southwell's method could be applied to plates supported on three and four sides, cylinders under axial compression and to struts in the plastic range provided that the buckling did not introduce appreciable second order stresses. The second order stresses are the stresses which occur when a developable surface buckles into a nondevelopable one.

(3) Harmonic analysis of deformations measured at a number of points could be used to obtain the appropriate critical loads.

Harmonic analysis of the deformation data to ascertain the critical conditions was the most important idea promulgated by Donnell. He realized that such an analysis should be particularly useful in more complex cases where the exact form of buckling mode is not accurately known in advance.

δ = elastic deflection
P = applied load
P_1 = Euler load
c = constant

δ is related, to a first approximation, to the load (P) which produces it and the Euler load (P_1) by the expression

$$\delta = \frac{cP}{P_1 - P}$$

Three possible arrangements of this form are:

Ayrton and Perry (1886)

formula $1/\delta = \left[\frac{P_1}{P} - 1\right]\frac{1}{c}$

variables $1/\delta$ and $1/P$

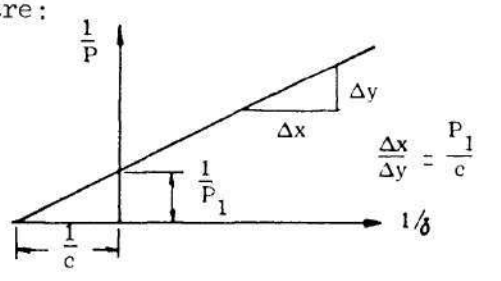

Southwell (1932)

formula $\delta\left[\frac{P_1}{P} - 1\right] = c$

variables δ/P and δ

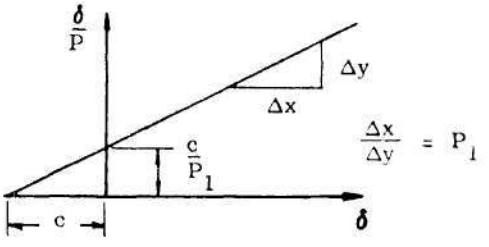

Donnell (1938)

formula $P_1 - P = c\frac{P}{\delta}$

variables P and P/δ

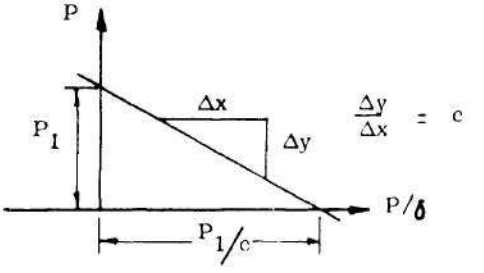

Figure 1. Linear Graphical Relationships for Columns.

The prime reason of discrepancy between the theoretical critical load and the actual critical load is due to the difficulty in the evaluation of realistic boundary conditions. Traditionally, experimentalists, in order to investigate the validity of various theories, devoted considerable attention to the construction of end fixity devices simulating the idealized boundary conditions. An excellent historical survey of the various boundary fixtures used by many researchers is given by Struble (16). It is evident from the kind of skill needed to attain the ideal under test conditions, that the absolute ideal boundary conditions are impossible to achieve in a real structure. The importance of the deviation of boundary conditions from ideality is well summarized by Salmon (17) in the conclusion of his work on columns.

> The most pressing point for future research on the subject of columns is undoubtedly the degree of imperfection common in practical fixed ends; in short, what value of K* should be assumed for such ends? A complete answer to this question is difficult, but at present the designer has no real data whatsoever regarding practical end conditions.

With the progress of time analysts have become more concerned about the effect of real boundary conditions on the behavior of compressed columns. Using current mathematical analysis, they have obtained the characteristic equations governing the instability of a strut with practical boundary conditions. However, these characteristic equations are at best transcendental and contain the eigenvalue and the boundary restraint parameters as implicit variables. These characteristic equations are, of course, solvable by the use of various numerical

---

* K; a factor when multiplied by Euler load gives actual critical load.

techniques.

From the practical engineer's viewpoint there are two issues of concern.

(1) What is the actual end fixity encountered in a given structure?

(2) Can simple design formulae for practical columns be developed?

The first issue has been resolved, in part, by the work of several researchers (16, 18, 19, 20). References (16, 18, 19) deal with nondestructive methods for determining actual critical load from a knowledge of the deformation produced by lateral loads. These researchers made no efforts to establish the individual end fixity. Their main concern was in the assessment of the gross effect on the instability load. On the other hand the study reported by Baruch (20) was aimed to determine the actual end conditions and from thence to determine the instability load level. In either case, however, substantial verification is lacking. The subject is discussed more extensively in Chapter II of this thesis. The data therein presented verifies the numerical results of the earlier work (18).

In Chapter V a simple method for dealing with the computational problem when end fixities are known is outlined.

The issues of plate stability are closely associatable with those of columns. In many respects analogous difficulties are encountered. There is uncertainty with respect to the actual boundary conditions encountered in practice and very little work has been done,

as yet, on practical means of determining them. This is due, in part, to the fact that there is a lack of analytical results relative to the behavior of plates with various boundary conditions. It is true that for a circular plate with uniform elastic rotational restraint along its boundary, the deflection under uniform lateral load and the critical load under uniform radial thrust can be readily expressed in terms of the restraint parameter. Thus for a given plate the actual boundary restraint is readily assessable from deflection information and the critical stress can be determined nondestructively. The appropriate expressions are,

$$\beta = \frac{64Dw - qa^4}{(5 + \nu)qa^4 - (1 + \nu)64Dw} \tag{1}$$

$$(\sigma_r)_{cr} = \frac{4.2D}{ha^2} \left\{ \frac{(145 + 36\nu)qa^4 - (1 + 36\nu)\ 64Dw}{(170 + 36\nu)qa^4 - (26 + 36\nu)64Dw} \right\} \tag{2}$$

where

w = deflection at the center of plate under lateral pressure

q = intensity of uniform lateral pressure

a = radius of the plate

D = bending rigidity of the plate

ν = Poisson's ratio

β = nondimensional restraining coefficient

$(\sigma_r)_{cr}$ = critical radial stress

The former expression is highly sensitive to small changes in the deflection parameter while the later is not. These expressions were obtained from the appropriate formulae derived in Chapter V. This emphasizes the value and necessity of the approximate formulae for the instability load of various structural elements. However, in general, the question is not so simply resolved. The analysis of a rectangular plate with unequal elastic restraint along its boundary still needs further study. The deflection function approach outlined in Chapter V should help in this regard. It is pertinent to note too that the rational function method of approximation for displacement functions effectively simplifies the problems of buckling and vibration of plates.

Just as was the case with columns much difficulty has been experienced with the interpretation of the data acquired from stability tests on plates. Despite the early success of Gough and Cox (9) there was a marked reluctance on the part of test engineers to use the Southwell method of data analysis. This was, in part, due to a misinterpretation of Donnell's (14) results. Many considered that Donnell's classic paper ruled out the hyperbolic relationship; this is not so. The equation which Donnell gives contains the Southwell relationship for plates with small imperfections and for which the deformations under load are small relative to the thickness. This question has been extensively reviewed by Horton, Cundari and Johnson (15). Moreover, not only is the Southwell expression given by Donnell's equation but it also shows that when the displacements are large,

compared with the imperfection magnitude, the relationship between load and displacement is parabolic. This parabolic law was derived and applied by Dunn (21) and subsequently used by Farrar (22) for the analysis of plate data. Its application to the inelastic case has been made by Yoshiki and Fujita (23).

Generally speaking, however, no matter what method of data interpretation is used, the agreement between the theoretical considerations and the results obtained from carefully conducted tests are reasonably satisfactory for column and plate structures. This is by no means the case for shell structures especially when the destabilizing force is primarily compression and the shell is thin walled and unstiffened.

The unstiffened circular cylindrical shell is one of the most common structural elements in general engineering use. For many years such structures have been made from metals and plywoods. Today, due to the development of fibers and a wide range of resins and bonding agents, such bodies can be filament wound. Generally speaking stability, in thin walled structures, rather than specific strength is the criterion for design. Thus, the buckling behavior of thin shell bodies, both homogeneous isotropic and heterogenecus aeolotropic is, like that of columns and plates, of vital concern to engineers.

At first sight the problem appears relatively straightforward. The geometry of the structure is comparatively simple and the loading conditions not overly complex. Yet despite much concentrated efforts the situation is largely unresolved even for the isotropic homogeneous

material. Indeed, the behavior of cylindrical shells under compressive loading condition is one of the most challenging problems in the field of structural analysis.

Historically, interest in the behavior of cylindrical shells dates back to Fairbairn* (24) who in 1859 made an experimental study of the collapse of tubes under external pressure. Thirty years later Bryan (26) examined the same question theoretically. By the turn of the century the behavior of cylindrical shells under a wider range of loading conditions was becoming of interest. Lorenz (27) and Timoshenko (28) were first to examine the behavior of a thin monocoque circular cylinder under axial compression on the assumption of an axisymmetric ring distortion sinusoidal along a generator line. In so doing they formulated the classical theory of buckling for homogeneous isotropic shells which predicts a critical compressive stress of

$$\sigma_{cr} = \frac{1}{\sqrt{3(1 - \nu^2)}} \cdot \frac{Et}{R} \qquad (3)$$

where

t = thickness of shell

R = radius of shell

ν = Poisson's ratio

E = modulus of elasticity

*Fairbairn was a pioneer in the field of stability of column and plate members. See Timoshenko's book on History of Strength of Materials (25).

σ_{cr} = critical compressive stress

The validity of this formula for the case of general instability of thin circular cylindrical shell was established later by Lorenz (29), Timoshenko (30), Southwell (31) and Flügge (32). The well known experiments of Robertson (33, 34) in 1928-29 showed that the classical considerations did not lead to results consistent with reality. He concluded that thin wall cylindrical shells under uniform axial compression failed on test at values much below the classical value and their mode of failure was not axisymmetric. Moreover, the buckling tests were characterized by wide scatter in the results. These sad findings were repeated in the extensive experimental work of Wilson and Newmark (35), Lundquist (36) and Donnell (37) between 1933 and 1934. These studies showed that as the R/t ratio increases the discrepancy between theory and practice grows. Critical load values as low as 15 percent of calculated value were recorded. This unsatisfactory state of affairs is best summarized in the work of Harris, et al. (38), reproduced in Figure 2, who compared the test results of many investigators (39, 10, 40, 37, 41, 38, 42, 43, 36, 33, 34, 35). The disparity between theory and the facts of experience caused many reconsiderations of the question of stability under uniform axial compression. Donnell (37), von Kármán and Tsien (44) and Yoshimura (45) all made important proposals relative to the issues. The theoretical views embodied in the Kármán-Donnell approach dominate the field despite the fact that they cannot describe the behavior of any realistic structure.

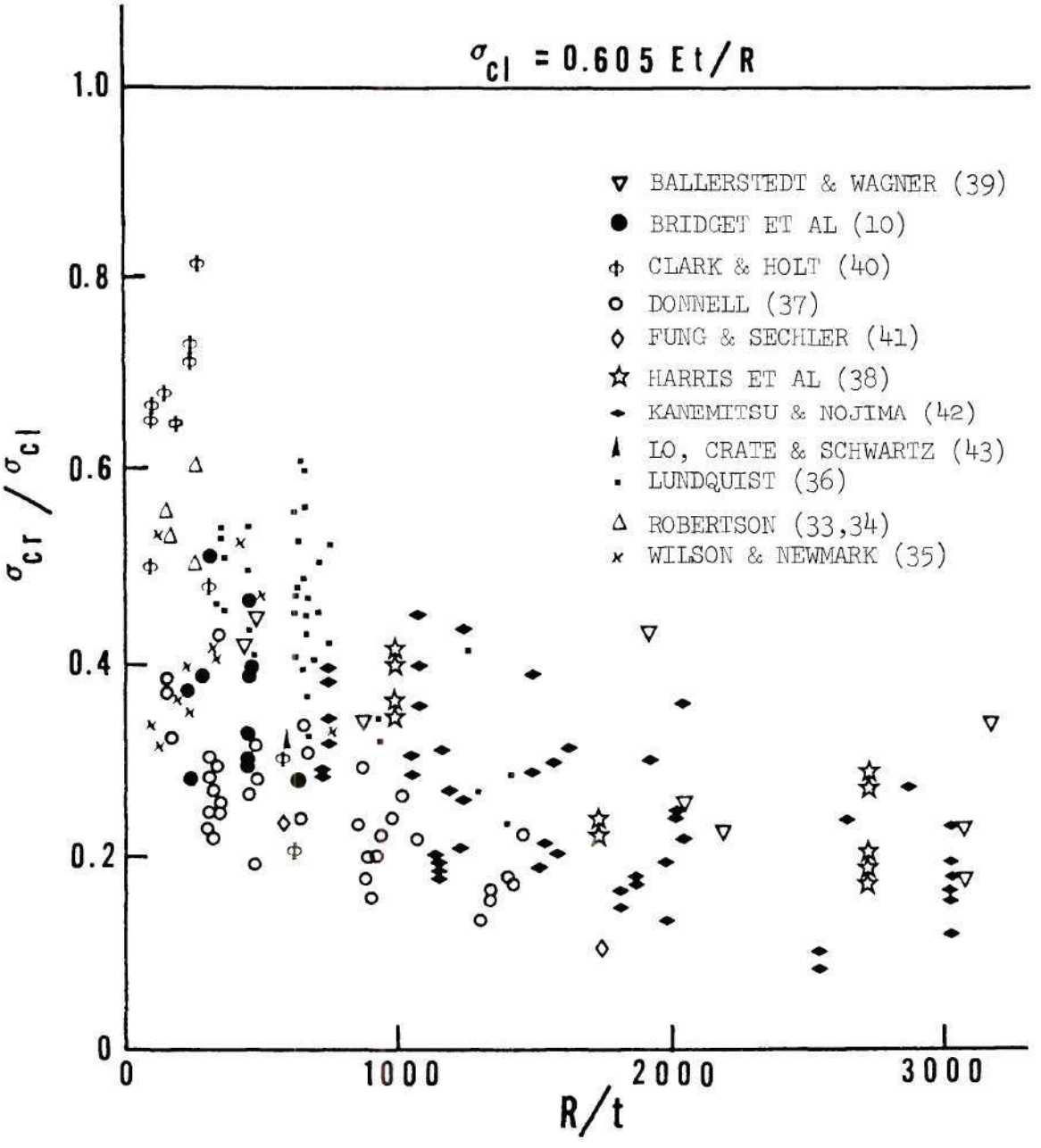

Figure 2. Comparison of Linear Buckling Theory with Test Data From Many Investigators for Circular Cylindrical Shells Under Axial Compression.

The possibility of boundary conditions having significant influence on the minimum load to produce instability has been considered by several authors (46, 47, 48). Recent analytical studies made by Mayers and Rehfield (49) have extended, in a way, the Kármán- Donnell concept and by so doing they demonstrated its inability to describe the buckling situation for the homogeneous isotropic shell under uniform compression. In addition to the large discrepancies which exist between theoretical and experimental load values, the axisymmetric buckle mode is never achieved except by plastic buckling of thick walled shells (50). The buckles which occur in reality are of a diamond shape. Sometimes these buckles are located at the ends of the shell, sometimes in a ring around the center and in other cases they tend to form a spiral. However, until the work described in Chapter III was completed, their location was indeterminate prior to collapse. Flügge (32) after careful study deduced that restraint to Poisson expansion of the shell caused by the testing machine and small initial deviation were sufficient degrading parameters to explain the departure from theory. Independently, Donnell (37) considered imperfections to geometric shape to be the main contributor. However, his theory could not account for such large differences. Kármán and Tsien (44), in their classic paper, ascribed test machine rigidity as the most important factor for imperfect bodies. This point of view had substantial following for many years. In the past few years, initial geometric imperfections have come to be accepted as the main degrading factor. Koiter (51) has shown this by assuming a very

special initial imperfection in the form of the axisymmetric buckling mode of the perfect shell. He concluded that an imperfection amplitude of 0.5 of the shell wall thickness would reduce the buckling load to about 0.3 of the classical value. Budiansky and Hutchinson (52) have demonstrated that a long thin walled cylinder under axial compression is the most imperfection-sensitive shell structure. They concluded that even very small geometrical imperfections could imply buckling loads smaller than the classical ones by amounts that are not entirely negligible. Recently, Arbocz and Babcock (53) investigated the effect of general imperfections. Their study showed that the correlation between the theoretical buckling loads obtained from nonlinear Donnell type shell equations and the experimental values was good for the case of "global" buckling. The difficulty of shell analysis in relation to design is well stated by Baker, et al. (54), "Development of more exact theoretical expressions does not necessarily assist in the solution of practical shell problems, since often the theoretical expressions can be solved only with great difficulty, and then only for special cases." In short, inspite of the voluminous (55, 56) work done in this field, the failure of the thin shells under axial compression remains to date the most frustrating yet, challenging problem. Unable to identify and account for several complex factors, namely, geometrical imperfections, load distribution and the realistic boundary conditions in the theoretical analysis one naturally turns to experiments for a nondestructive method of testing.

Development of Nondestructive Techniques of Shell Testing

Experiments on shell bodies have been made for many years, as noted earlier. Nevertheless, until recently they were plagued with uncertainty especially in those cases for which the destabilizing load was primarily compression. Donnell (14) indicated that the Southwell method for data reduction should probably be applicable to shells under axial compression. Flügge (57) reported its successful application to unstiffened cylindrical shells under axial compression. Galletly, et al. (58) demonstrated that the Southwell plot appears generally to be pertinent and accurate for cylindrical shells subjected to external pressure loading. Their results showed a good correlation between the actual and predicted value of the critical load and the agreement was within 5 percent in all cases. The consistency of the values derived by the Southwell process for the external pressure case is further illustrated in the work of Galletly and Reynolds (59) and of Sturm (60). Bank (61) demonstrated its application to orthotropic shells under torsion. The first published Southwell plot for a cylinder under axial compression was obtained by Tenerelli and Horton (62).

The difficulty as pointed out by Flügge (57) lies in the determination of the relevant station at which to make observations. Moreover, it is clear from the data of Craig (63) that the points of maximum deformation move around the circumference as the load level increases. This type of motion of the wave was also observed by Gough and Cox (9) in their tests on thin strips and their Southwell plots

were obtained for crest readings. To some extent these problems can, however, be resolved by acquiring data not at an isolated point but at a series of stations located on a circumferential line. In some cases it has been found that when this is done good Southwell plots can be obtained at the various stations. These tend to several values of the critical load for the shell and in fact can be shown (64), statistically, to constitute a family. Generally, however, the harmonic analysis must be used to interpret the data. Such analysis was first mentioned by Donnell (14). Tuckerman (65) applied it to the problem of the strut and subsequently Craig (63) developed this scheme for an unstiffened cylinder in torsion.

The researches mentioned in the previous paragraph indicated that a Southwell type approach such as that described in reference (63), or some modification thereto would be applicable to the question in hand. Ford (66), consequently, undertook a study on a family of shells under axial compression. Deflections of the shell wall as a function of load were determined at 45 equally spaced stations at the equatorial plane of the cylinder. Ford then used harmonic analysis to determine the distortion amplitudes corresponding to the several harmonics. From this analysis Ford was able to determine the predominant harmonic and to construct appropriate Southwell plots. Table 1 summarizes his results for all cases in which he ascertained both the Southwell critical load and the actual critical load. It is interesting to note that the ratio of $P_{exp}/P_{Southwell}$ is nearly 0.9, thus predicting a higher value of critical load than the actual value of

Table 1. Summary of Ford's Results.

Shell Number	P_{exp}	P_{sw}	P_{exp}/P_{sw}	P_{msw}	P_{msw}/P_{exp}
0601	5290	5700	0.93	4700	0.89
0814	8100	9060	0.89	4300	0.53
0911	11900	14800	0.81	6000	0.50
1000	3720	4100	0.91	2000	0.54
1002	4130	4600	0.90	2400	0.58
1006	5160	5430	0.95	2600	0.50

P_{exp} = Actual Buckling Load.

P_{sw} = Critical Load Predicted From Southwell Plot.

P_{msw} = Maximum Load Level Used to Get Southwell Data.

critical load. Of equal significance is the fact that the analysis cannot reveal the weak locations nor is it in general simple to decide where the many displacement readings essential for the process should be taken. Also the load level which must be used is a high percentage (50 percent or more) of the critical value. This percentage, of course, would be expected to rise with the improved quality of the specimen as well as with the decreasing sensitivity to imperfection which results from greater stiffening. Moreover, the method is difficult, if not impossible, to apply to bodies other than right circular cylinders. However, the process has merit in the sense that it gives valuable nondestructive test data. It has great potential in parametric studies for which the basic test vehicle is repeatedly used in various stages of modification. Nevertheless, it is far from an ideal method.

The restraining mandrel technique for nondestructive testing of shell bodies has been developed considerably in the last decade. The first known application of such a method was made by Sturm (60) in 1941. Almroth, et al. (67) presented an interesting experimental study of the buckling of cylinders under axial compression at the 1964 spring meeting of the Society for Experimental Stress Analysis. They presented a technique of testing cylindrical shells using an interior mandrel to obtain repeatability of the buckling load. Horton and Durham (68), in an independent study, developed a very similar process. They concluded that if a mandrel is placed at a distance equivalent to the shell skin thickness from the inside surface of the shell then

it is possible to elastically buckle the shell. They demonstrated that the buckling load of the shell could be repeated if a restraining mandrel is used and that the load progressively falls if the mandrel is removed. They discovered that by placing a mandrel inside the shell, it was possible to buckle the shell elastically until the entire shell surface was completely filled with buckles. They showed that the relationship between the number of buckles and the load follows a typical population distribution curve. Moreover, they discovered that the most probable value of the buckling load for the perfect shell, as derived from this population curve, is in fact the critical load computed from the classic stability formula. Having established a sound nondestructive method, Horton and Bailey (69) conducted tests on a number of cylinders in different test machines. They discovered that the Kármán and Tsien (44) criterion that the test machine rigidity influences the buckling load has no foundation.

The restraining mandrel technique for nondestructive testing of shell bodies is excellent for small specimens. However, as the specimen size increases, this method becomes increasingly difficult to apply. This is clearly evident from Figure 3 which shows a specimen currently being tested in the School of Aerospace Engineering. The amount of time and expense involved in the manufacture of a mandrel for such a specimen would be excessive.

The "strain reversal" method of predicting the buckling load has received the attention of a few researchers (70, 71, 72). A number of strain gages are placed on the shell wall. The buckling is

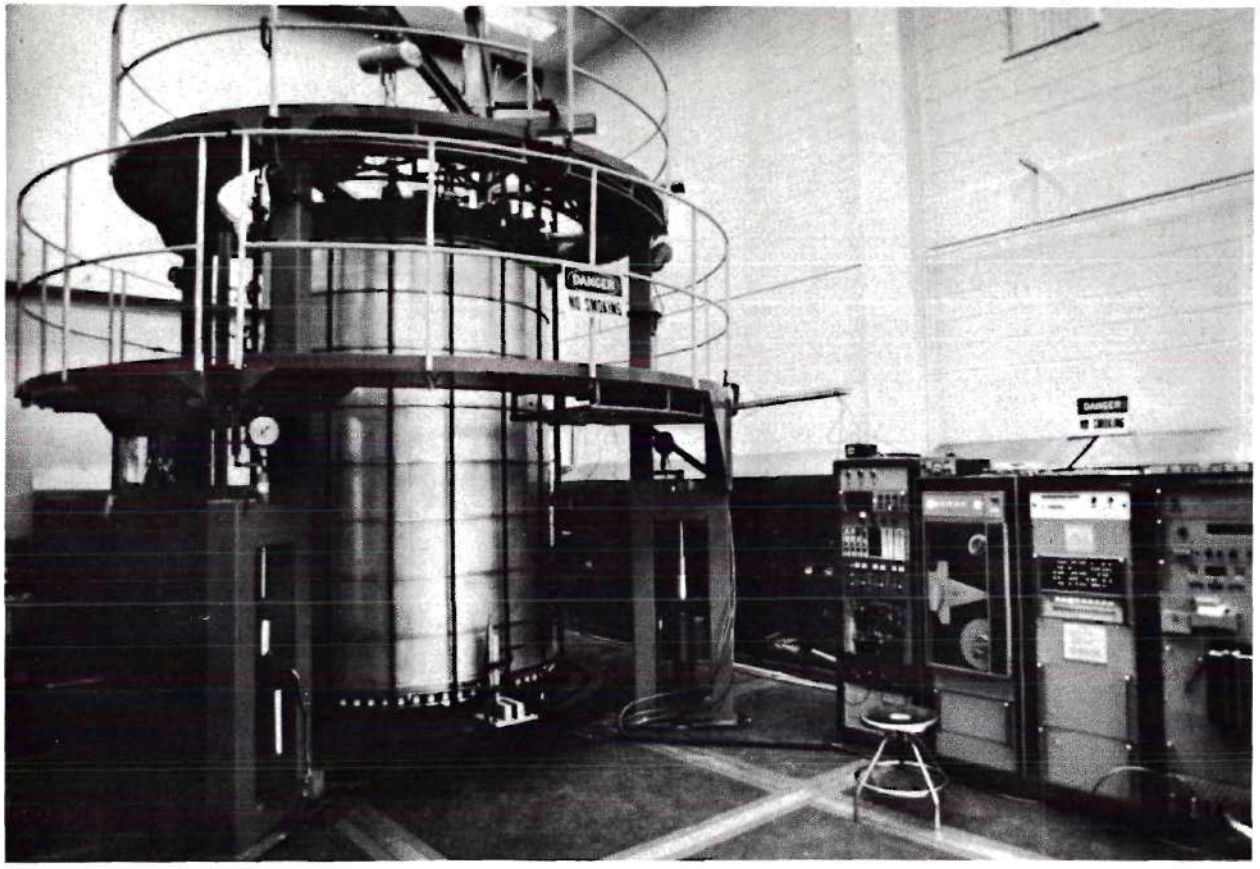

Figure 3. Large Shell in Test Rig.

then "assumed" to occur when the strain gages in the vicinity of the buckles experience bending strains from buckle growth of sufficient magnitude to reverse the rate of strain on one side of the wall. The corresponding load is then the "strain reversal" load. The disadvantages of this method are obvious.

(1) A lack of knowledge of the position of buckle formation on the surface of the shell necessitates the use of a large number of strain gages.

(2) The critical load is predicted at such a high level of the destabilizing load that failure of the specimen is inevitable.

It is clear from the preceding remarks that small shells can be successfully nondestructively tested in virtually any loading environment. However, this is not so for large specimens. Admittedly, the Southwell plot technique enables viable predictions to be made in many cases for such bodies. Nevertheless, the level of destabilizing load required for the application of such a process is uncomfortably high. Moreover, the region of failure of the shell surface is not defined. There is, therefore, a pressing need to develop a method which will positively locate the region of failure prior to the event occurring and from which an accurate assessment of the critical load level can be made.

A concerted effort to establish such a process is reported in Chapter III.

CHAPTER II

INSTABILITY OF COLUMNS

In the previous chapter the nondestructive methods of determination of the instability loads of structures have been discussed. It was therein stated that the oldest nondestructive method of ascertaining stability load level for an imperfect column was by the use of the hyperbolic relation between the load and deflection of the column. Columns, of course, can frequently carry loads in excess of the normally defined stability load. In fact they have considerable post buckling strength.

A pin ended column under axial compression has a load versus central deflection curve much as depicted in Figure 4.

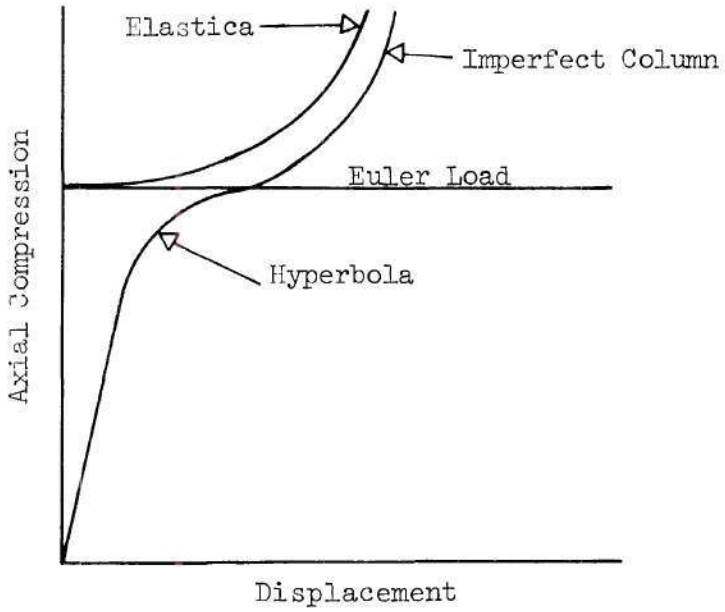

Figure 4. Load-Displacement Plot for a Column.

Initially, for an imperfect column, the load-displacement relationship is linear but as the load increases a hyperbolic form develops. When the central deflection becomes large this hyperbolic curve fades away and the displacement begins to approach the elastica. This curve for end slope angles between 5° and 25° is very nearly parabolic.

It is these two behavior patterns, namely, hyperbolic and parabolic portion of the curve that enable the nondestructive evaluation of the critical load. The hyperbolic portion of the curve, whose precise shape and location depends upon the degree of imperfection, is always a rectangular hyperbola and its asymptotes are the load axis and the Euler load line. Thus the determination of the critical load, which in essence is the definition of the horizontal asymptote, is in no way influenced by the degree of imperfection. Likewise the large deflection analysis, the so called $P\text{-}\delta^2$ plot, yields an intercept value as a critical load which is uninfluenced by the initial imperfection. Boundary condition variations plays an important role as they determine the vertical location of the asymptote.

A similar situation is true for plates. Donnell (14) in his paper on the Southwell method gives the following equation between load, displacement and initial imperfection for flat panels.

$$P = \frac{W}{W+W_i} P_c \left\{ 1 + \frac{3(1-\nu^2)}{8t^2} (W + 2W_i)(W + W_i) \right\} \qquad (4)$$

where

t = thickness of plate

ν = Poisson's ratio

W_i = amplitude of the initial imperfection

W = amplitude of the deformation

P_c = classic critical load

It is readily seen that only so long as the second term inside the brackets is small can the Southwell method give good results. It is also clear from this equation that when the deflections as compared to the initial imperfections are large, a $P\text{-}\delta^2$ arrangement is found.

Just as was the case with columns, plates have appreciable post buckling strength. There is no definable load arising from stability analysis which will cause collapse or one might say that there is no critical load. However, the columns and the panels experience a softening and hardening, a change of phase when small changes in the load causes large deformation changes, they then have a critical load in the classic sense. It is this value of the load which both the Southwell and the $P\text{-}\delta^2$ approaches give.

The Southwell relationship is derived from the consideration of an imperfect column. However, this imperfection need not be merely a bent centerline, as considered by Southwell in his analysis. The imperfection can be caused by a side force. This leads to a slightly different interpretation of the Southwell approach that the lateral stiffness of an axially compressed column or plate tends to zero as the axial load tends to the critical value.

The idea that the normal stiffness tends to zero as the compressive load tends to the critical value has been emphasized for the stability of frameworks by Gregory (73). In order to fix the thoughts, we examine the behavior of a beam column. Consider a uniform column with pinned ends subjected to axial compression 'P' and a concentrated normal load 'N'. The deflection 'w' at the midspan is

$$w = \frac{NL}{2\lambda P} \tan\frac{\lambda}{2} - \frac{NL}{4P} \tag{5}$$

where $\lambda^2 = PL^2/EI$. This simplifies to the following convenient form by the use of rational function approximations,

$$w = \frac{NL^3}{48EI} \left[\frac{1}{1 - P/Q}\right] \tag{6}$$

where E and I have the normal significance and $Q = \pi^2 EI/L^2$ is the Euler load.

The lateral or normal stiffness, henceforth termed stiffness, defined as the ratio of the side load to the deflection produced by the side load can then be written as

$$\text{Stiffness} = \frac{N}{w} = \frac{48EI}{L^3}\left[1 - (P/Q)\right] \tag{7}$$

i. e., the stiffness varies linearly with the compressive force and tends to zero when the axial load reaches the critical value. Equation (7) is, of course, really only another way of stating the Southwell relationship. It can be derived directly from this by taking the imperfection to be the displacement caused by a concentrated load 'N' applied at the midspan.

Engineers, in dealing with problems of stability for both column and plate structures are concerned with the behavior of real systems. The buckling of a realistically restrained element rather than the knowledge of the buckling of a pinned or clamped element is, therefore, of more vital concern to them. It is true that the Southwell plot could be used for this purpose but high load levels would be needed to generate the pertinent data.

More recently other methods have been proposed. The first of these was developed by Horton, Craig and Struble (18). They pointed out that the instability load for a column could be associated with the displacement produced by a unit concentrated lateral load applied at the point of maximum compliance. They concluded that under these circumstances the product of the critical load (P_{cr}) and the displacement (δ) defined above is substantially constant.

$$P_{cr} \cdot \delta = \frac{\pi^2 L}{48} \tag{8}$$

where L is the length of the column.

In a subsequent study Iwamoto (19) showed that the behavior of a beam under uniformly distributed lateral load could also be used as a

means of determining the critical load level for the column. For a column with elastic rotational restraint at its ends the appropriate expression is

$$\frac{(\frac{P_{cr}}{EI})\cdot(2\cdot l^3)}{(L + l)} = \pi^2 \qquad (9)$$

where l is the distance apart of the two inflection points and EI is the bending rigidity of the beam.

The results of Horton, et al. (18) and Iwamoto were essentially derived from detailed numerical calculations. However, Bank (74) using the results generated in Chapter V demonstrated that the formulae of Horton, et al. and Iwamoto could be directly verified. Nevertheless, to this time no practical verification has been given nor has any clear meaning of the results been promulgated.

Baruch (20) starting from the concepts of Horton, et al. went on to outline an "exact" method of determining the end fixities from the lateral displacements and rotations measured at the ends of the beam. He then used these in the characteristic equation governing the instability of a column to ascertain the critical load. There is some difficulty in Baruch's approach. It arises from the fact that the deflections and rotations at all points on a realistic body are rational functions in terms of the end restraint parameters. These restraint parameters can vary in value from zero to infinity while the displacements and rotations remain finite. Consequently, the

displacements and rotations are not highly sensitive to small changes in the stiffness parameters. The reverse is of course not true. This is clearly evident from Table 2 (reference (75)) where the sensitivity of these restraint parameters to 5 percent changes in the values of deflections and rotations are shown.

The direct relationship between the displacement due to a normal load applied at the point of maximum compliance and the instability load, as proposed by Horton, et al. (18), is easier to apply and probably as instructive.

The P-δ relationship (equation (8)) can be looked at from another viewpoint. It is merely an expression of the fact that the straight lines which represent the decrease in lateral stiffness with increase in compressive load are parallel or nearly so. This, of course, gives rise to an elegant method of verification of the P-δ law.

An experimental study based upon this observation was made on an aluminum column of 1/2" x 3/4" x 27.25" dimensions. The test set up is shown in Figure 5. The rotational end fixities of the column were varied by shifting the position of the support screw in the elastic spring. The central deflection of the column was measured by using a Hewlett-Packard 24DCDT250 linear variable-differential transformer (described in Chapter III). The lateral load for the stiffness measurement was applied through a pulley arrangement. The magnitude of the applied lateral load was 2003.6 grams.

Table 2. Sensitivity of Baruch's Method for the Determination of the End Fixity Parameters.

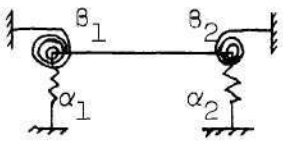

Where α and β are the nondimensionalized parameters associated with lateral and rotational elastic restraints, respectively.

Exact Values				New Values*			
α_1	α_2	β_1	β_2	α_1	α_2	β_1	β_2
3	3	1	2	4.3	1.9	2.8	-1.2
5	5	2	9	6.4	3.8	3.7	3.9
5	6	4	5	6.4	4.7	6.5	2.8
10	10	2	5	11.5	8.7	2.6	3.9
10	10	6	7	11.6	8.6	7.3	5.4
20	20	3	9	21.9	18.4	3.2	8.6
∞	∞	0	1	∞	∞	-0.27	1.4
∞	∞	0	2	∞	∞	-0.26	2.5
∞	∞	0	5	∞	∞	-0.24	5.7
∞	∞	1	5	∞	∞	0.7	5.6
∞	∞	1	10	∞	∞	0.72	11.0
∞	∞	2	5	∞	∞	1.65	5.6
∞	∞	5	5	∞	∞	4.48	5.58

* Values obtained when,

1) Deflection at left end is measured 5% too low.
2) Deflection at right end is measured 5% too high.
3) Slope at left end is measured 5% too high.
4) Slope at right end is measured 5% too low.

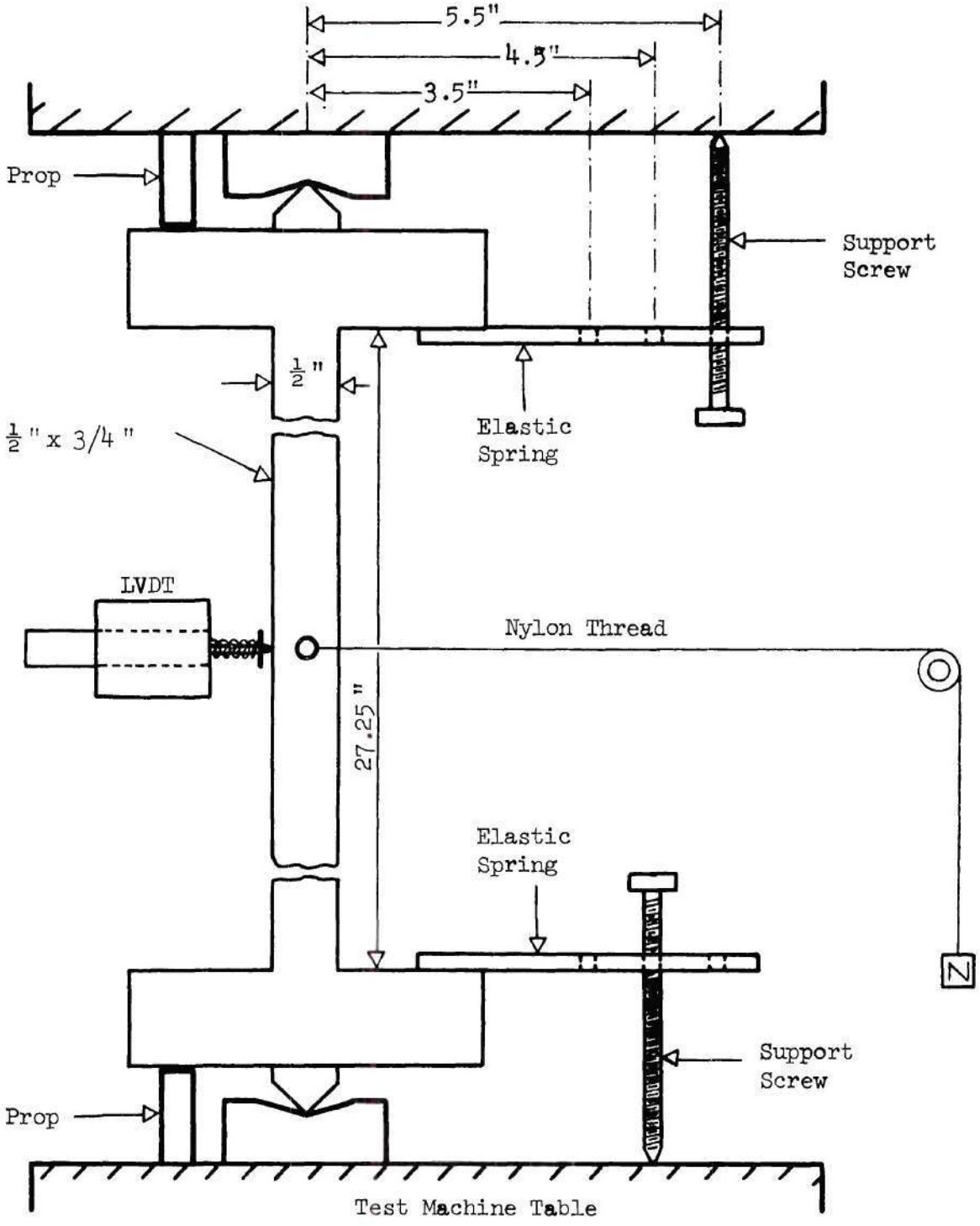

Figure 5. Diagramatic Representation of Column Test Set Up.

The stiffness-axial load plots for the four different conditions of the edge restraints are shown in Figure 6. The computed value of $P_{cr} \cdot \delta$ (from equation (8)) is

$$P_{cr} \cdot \left(\frac{\delta}{l}\right) = \frac{\pi^2 \times 27.25}{48} = 5.603 \tag{10}$$

and from Figure 6 we get

$$P_{cr} \cdot \left(\frac{\delta}{l}\right) = \frac{1260}{233} = 5.408 \tag{11}$$

The agreement between the theoretical and computed values of the constant in P-δ law is within 3.5 percent.

The stiffness method, so clearly a consequence of the Southwell relationship would be equally pertinent to the plate structures. Its application to the shell bodies is investigated in the following chapter.

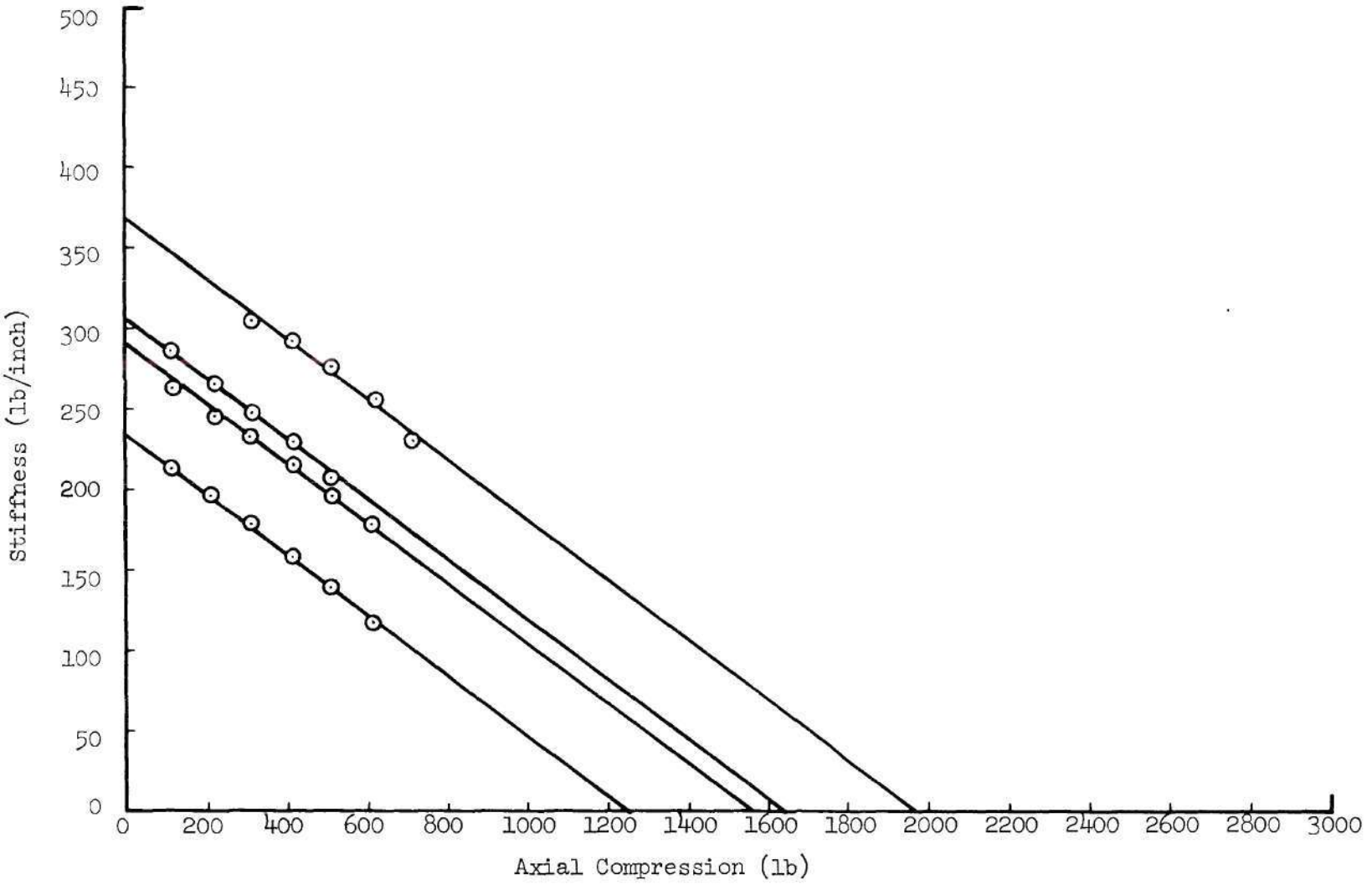

Figure 6. Stiffness-Axial Load Plots for a Rotationally Restrained Column.

CHAPTER III

NONDESTRUCTIVE TESTING OF THIN CYLINDRICAL SHELLS

The behavior of cylindrical shells, both stiffened and unstiffened, under axial compression differs appreciably from that of columns and plates. Such bodies show a marked reduction in load carrying capability in the post buckling region.

For a perfect plate or a column, the load-deflection curve is concave upwards and symmetric about the load axis since motion in either of the two directions is admissible. This is, however, not true for a shell body. Consider the characteristic "load-deflection" diagram shown in Figure 7.

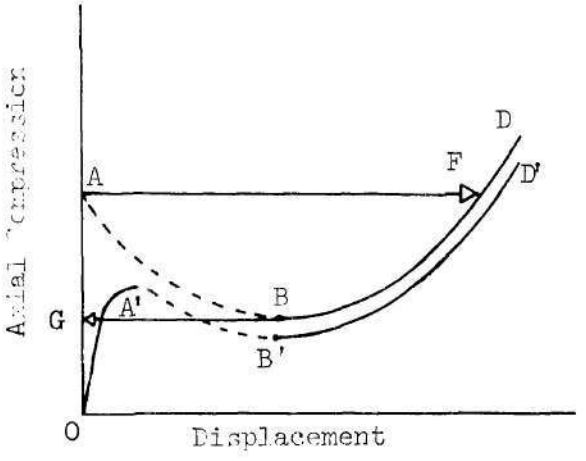

Figure 7. Characteristic Load-Deflection Diagrams for a Perfect and an Imperfect Shell.

It can readily be shown that the general tendency of the shell is to buckle inwards; towards the center of curvature. In Figure 7 the deflection towards the center of curvature against the axial compression is plotted. Asymmetry of the diagram of equilibrium states is due to the fact that branch ABF of the diagram lies below the point of bifurcation A. On section AB of the curve OABD for a perfect shell, the equilibrium forms are unstable and on section BF they are stable. Section FD corresponds to stable states. The upper critical load is defined as the greatest load below which initial equilibrium state is stable in the small. In Figure 7 the upper critical load for a perfect shell refers to the load at bifurcation point A. The lower critical load is the load below which the initial state is the only stable state, thus there is stability in the small as well as in the large. If an ideal shell is loaded by a static load (soft machine) in such a way that the state of strain is strictly momentless, then the load applied to shell increase to A, the upper critical load, then the shell will experience a jump from equilibrium position A to F, after which the load starts increasing along the branch FD. The reverse process consists of drop of the load along DB, then a jump of the shell along line BG and then to the starting point of loading along GO. The behavior of a real shell (imperfect shell) as explained by the curve OA'B'D' is similar to that of a perfect shell, except that, due to the bending occurring the branch of the equilibrium states with growing load no longer coincide with the axis. The upper and lower critical loads, in a similar way, are defined by A' and B' respectively. It

is thus clearly seen that the highest critical load for an imperfect shell is lower than the classic value. Thus the buckling load value derived from a Southwell plot must always be lower than the theoretical ideal. This is in contrast to the case of an imperfect column where, as stated in the previous chapter, the hyperbolic relation between load and deflection (from whence Southwell plot is obtained) always asymptotes to the classical instability load level. However, for shell bodies under loadings other than compression, the disagreement between the Southwell load and the theoretical load is frequently smaller. The introductory chapter of this dissertation contains a discussion on the question and gives a number of supporting references.

Donnell (14) in his classic paper of 1938 discusses the issue at some length and our attention is now directed to his findings. An approximate solution for the case of cylinders under axial compression, which considers initial deviations from a cylindrical shape, was given by Donnell (37) in 1934. He assumed, and this assumption is well born out by experience, that the lengths of half waves in the longitudinal and circumferential directions are the same. From this assumption he arrived at the following expression for radial displacement,

$$w = W \sin \frac{\pi x}{L} \sin \frac{\pi s}{L} + W(W+2W_i) \frac{\pi^2 R}{8L^2} \cos \frac{2\pi x}{L} \qquad (12)$$

and the initial derivation from a cylindrical form was taken to be

$$w_i = \left(\frac{W_i}{W}\right)w \tag{13}$$

He then arrived at the following expression for the compressive load 'P';

$$P = \frac{W}{W_i + W} P_c \left\{ \frac{1 + \frac{\pi^4 R^2}{4L^4}(W + 2W_i)(W + W_i)}{1 + \frac{\pi^4 R^2}{8L^4}\frac{(W + 2W_i)^2(2W + W_i)}{(W + W_i)}} \right\} \tag{14}$$

where P_c is the classic instability load.

The expression in the brackets, given above, is really an attenuation factor on P_c and is, clearly, always less than unity for positive values of W and W_i. Also this expression can be demonstrated to be a function of the initial imperfection and the weighting factor W_i. Practical experience demonstrates that for shells in compression good Southwell plots can be attained. This is possible if the observation point is chosen with great care or if the total deformation pattern around the circumference is harmonically analyzed. The results so obtained appear to indicate that the value of critical load so derived is very nearly the actual buckling load. However, this "gross" treatment method can give good answers only after considerable expenditure of time and effort in computation. It requires, moreover, the amassing of considerable amount of data at relatively high load levels. The direct approach, the determination of the Southwell load for the specific critical region is even more difficult.

The measurement point for such an approach is, with current techniques, virtually indeterminate. It is this state of affairs which directs one's attention to the wall stiffness approach which, as we have indicated before, is directly associatable with the Southwell approach. The virtues of this wall stiffness technique, as subsequent experiments clearly indicate, are

(1) Observations are taken at the point of the application of normal force.

(2) Very low load levels are necessary to achieve success.

The study starts from the single test observations of Bank (74). He has demonstrated the effectiveness of this approach for one particular longitudinally stiffened shell. He has shown that the wall of a stringer reinforced shell underwent a progressive loss of stiffness as the axial compression was increased. His study also indicated that the variation in lateral stiffness with increasing axial compression was apparently nonlinear for some region of smaller axial load but there was a usable region of linear variation of stiffness for compressive loads considerably lower than the critical load. He was able to predict the actual buckling load of the shell as the zero stiffness intercept obtained by extending the linear portion of the stiffness versus axial load plot. However, the study did not clearly indicate the restrictions that must be placed on the magnitude of the side force used, nor did it indicate how the region of instability should be determined. Moreover, it is not possible from a single test to determine the generality of the method.

The analysis of Donnell (14), as pointed out earlier, is dependent upon the initial imperfection being of the same form as the final buckle pattern. To a large degree this is frequently the case as Ford's (66) study shows. But it is crucial to recognize that in some circumstances a point load normal to the shell wall will not produce a deformation which is consistent with the buckle deformation. For unstiffened shells, both circular and elliptic, there is a reasonable correspondance. For longitudinally and circumferentially stiffened shells of a classic pattern the situation is similar. However, for spirally stiffened shells this is not so. This will not be true for shells with internal or external pressure in addition to axial compression, particularly if the pressure level is reasonably high. This is evident from the work of Horton and Durham (76). They conclude that as the pressure (p) goes from negative to positive the buckle changes from a vertical fold to a ring type shape, passing through a rhomboidal shape at $p = 0$.

The studies reported in this chapter deal with these issues. They bring clarity to the magnitude of the lateral force needed to determine the wall stiffness and indicate the influence of the curvature and the applicability of the method to noncircular shells. Also the method demonstrates that the region of high probability of instability can readily be ascertained under zero or low load level conditions, and it verifies that the critical condition predicted on the basis of linear extrapolation of the load-stiffness curves generated for low values of axial compression agrees extremely well

with the actual failure load.

Experimental Program

To clarify the issues discussed in the previous section it was essential to conduct tests on a variety of cylinders. Because of the expense which would have been involved if realistic large scale shells had been used, the program was centered around model shells. This is a well established procedure and the deductions therefrom are known to be consistent with reality. A detailed treatment of this topic is given by Horton, Singhal and Haack (77).

Six cylinder types were chosen for this investigation. These cylindrical shell models were unstiffened circular, longitudinally stiffened circular, longitudinally and circumferentially stiffened circular, unstiffened elliptic, unstiffened elliptic with a rectangular cutout and spirally (symmetrical) stiffened circular. Details of the choice of material and fabrication of models, the instrumentation used and tests procedure followed are described in subsequent sections.

Design and Construction of Specimens

Choice of Material

It is expensive and time consuming process to build thin walled metallic shells. Their modification while they are rigged for the test is almost impossible and hence parametric studies cannot be efficiently carried out with them. Plastics have, therefore, been used by many investigators (see reference (77)) in the past.

Plexiglas (Methyl Methacrylate) was chosen for the fabrication

of the models used in this program. The reasons to choose plexiglas over the other plastics were as follows:

(1) It behaves in a linear elastic fashion below its yield point (6000 psi).

(2) Excellent quality thin sheet and bar stock is available at reasonable cost.

(3) The material is easily glued, machined and hot formed. Tests made at Georgia Institute of Technology (66) show that the modulus of elasticity value of plexiglas acquired from a single supplier lie between 4.47×10^5 and 4.54×10^5 psi.

Plexiglas is, however, not the perfect material. The material properties are influenced by temperature, relative humidity and strain rate (77). In contrast to metallic materials plexiglas is creep sensitive. Nevertheless, in our particular application these disadvantages in no way outweighed the advantages. The reasons will become clear when we discuss the test procedures used.

Method of Construction

Models used in this study were basically of two categories, right circular cylinders and right elliptic cylinders. The stiffening used was both of conventional nature viz, longitudinal stringers and circumferential rings and of unconventional nature, namely, the waffle or spiral stiffening. The stringers were internal and the rings were external. All shells were 16.5 inches long and had skin of 0.030 inch thick plexiglas sheet. The sheet was made to size by a scratch and fold process.

In the case of conventional stringer stiffening, the sheet was then placed in a holding fixture and the appropriate stringers were then attached to it by using B-1 solvent supplied by the plexiglas manufacturer. This process of gluing was easily carried out. The two pieces of plexiglas to be joined were placed in close contact under slight pressure and the common edge wetted with the liquid glue (solvent) using a hypodermic syringe. The transparency of the material aided in this process because the degree of penetration into the joint was thereby easily monitored. Care was exercised to ensure complete penetration during the process because subsequent filling was almost impossible. After the stringers were attached to the sheet, the two ends of the sheet were butt jointed together and a 3/4 inch wide reinforcement of the same thickness as the skin was glued overlapping the joint.

In the case of the unstiffened shell and the spiral stiffened shell, a similar "loop" of the skin sheet was made as was done for the conventionally stiffened shell described in the preceding paragraph. At this stage the "loop" of the skin was formed into a right circular or elliptic cylinder by adding 0.030 inch thick and 3/4 inch wide doubler plates and 1/4 inch by 1/4 inch hot formed rings externally at the shell extremities. The fabrication of hot formed sections is described in detail by Haack (78).

The waffle stiffeners, in the case of symmetrical spiral stiffened shell, were then placed, internally, at 30 degrees to the generator. The stiffeners were 0.060 inch deep and 1/4 inch wide.

They consisted of two layers of 0.030" x 1/4" strips of plexiglas. First, a bottom layer consisting of the continuous strips described above was laid in one direction. The top layer of the symmetrical stiffener in the other direction was then laid overlapping this bottom layer. The remaining two layers in each direction then consisted of small appropriate discontinuious strips. They were carefully cut to the size and laid so as to make the necessary 0.060 inch deep and 1/4 inch wide symmetrical waffle stiffening. The spacing between these stiffeners was adjusted such that the perpenidcular distance between their center lines was one inch.

The internal doubler plates and hot formed rings, similar to the external doubler plates and rings, were then attached at the shell extremities. The proper circumferential stiffening (for conventionally stiffened shell) could then have been carried out. However, due to the simplicity of the process this operation was performed with the specimen rigged for testing. A typical plexiglas shell construction (Specimen 2) is shown in Figure 8.

Design and Construction of Stiffness Probe

The tool used in the determination of the stiffness of the shell wall was a special pushing force-deflection measuring device; hereafter called "stiffness probe". A schematic diagram of this apparatus is shown in Figure 9 while a picture of this device is given in Figure 10. It consists of a case hardened steel rod sliding horizontally in two Thompson ball bushings. The pushing end of the steel rod was hemispherical and was 1/8 inch in diameter. An aluminum bracket supported a

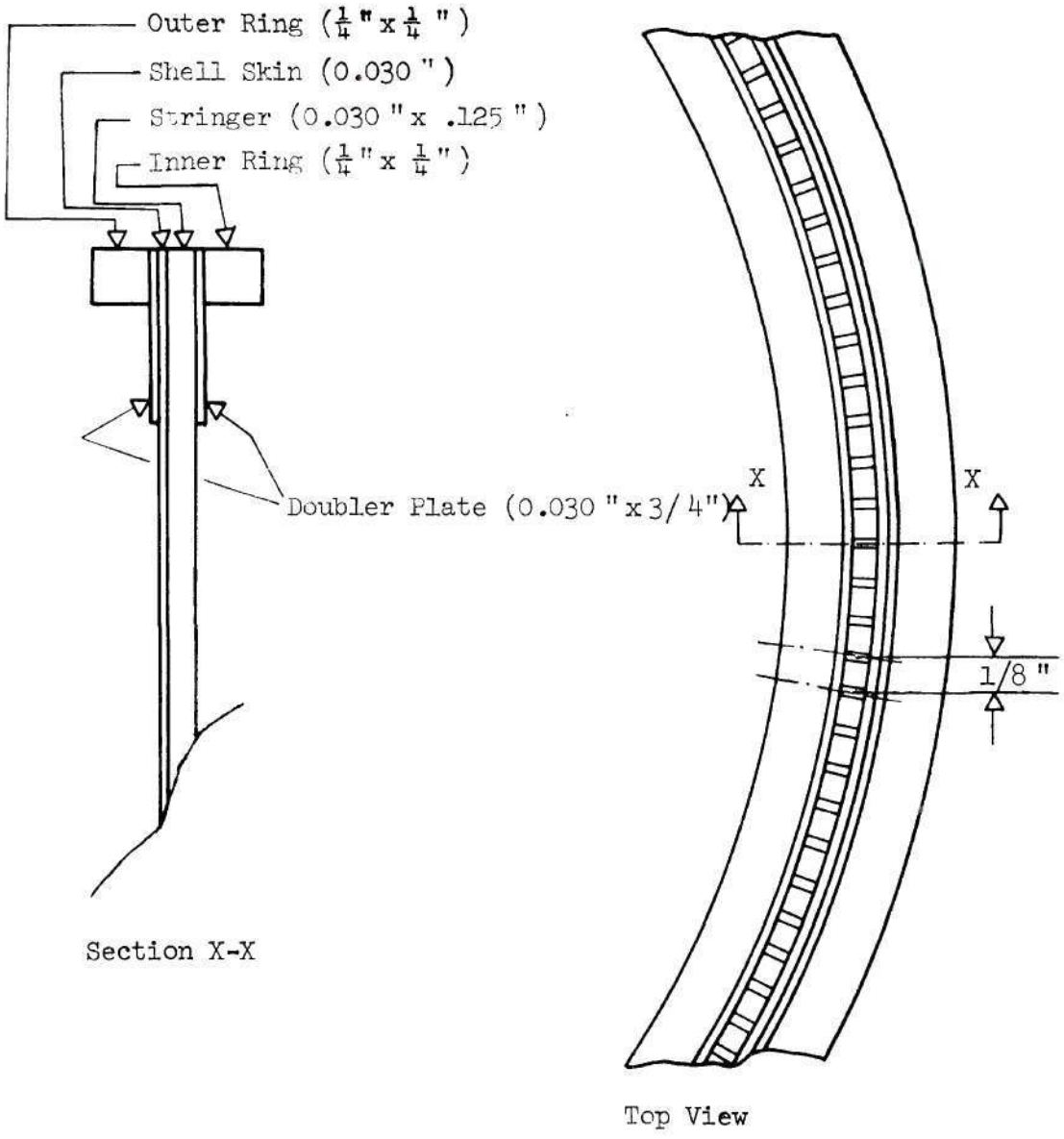

Figure 8. Typical Plexiglas Shell Construction (Specimen 2).

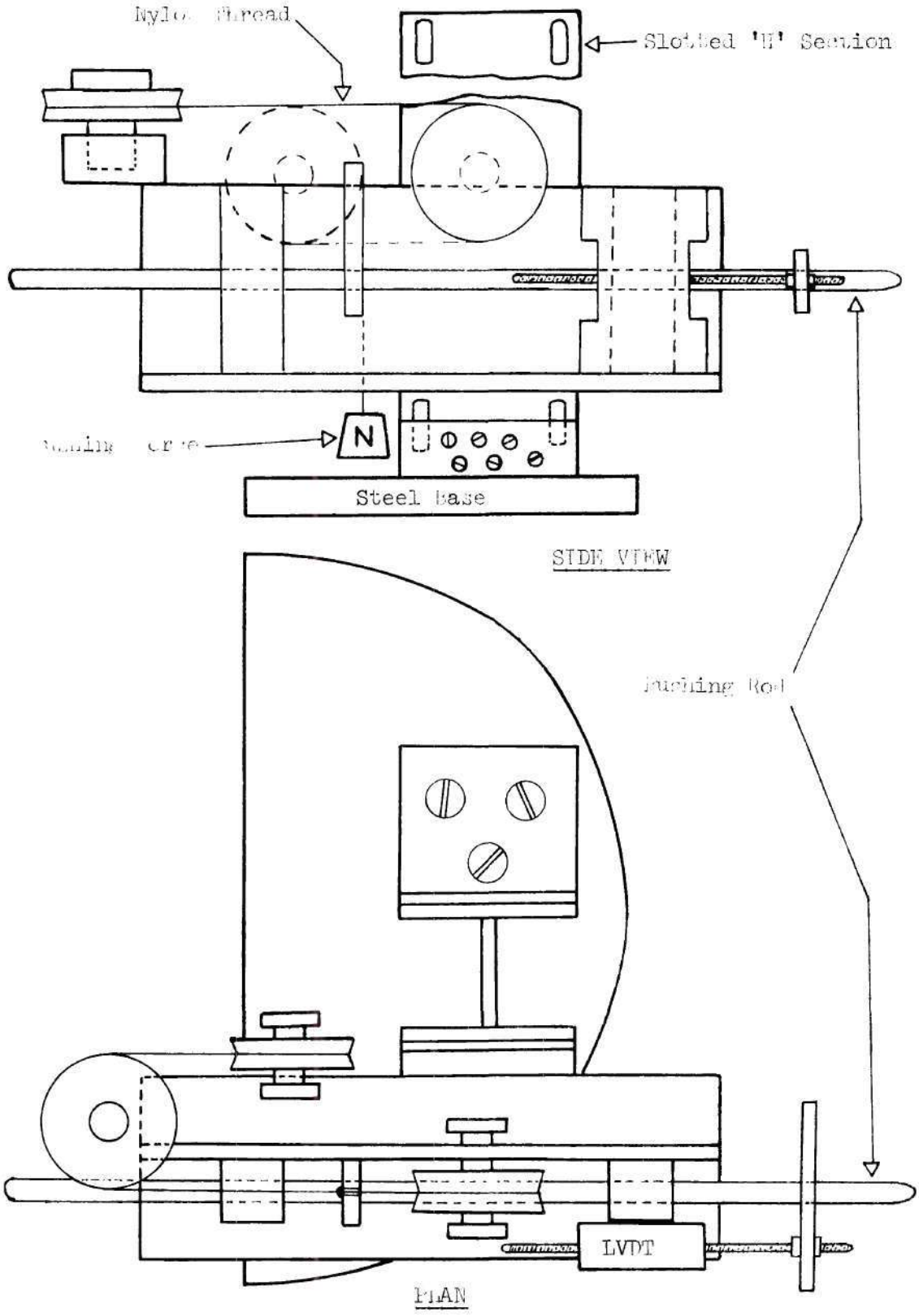

Figure 9. A Schematic Diagram of the Stiffness Probe.

system of pulleys through which a nylon thread transmitted to the pushing rod the force caused by placing a known weight in the scale pan. A linear variable-differential transformer was clamped to the bracket and its core rigidly connected to the pushing rod through a 1/4 inch thick aluminum strip. The bracket in turn was clamped to a vertical slotted H-section mounted on a one inch thick steel base. To prevent rigid body motion, if any, caused when a weight is added in the scale pan the base of the stiffness probe was clamped down to the testing machine bed. This design of stiffness probe enabled the measurement of the deflection caused by the known side force without the displacement transducer coming in direct contact with the point probed. The high quality bearings and the excellent surface finish on the pushing rod reduced friction to a minimum. In fact a weight of five grams in the scale pan was sufficient to slide the pushing rod in the bushing. This sliding friction force was, in part, compensated by the stiffness of the LVDT spring (one gram per 0.010 inch of displacement). However, in our plot of stiffness versus axial compression these "constant" but unknown forces will not change the zero stiffness intercept on the axial load axis. They will merely alter the slope of this plot.

Instrumentation

Under axial compression alone the shell wall deflections were a few thousandths of an inch. The normal force used to determine the stiffness caused an increase of tens of thousandths of an inch. The accurate measurement of this variation in displacement, thus, demanded

a high resolution large range displacement transducer. The Hewlett-Packard 7DCDT100 linear variable-differential transformer (LVDT) met the above requirements and was readily available in the laboratory. The linear measurement range of this LVDT as prescribed by the manufacturer was $\pm$ 0.100 inch and the error in linearity claimed to be less than 1/2 percent. However, it was found that this accuracy in linearity was lost when the measurements were made in the neighborhood of electrical zero. Nevertheless, the linearity was good when the measurements were made away from the electrical center. The stiffness probe position with respect to the shell wall was, therefore, adjusted in such a way that all motions of the pushing rod caused the LVDT magnetic core to travel only on one side of the electrical zero. For the circularity check and end shortening measurements (required for centering the axial load) the Hewlett-Packard 24DCDT250 displacement transducers were used. These LVDT's had a linear measurement range of $\pm$ 0.250 inch.

Hickson self-adhesive gages were used to check the uniformity of the load distribution accomplished on the basis of uniform end shortening sensed by three LVDTs. These gages are reusable since they utilize the natural cohesive properties of plate cured Poly-Vinyl-Cloride material from which the gage body is manufactured. The sensing element is made of a very thin gold strip formed by vacuum deposition. They are easily stuck to the shell surface by rolling action and peeled off after lifting a corner of the gage with a knife edge. For a good adhesion the only requirement is that the gage and specimen surface

be cleaned with a dilute detergent solution. These gages have a nominal resistance of 120 ohms and their limiting current carrying capacity is 10 ma. They can be calibrated individually. However, they are highly temperature sensitive and hence require a close temperature and air draft control.

The axial load was sensed by a strain gage load cell of the Baldwin test machine and read on the indicator dial. Provision for an electrical output proportional to the load was available through a voltage divider network driven by the indicator system of the machine. All the instrumentation used in this program are standard in a structures research laboratory.

Data Acquisition System

The large amount of data acquisition and reduction became possible due to an on line Hewlett-Packard 2115 digital computer. The computer was interfaced with a 200 channel crossbar scanner, a digital integrating voltmeter, a digital magnetic tape recording unit, a 16 channel digital to analog and analog to digital converter, a photo-reader, a high speed paper tape punch unit and a teletype unit. With the exception of digital to analog and analog to digital converter all other units were used in this experimental study.

The computer had a 8000 word memory and BASIC language was used to acquire and analyze the data. BASIC language was chosen for the reason that it allows the modification of the operating program through a simple teletype input. The data acquisition and reduction consisted of reading the output from the stiffness probe, the end shortening LVDTs

and the test machine load, scaling and displaying them on the teletype unit as desired. An operating program in BASIC language and the flow diagram of the data acquisition system is given in Appendix A.

Magnitude of the Side Force

For columns, compressive forces are destabilizing but lateral loads are not. Under combined loading conditions the deflection due to the side force is amplified in the stable region by the compressive load present. The net deflection is, in fact, obtained as the product of the displacement due to side force alone and a factor dependent upon the ratio of the compressive load and the instability load. The basic deflection term is, therefore, linearly dependent upon the lateral load and hence, the measured lateral stiffness is independent of the magnitude of the lateral force, in linear theory range.

Shell bodies, on the other hand, are unstable both under axial compression and normal force. Consequently, under combined loading the instability load level depends upon both loading actions. The lateral stiffness, hence, is a function of the side force applied and decreases with the increase in the side force.

In conducting the tests on the various shells we limited the normal force employed for the stiffness determination purposes to that magnitude which, at zero axial compression, deflected the weakest region between 1/4 and 1/3 the effective wall thickness. The validity of this restriction was substantiated by conducting tests with different levels of side force. These tests were made on all specimens. It was ascertained that the plots of stiffness versus axial force for all

values of side force, which did not produce a net deflection in excess of 1/2 the effective wall thickness at the maximum value of the compressive force, indicated the same critical load.

Size of the Gridwork and Station Identification Code

All shells were marked with one inch orthogonal gridwork consisting of vertical longitudinal lines and circumferential latitudinal lines. The longitudes were numbered in the counterclockwise direction (looking from top end of the shell) starting with the one next to the seam of the shell. The latitudes were numbered according to their distance from the equator, e. g., the latitudinal line one inch above the equatorial line as +1 while that one inch below the equatorial line as -1. The code which identifies a particular station consists of three digits. The first digit with the appropriate sign denotes the latitude and the last two digits the longitude of the station.

Test Procedures

The tests were carried out in a laboratory in which the temperature and humidity did not vary significantly. A Baldwin 120,000 lb. screwjack universal test machine was used and this was operated at a fixed strain rate. Thus, the basic disadvantages of plexiglas as pointed out in earlier discussion were minimized.

To begin with the ends of the completed circular shell were "potted" in epoxy in aluminum rings. These rings were machined on a lathe from one inch thick aluminum plate. Their inner and outer radii were four and seven inches, respectively. A one inch wide and 1/4 inch

deep groove (with the six inches radius line as the center line) was turned for the seat of the shell ends. The elliptic shell was potted on two 18" x 18"x 1" precision ground flat steel plates.

A circularity and stiffness scan of the circular shells over the mid 2/3 rd length was then made. The shell to be probed was mounted on a turntable and a LVDT and the stiffness probe were used for the relevant data acquisition. Having established the "weak regions" of the shell body the specimen was then placed in the Baldwin universal testing machine. An annotated picture of Figure 11 illustrates the test set up. To prevent the various pieces of test fixture from falling in case of catastrophic failure of the shell body, a pair of safety cables were attached between the upper ring or plate and the test machine crosshead. The three end shortening LVDTs mounted on the magnetic base stands were positioned 120 degrees apart in such a fashion that each picked up the vertical motion of the outside upper end frame of the shell. The position of the spherical bearing on the two inch thick steel disc was thereafter adjusted until the end shortening under axial load was identical at the three measurement locations. Hickson strain gages were then used to determine the circumferential distribution of the axial strain. This distribution was found to be uniform within 15 percent. The uniformity of axial strain and the uniformity of axial load distribution are clearly synonymous at low load levels. The uniformity of the applied axial compression is necessary to ensure that failure occurs at the weakest region as determined by the stiffness profile. Care was taken not to

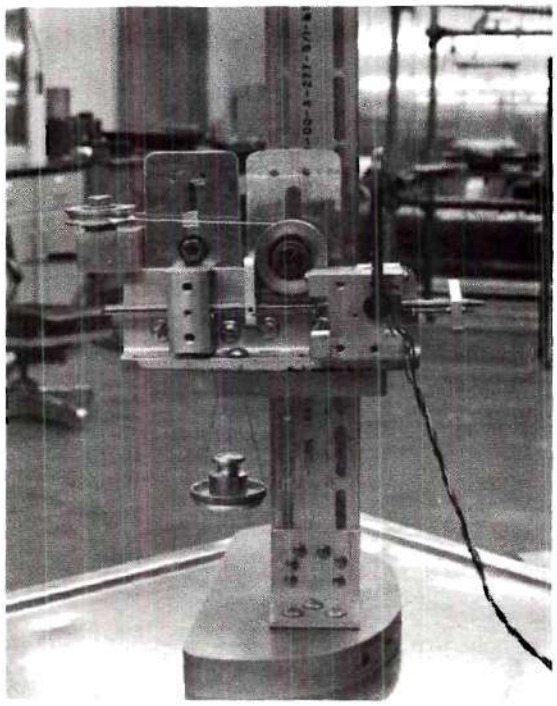

Figure 10. Stiffness Probe.

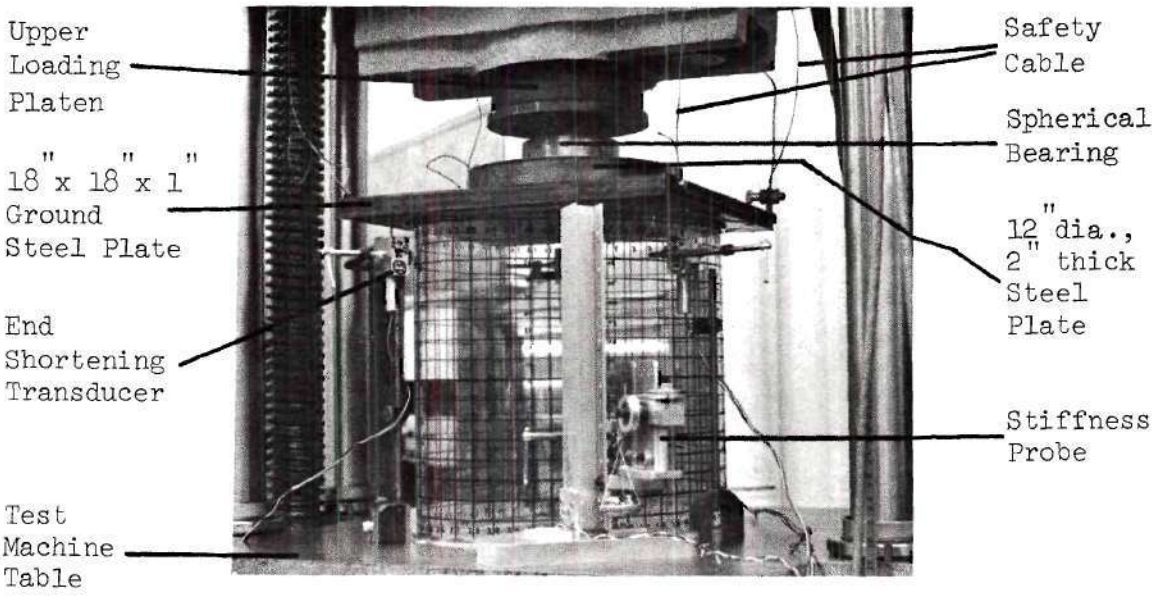

Figure 11. Elliptic Shell Rigged Up for Test.

change this set up during the whole test sequence. The variation in stiffness with increasing axial compression was then determined in the anticipated first unstable region. When this region had been thoroughly "mapped" the shell was loaded to instability. In this way the actual unstable region was located and the value of critical load established.

Summaries of the tests made on each of the six specimens are given in the subsequent sections.

Summary of Tests on Specimen 1

(Unstiffened Circular Cylindrical Shell)

An unstiffened circular cylindrical shell of 11.45 inches diameter and 16.5 inches length was constructed from a single 0.030 inch plexiglas sheet according to the method described earlier. It was thoroughly checked for circularity over the mid 2/3 rd of its length. The variation in nominal diameter was less than fifty thousandths of an inch, i. e., the error in circularity was less than 0.5 percent of the base diameter. The quality of the specimen was excellent.

The static stiffness values, under zero axial compression, determined at the middle 13 latitudinal planes are listed in Table 3. The side force used to determine this stiffness profile was 200 grams. The region of minimum stiffness is clearly evident. A detailed study of the variation in stiffness of several points in this region with increasing axial compressive force was made. The plots of stiffness versus axial load are given in Figure 12. The disagreement between the stiffness values determined on the turntable and in the test machine is probably due to the slight motion of the turntable bearing.

Table 3. Stiffness Profile of Unstiffened Circular Shell Under Zero Axial Compression.

Generator	Normal Stiffness (lb/inch)												
	Distance of the Measurement Plane From the Equatorial Plane of the Shell												
	6"	5"	4"	3"	2"	1"	0"	-1"	-2"	-3"	-4"	-5"	-6"
1	53.3	67.8	65.6	58.6	52.5	53.8	44.1	43.4	48.0	53.1	54.7	63.7	64.5
2	72.0	52.8	63.1	50.4	42.1	45.7	44.8	40.7	47.3	47.9	51.9	53.4	67.0
3	65.4	52.6	56.0	48.0	41.0	45.4	43.6	39.6	46.3	49.7	52.1	52.0	66.4
4	71.0	50.8	56.0	43.1	41.7	45.5	42.6	38.5	48.7	45.7	47.1	50.0	62.1
5	68.4	46.5	48.4	40.6	39.8	45.5	42.6	40.8	47.2	45.1	46.2	48.7	61.8
6	69.9	46.8	47.7	41.6	38.2	40.7	40.6	37.7	41.8	42.5	45.4	47.5	61.6
7	74.2	49.2	45.5	40.6	37.6	39.8	37.8	37.8	40.8	40.3	45.6	46.5	57.3
8	68.0	48.8	49.7	41.6	37.9	40.6	37.5	38.3	38.5	41.8	43.1	46.2	59.5
9	74.9	47.1	43.8	40.7	37.7	46.2	35.7	37.5	39.1	40.0	41.2	45.8	66.7
10	67.0	51.3	38.8	41.0	36.8	45.0	39.1	37.6	40.4	43.3	41.8	46.8	63.3
11	68.7	47.6	44.2	38.2	37.8	43.2	41.6	40.3	43.6	48.2	44.9	49.6	54.4
12	69.4	49.7	49.0	47.8	40.4	46.2	43.2	42.3	42.5	48.2	48.0	53.2	61.8
13	78.7	52.5	47.4	45.0	43.1	47.4	46.1	45.3	43.0	42.8	48.3	52.1	61.2
14	77.5	54.8	54.6	44.8	43.9	51.8	47.1	41.7	47.8	47.7	51.3	52.3	63.9
15	66.8	61.6	58.9	51.5	42.7	53.2	44.7	47.1	48.2	53.0	53.5	52.4	62.2
16	64.5	53.8	49.3	50.2	44.8	56.1	48.7	45.1	47.5	52.0	56.0	56.8	63.0
17	63.0	61.4	63.0	48.4	44.5	49.3	50.1	48.6	46.7	48.3	58.2	55.1	63.4
18	72.4	63.4	61.6	52.7	49.1	52.2	52.8	55.8	47.4	51.4	60.1	54.2	66.4
19	75.4	72.2	74.0	55.1	49.6	58.2	55.6	56.6	47.1	91.1	62.1	62.9	72.7
20	70.0	65.6	71.7	68.7	55.3	62.6	59.4	55.0	52.0	54.5	56.0	58.8	74.6
21	76.6	69.5	80.4	67.5	54.2	66.6	60.3	60.7	53.4	56.8	62.3	59.2	80.6
22	96.0	71.9	81.0	71.2	57.5	79.3	65.5	61.2	52.4	61.0	68.6	59.5	78.7
23	136.6	78.5	88.6	70.2	61.2	82.1	69.8	71.8	57.5	58.5	69.4	65.4	83.4
24	145.9	88.5	77.3	76.5	58.8	78.5	80.5	80.8	72.8	67.1	67.5	77.8	89.9
25	111.1	83.6	83.4	93.5	64.2	75.5	69.2	76.3	70.7	67.3	73.4	70.4	77.7
26	178.9	77.4	92.8	73.0	63.3	78.2	81.2	78.0	70.3	66.9	75.4	67.4	84.4
27	114.8	74.3	98.2	86.0	75.2	77.3	78.1	74.9	74.6	70.4	69.0	67.2	86.1
28	110.0	102.0	98.1	76.8	69.9	74.0	86.7	73.4	72.9	75.3	68.4	69.1	89.1
29	98.8	80.5	106.4	70.2	62.9	65.6	78.8	65.1	67.8	69.3	63.9	69.7	92.3
30	104.1	88.3	90.6	67.5	60.3	58.6	68.7	61.9	59.7	63.7	65.4	70.1	82.1
31	91.2	112.4	77.3	68.2	56.8	62.7	69.4	68.4	68.2	62.3	57.5	70.3	84.4
32	100.4	88.7	100.9	106.4	63.1	106.0	80.9	80.2	83.9	100.9	89.8	76.8	132.3
33	105.7	105.8	76.4	84.1	76.1	81.2	78.7	79.7	87.1	84.4	101.5	77.2	118.8
34	116.1	107.3	101.4	98.5	64.3	73.2	57.3	67.9	75.9	79.9	80.5	71.1	91.5
35	117.0	78.1	85.5	62.0	47.5	52.7	52.6	46.8	57.0	48.6	60.1	58.6	74.2
36	..... Seam of the Shell - Data not acquired.												

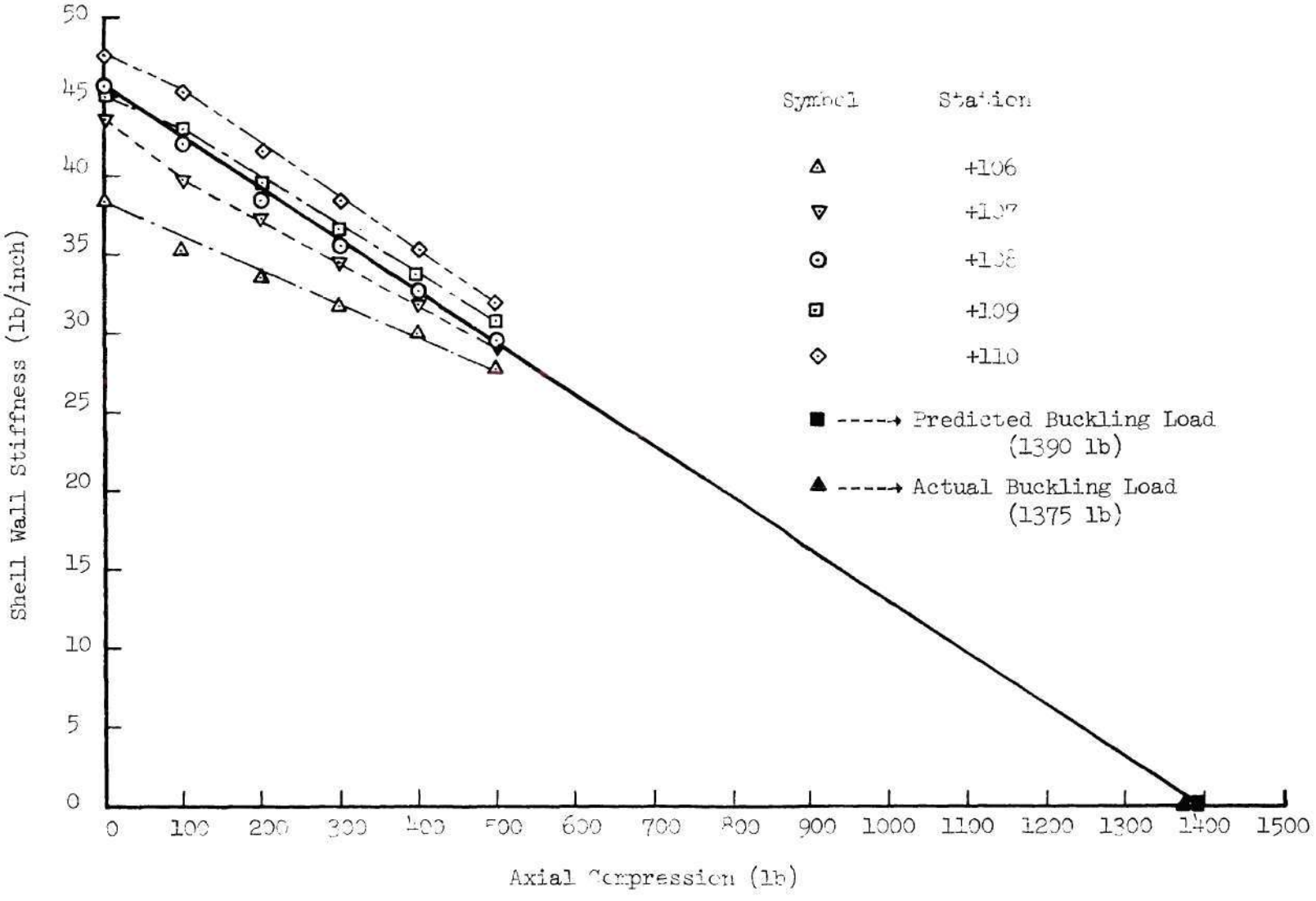

Figure 12. Stiffness-Axial Load Plots for Unstiffened Circular Shell.

It is evident from the plots of stiffness variation in the region of minimum stiffness that they lead to a good estimate of the buckling load. The lowest critical load predicted from the data, corresponds to point +108, and has the value of 1390 lb. This is in excellent agreement with the measured buckling load of 1375 lb. The disagreement of 1.09 percent is negligible.

Summary of Tests on Specimen 2

(Stringer Stiffened Circular Cylindrical Shell)

Having established the validity of the stiffness method for prediction of the buckling load for an unstiffened circular cylindrical shell we proceed to explore the possibility of its application to stiffened shell bodies. For this purpose a plexiglas specimen of 11.45 inches diameter and 16.5 inches length and of 0.030 inch thick skin reinforced by a multiplicity of stringers was constructed. These stiffeners, 0.125 inch deep and 0.030 inch thick, were placed 1/8 inch distance apart on the internal surface of the shell. In this case a differential method for the determination of the stiffness profile was employed. The differential stiffness at a point is defined as the ratio of the difference of two normal forces (applied at this point) to the difference of deflections produced by these normal forces. The normal force levels used for the determination of this differential stiffness were 200 grams and 500 grams. The differential stiffness profiles at the equatorial plane of the shell under zero and 400 pound axial compression are shown in Figure 13. The plots of differential stiffness versus axial force at several stations of the anticipated first buckle region are

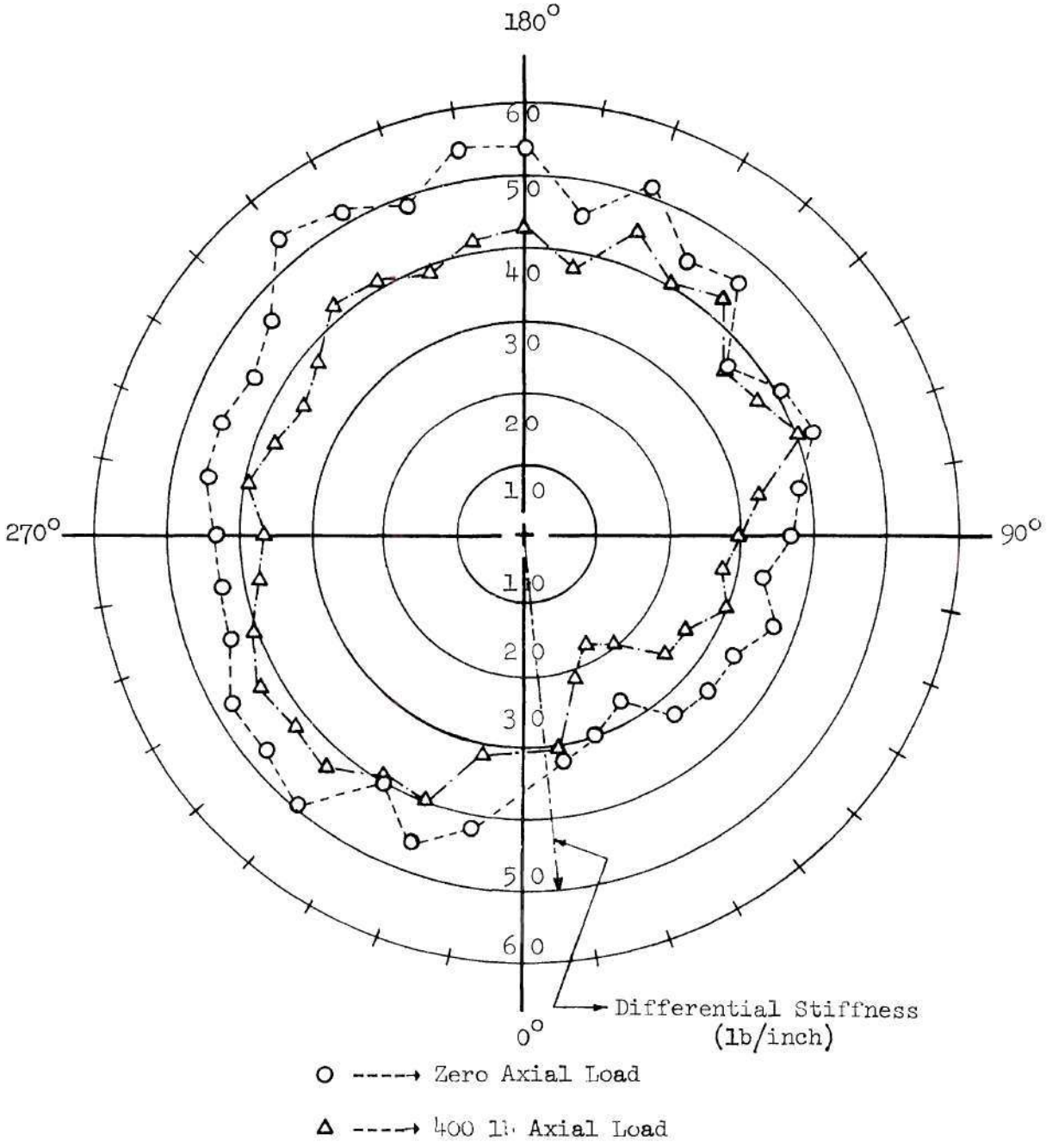

Figure 13. Differential Stiffness Profile at the Equatorial Plane of the Stringer Stiffened Circular Shell.

shown in Figure 14. The predicted value of 1060 lb. for the buckling load compares well with the actual buckling load value of 1080 pounds. The error in the prediction is less than 2 percent.

Summary of Tests on Specimen 3

(Stringer and Ring Stiffened Circular Cylindrical Shell)

Two frames, 0.060 inch thick and 0.25 inch wide, were attached to the longitudinally stiffened shell used in the previous test program. There were placed at 2.5 inches above and below the equatorial plane of the shell. A 500 gram side force was used for the stiffness measurements. The stiffness profile indicated that station 004 was the center of the most probable unstable region. The stiffness variation with increasing axial compression measured at this point is shown in Figure 15. The predicted value of the buckling load obtained by extrapolating this plot (linearly) to the zero stiffness ordinate on the load axis was 1950 pounds. The actual value determined by loading the shell to the buckling was 2000 pounds. The disagreement of 2.5 percent between the predicted and actual value is negligible for all practical purposes.

Summary of Tests on Specimen 4

(Unstiffened Elliptic Cylindrical Shell)

In order to investigate the applicability of the stiffness method to cylinders other than circular an elliptic cross-section shell was constructed. The skin thickness and the length of this shell were the same as of the unstiffened circular shell, namely, 0.030 inch

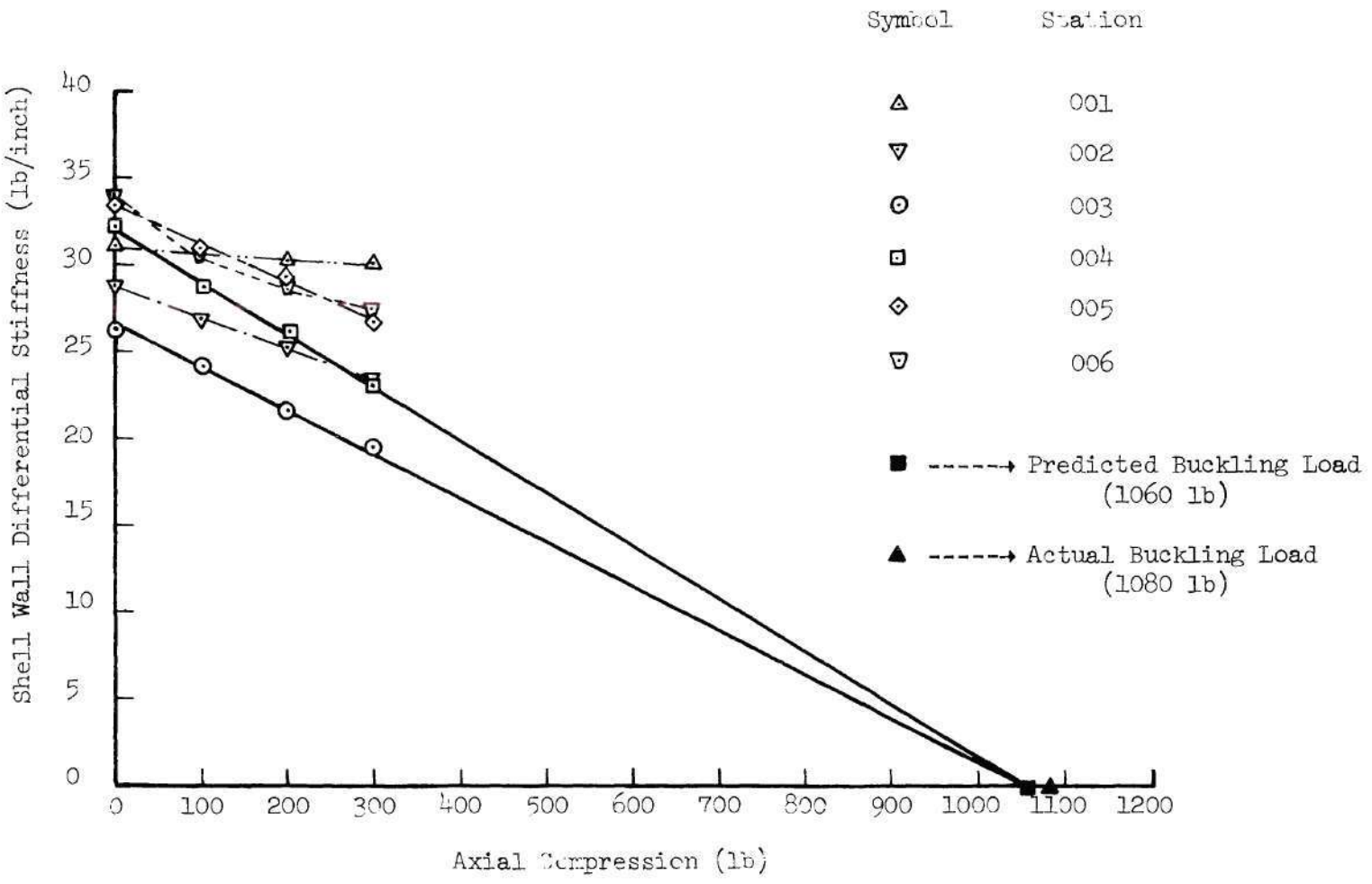

Figure 14. Differential Stiffness-Axial Load Plots for Stringer Stiffened Circular Shell.

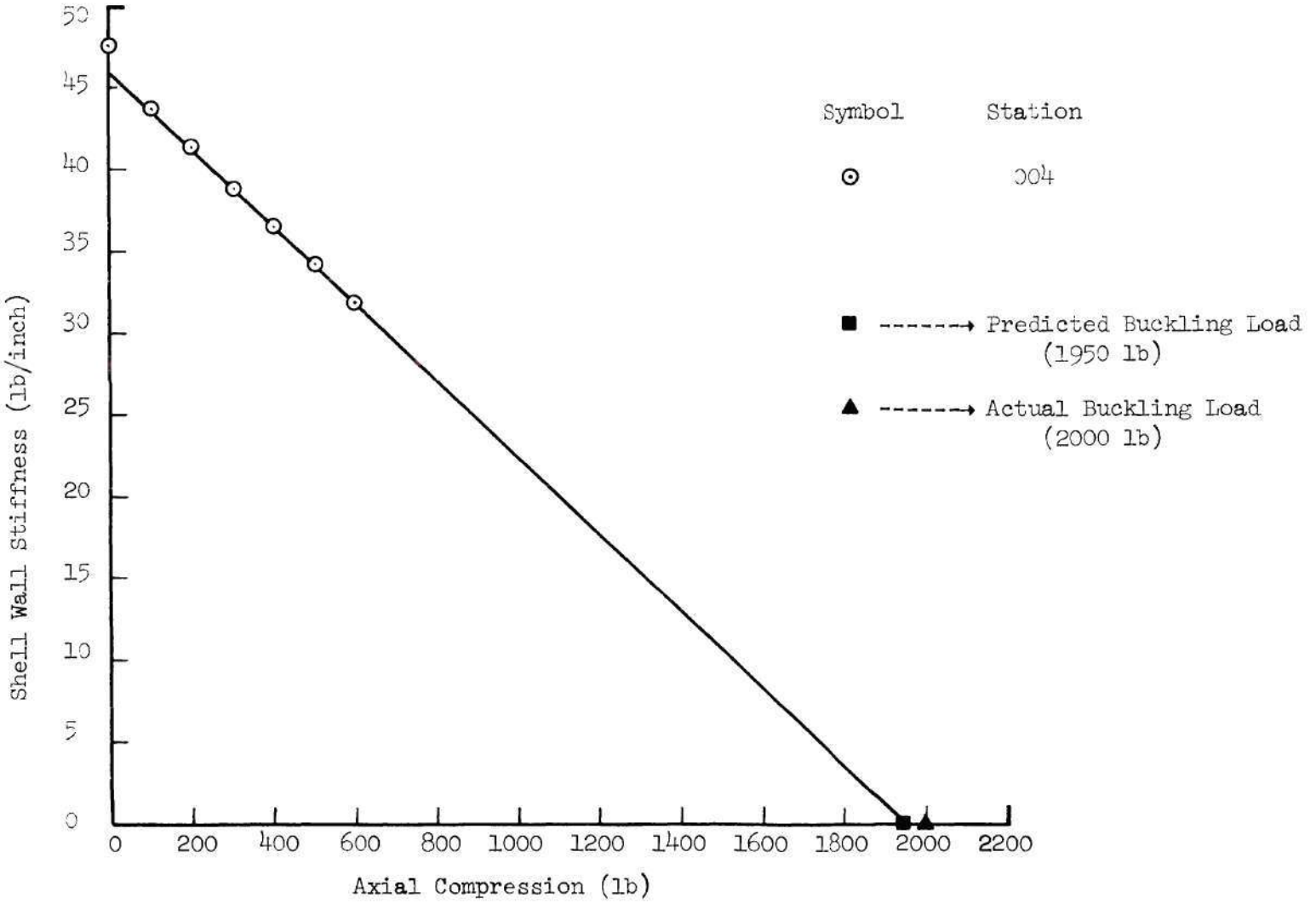

Figure 15. Stiffness-Axial Load Plot for Ring and Stringer Stiffened Circular Shell.

and 16.5 inches respectively. The circumference, major axis and minor axis were 47.1, 17.7 and 11.9 inches, respectively. The elliptic profile was approximated by the four arc method (79). This approximation is excellent and simple enough to permit inexpensive manufacture of a fixture for making the end rings. The seam of the shell was placed at one end of the major axis. In order to locate the weaker areas of the shell, the stiffness determination under no axial load was carried out in the large radius of curvature regions only (for obvious reasons). A normal force of 75 grams was employed for the stiffness measurements. The anticipated first buckle region was established between stations -332 and -338. The plots of variation in normal stiffness, at several stations of this area, with increasing axial compressive force are given in Figure 16. It is seen that the stiffness variation plot corresponding to the central station -335 of the first unstable region, gives an excellent estimate for the buckling load. The agreement between the predicted buckling load value of 360 pounds and actual buckling load value of 371 pounds is within 3 percent.

Summary of Tests on Specimen 5

(Unstiffened Elliptic Cylindrical Shell With a Rectangular Cutout)

So far our study has been limited to continuous cylindrical bodies. A natural extension of the research is to the bodies with definite discontinuities. For that purpose a 3" x 4" rectangular hole was cut from the elliptic shell used in the previous test. The coordinates of the corners of the cutout were -110, +210, -114 and +214. The magnitude of the side force used for the stiffness measure-

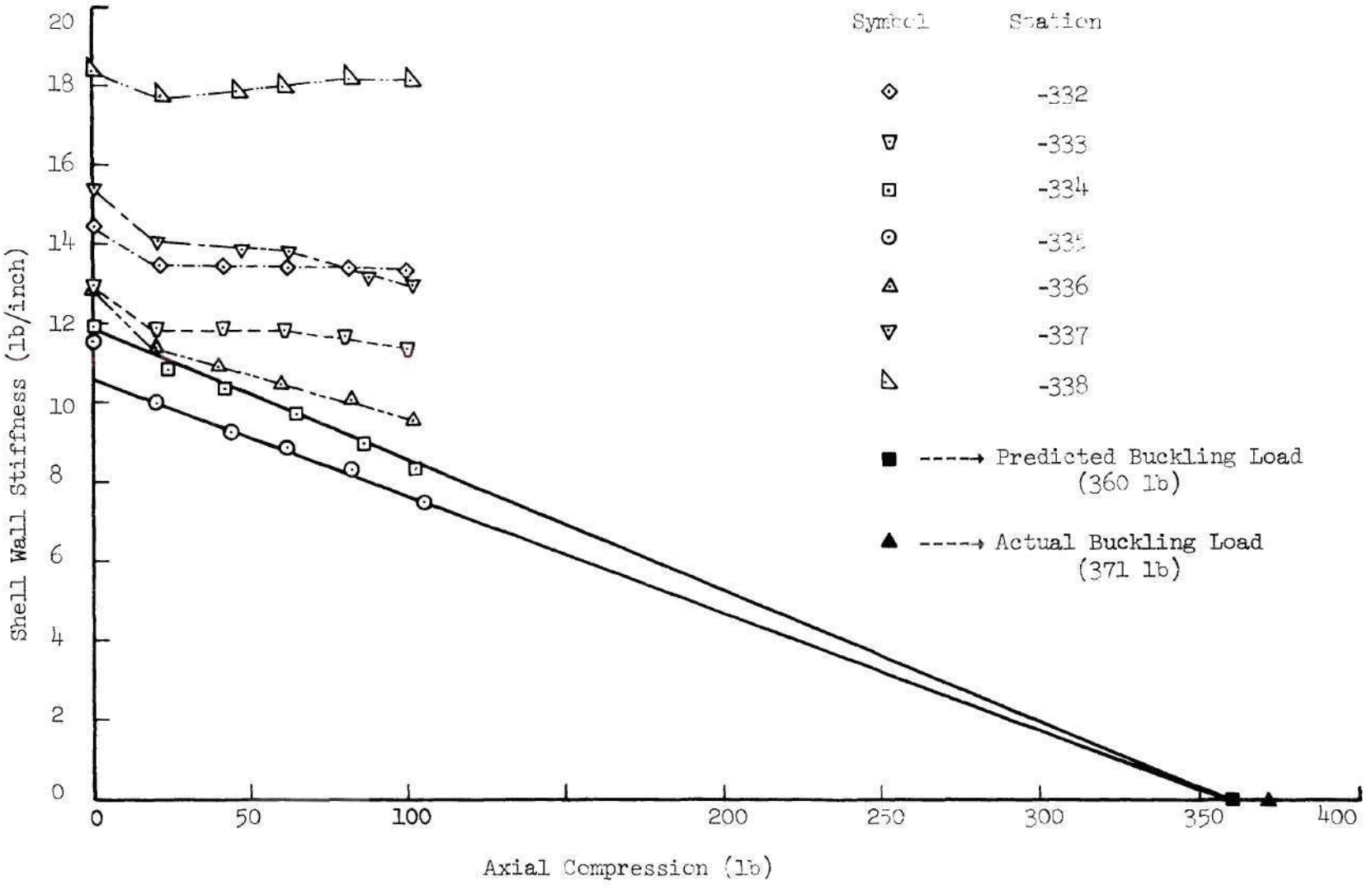

Figure 16. Stiffness-Axial Load Plots for Unstiffened Elliptical Shell.

ments was 75 grams which is the same as that employed in the previous test program. Thorough stiffness probing around the cutout was carried out. Station -215 was anticipated as the center of the weakest region. The variation of normal stiffness with increasing compression at this station is given in Figure 17. The linear extrapolation of this plot gave 180 pounds as the critical value of the axial compression. The actual buckling load was determined to be 191 pounds. The agreement is within 6 percent.

Summary of Tests on Specimen 6

(Symmetrical Spiral Stiffened Circular Cylindrical Shell)

The agreement between the actual failing load and the predicted buckling load by stiffness method for the five model test specimens, described earlier, is excellent. We now turn to the crucial issue of generality. To do so an investigation was made on a symmetrical spirally stiffened shell. Such shells buckle in either diamond or ring forms depending upon the degree of stiffening. However, under the normal force applied at the center of a panel or at the intersections of the stiffening members, the deformation pattern tends to differ from these forms. Thus, it is clear that the shape of the imperfection caused by the side force is of different nature to that of the buckle pattern formed under axial load.

A plexiglas circular cylindrical specimen of 11.45 inches diameter and 16.5 inches length and of 0.030 inch thick skin reinforced

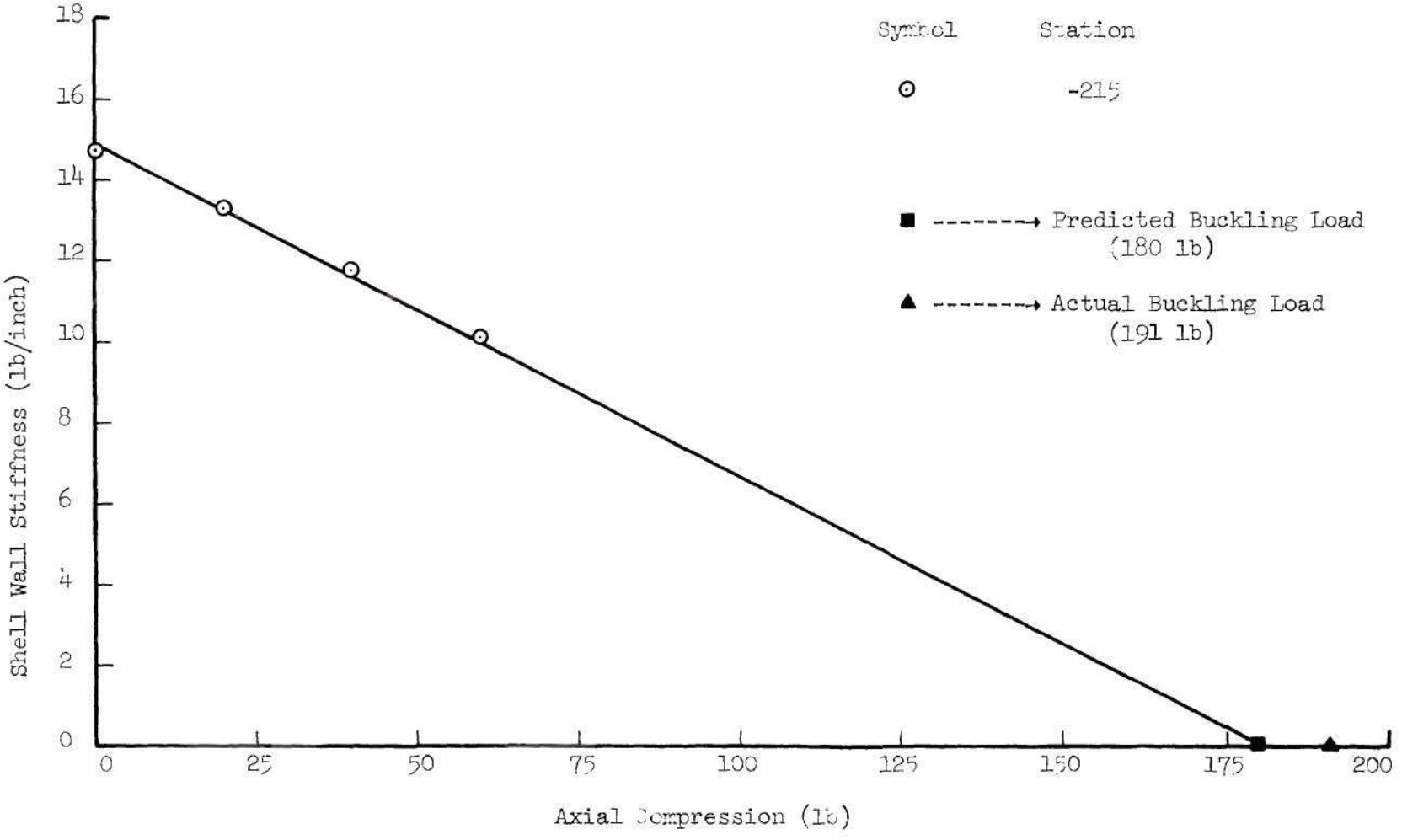

Figure 17. Stiffness-Axial Load Plot for Unstiffened Elliptic Shell With a Rectangular Cutout.

by symmetrically placed spiral stiffeners was constructed. These stiffeners, 0.060 inch deep and 0.25 inch thick, were placed at 30 degrees to the generator (longitude). They were spaced such that the perpendicular distance between their center lines was one inch. The method of attaching these stiffeners to the internal surface of the shell has already been described in an earlier section. A 600 gram side force was used for the stiffness measurements.

The buckling load values, as predicted by the stiffness method, at the various stations of the shell are shown in Figure 18. It should be noted that these loads were determined by the stiffness measurements at the points where the stiffeners meet or the "diamond verticies". The probing of the weakest area, marked by a bigger diamond in Figure 18, was then carried out in detail and the corresponding values of the predicted values of the buckling loads are shown in Figure 19. In this study the buckling loads were determined both at the "diamond verticies" and at the "diamond centers". From the initial stiffness scan of the shell surface, the section of the shell body on the +1 latitudinal plane between the longitude 16 and longitude 26 was found to be the weakest. The stiffness variation with increasing axial compression measured at the diamond verticies and diamond centers of this section are shown in Figures 20 and 21, respectively. It should be noted that since these diamond verticies and diamond centers did not exactly coincide with the one inch orthogonal grid work intersection points on the shell surface, the station identification code used for this shell is, therefore, a little different from that used for the previous five specimens. Each diamond vertex or diamond

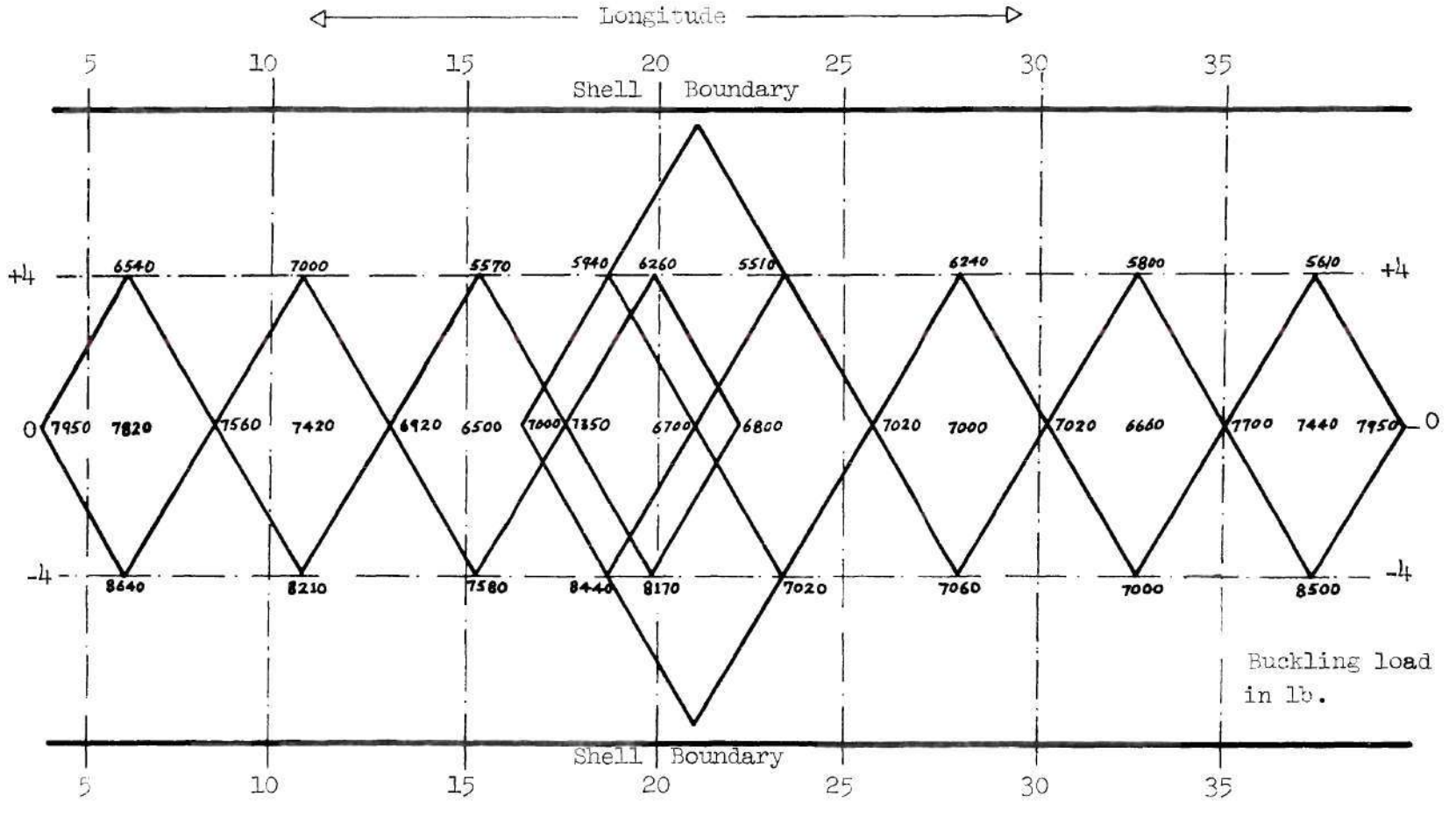

Figure 18. Predicted Buckling Load Values at Various Stations of the Spiral Stiffened Shell.

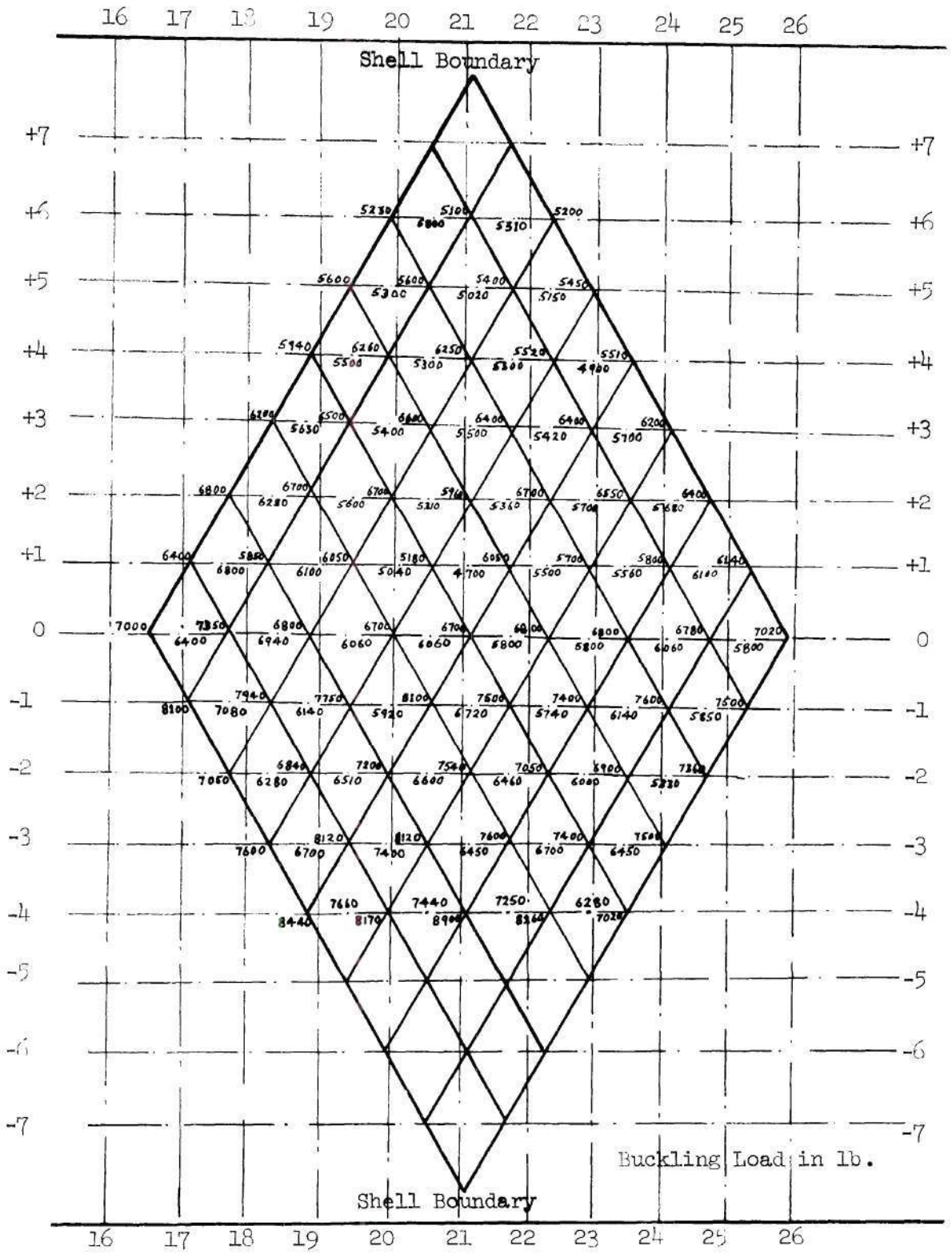

Figure 19. Predicted Buckling Load Values at Various Stations of the Weakest Region of the Spiral Stiffened Shell.

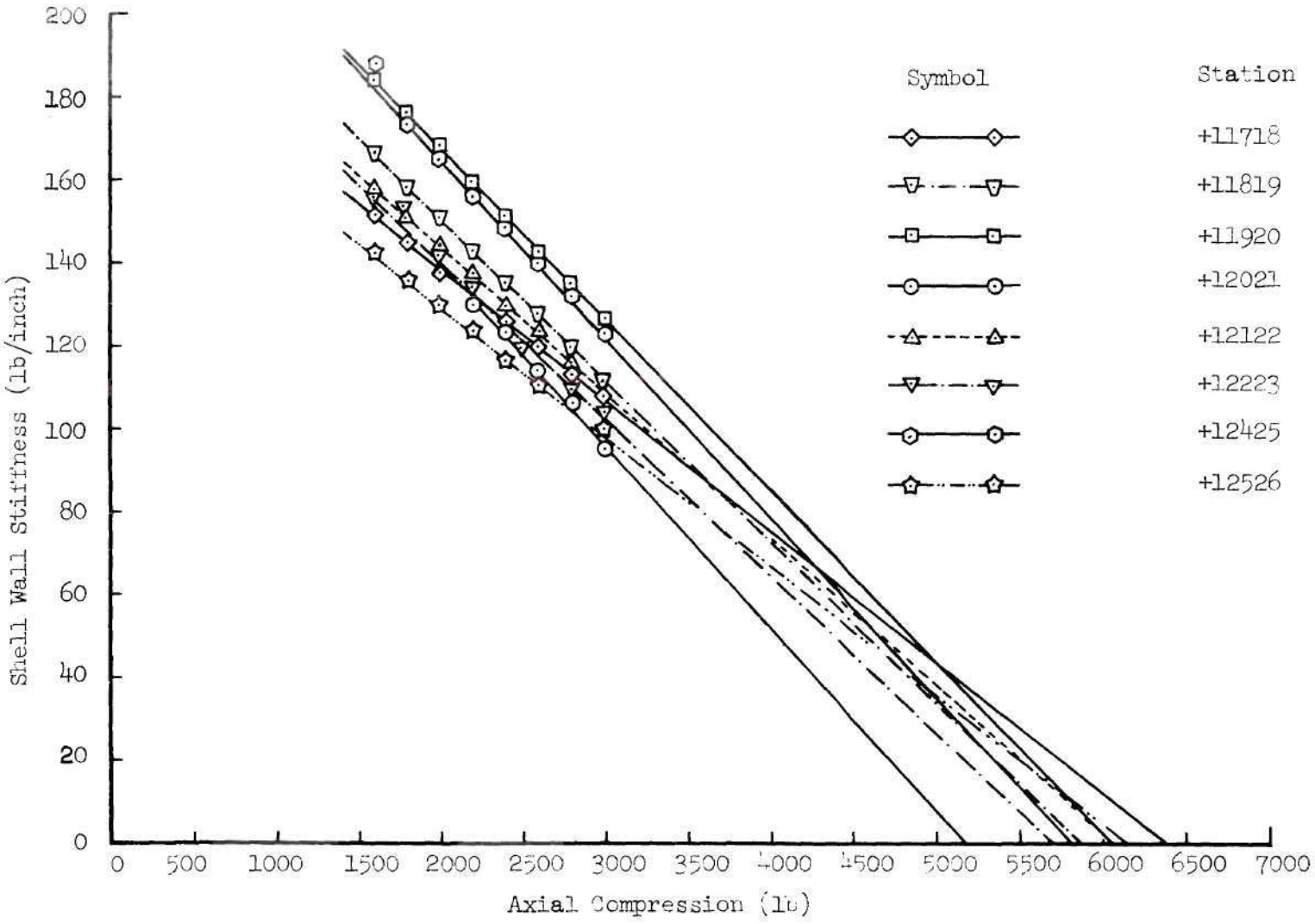

Figure 20. Stiffness-Axial Load Plots at the Diamond Vertices on +1 Latitudinal Plane of the Spiral Stiffened Shell.

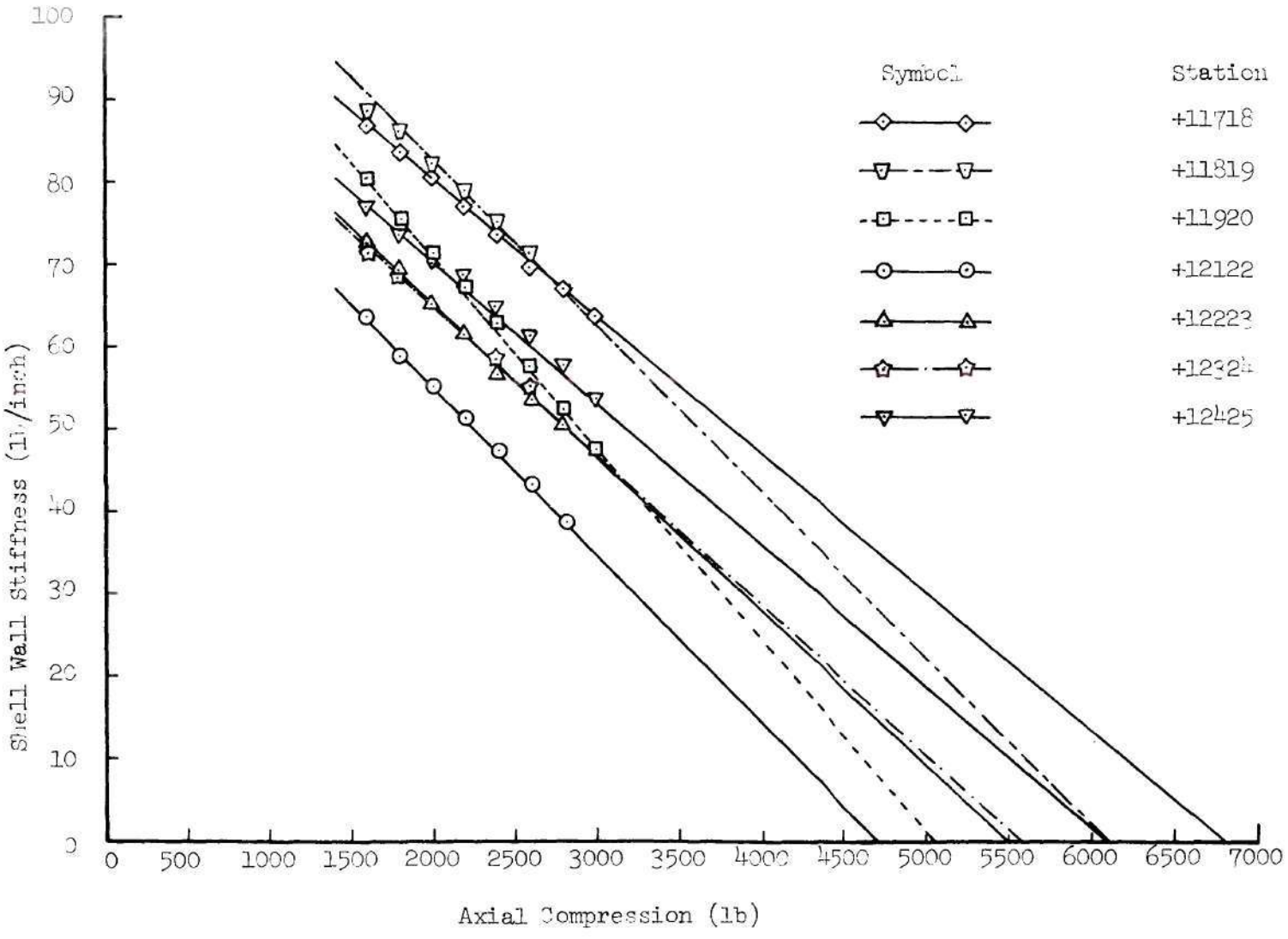

Figure 21. Stiffness-Axial Load Plots at the Diamond Centers on +1 Latitudinal Plane of the Spiral Stiffened Shell.

center is identified by a five digit code. The first digit with appropriate sign denotes the latitude and the last four digits represents the two longitudes between which the diamond vertex or diamond center is located.

The minimum values of the buckling load predicted from Figures 20 and 21 are 5180 pounds and 4700 pounds, respectively. The actual value of the failing load determined by loading the shell to instability was 3400 pounds. The disagreement between the actual buckling load and the predicted buckling load is so large that it is unlikely to be due to errors in observations. The discrepancy seems to be due to the reason that imperfection caused by lateral load is not of the same nature as the buckling pattern formed under compressive load.

The predicted and actual values of the buckling loads of these six cylindrical shell specimens are given in Table 4.

Table 4. Summary of Tests on Cylindrical Shells.

Specimen Number	Shell Construction	Level of Side Force Used (Grams)	Predicted Buckling Load (lb)	Actual Buckling Load (lb)	% Error	Remark
1	Unstiffened Circular	200	1390	1375	+1.1	Buckled Elastically
2	Stringer Stiffened Circular	200 & 500*	1060	1080	-1.9	Buckled Elastically
3	Ring and Stringer Stiffened Circular	500	1950	2000	-2.5	Buckled and Cracked
4	Unstiffened Elliptic	75	360	371	-3.0	Buckled Elastically
5	Unstiffened Elliptic With A Cutout	75	180	191	-5.8	Buckled Elastically
6	Spiral Stiffened Circular	600	4700	3400	+38.2	Buckled and Cracked

* The differential stiffness was measured in this case

CHAPTER IV

ANALYSIS OF A SPIRAL STIFFENED SHELL

In the preceding chapter the results of a study on a specific symmetrical spiral stiffened shell under uniform axial compression were presented. The critical load predicted by the wall stiffness variation method was 4700 pounds if the stiffnesses were measured at the center of a diamond and 5180 pounds when the measurement point was a stiffeners intersection point. In both cases the stiffness-axial load plots from which these predictions were made were of high quality. In fact, they were among the best obtained in the whole test program. However, neither result is close to the actual failing load of 3400 pounds. The opinion has been expressed that the discrepancy is due to the fact that the buckle shape and the imperfection shape, caused by the lateral force, were different. One cannot, however, ignore the fact that due to the fabrication difficulties the joints at the meets of the stiffeners may not be ideal and as a consequence may cause a stress concentration and thus a reduction in load carrying capability. Visual inspection prior to and during the test did not reveal any difficulty in this field. Thus, to be more certain that the previous conclusion is substantially valid a detailed analysis of the shell was carried out.

This analysis is based upon the theoretical solution published by Soong (80). It takes the smeared thickness approach and

includes the effects of stiffener eccentricities which were promulgated by Baruch and Singer (81). It assumes that the buckle pattern is of a diamond kind. Comparison between the buckling loads determined from this analysis and the test results achieved by Meyer (82) on 45° waffle stiffened cylinders was made by Soong. The agreement is good and the average value of the ratio of Meyer's test results to the Soong's theoretical analysis is 0.96. We feel confident, therefore, that the theoretical buckling load for the shell tested in this program should be in reasonable agreement with the actual failing load unless, some serious reduction occurred due to local effects at the stiffener joints. Such effects were absent from the specimens tested by Meyer since those specimens were machined from a thick body.

The analysis indicates that a buckling load of 3215 pounds should be anticipated. This is in excellent accord with the test established value of 3400 pounds. The ratio of the actual buckling load value to the theoretical value is 1.06. We feel confident, therefore, that the explanation given for the fact that the stiffness method indicated a higher value than achieved is probably correct.

In making the above referenced analysis a thorough study of Soong's (80) work was done. It was determined that the analysis contained several errors. These errors were of no significance for symmetrical spirals, and thus in no way reflect upon the comparison with Meyer's test data. However, they have been corrected and the corrected values are given in Appendix B.

It is felt that the tests outlined in the previous chapter and the strong analytical support given above are ample evidence that

the stiffness method can not be directly used with all kinds of structures and/or loading. We suggest that this issue is worthy for a more detailed study. For this study we believe that the compressed shells subjected to internal and external pressure would be the ideal media. In such loading environment there is a distinct change in buckle pattern as is evident from the work of Horton and Durham (76). The deformation patterns due to normal force are also at variance with these shapes.

CHAPTER V

APPROXIMATIONS TO STRUCTURAL PROBLEMS UTILIZING RATIONAL FUNCTION TECHNIQUE

Horton (83) recently pointed out that many engineering solutions are expressed in terms of the sums of an infinite series. Such expressions are inconvenient due to the fact that they converge slowly and thus the sum to a sufficiently large number of terms can present computational difficulty. However, in certain cases the infinite series can, if the coefficients are properly adjusted, be adequately represented by a rational function. The discrepancy between the real sum of 'n' terms of the infinite series and the rational function value is relatively small. This is well illustrated by Newmark's (84) approximation for the instability load of an elastically restrained column, and by Gregory (73) in the solution of an eccentrically loaded column. Rational functions, being the quotient of two polynomials, are unique in the fact that infinite values of the dependent variable can exist for finite values of the independent variable. On the other hand such functions can remain finite when the independent variable has values extending over an infinite range. These properties form the basis of many useful approximations to various kinds of engineering problems. For example, all eigenvalues for elastically restrained columns are finite but the end fixity parameter can range from zero to infinity. It would, thus, seem reasonable to expect that

a rational function approach might have significance in deriving approximations for buckling loads and vibrational frequencies of the said column in terms of the end fixity parameters. It should also be noted that similar conclusions apply to the displacement function as well. Thus we are led to the thought that a study of rational function use in connection with displacement, instability and vibrational behavior of a column might lead to useful results. Such results could be of value to the practical engineer in that they should simplify his computational work and to the test engineer in that they might lead to simple relationships between different behavioral patterns. This then is the motivation for the studies reported in this chapter.

Transcendental Functions

From a classical point of view the determination of the value of any transcendental function is a straightforward matter. However, their presence in most structural problems demand a great deal of computational time. Berry functions (85) encountered in the solution of beam column problems, could possibly be simplified if we could derive good approximations to the transcendental functions. As an example of what can be done in this regard, we examine the quantity 'q'

$$q = \left\{ \frac{\tan\left[\frac{\pi}{2}\sqrt{\frac{P}{Q}}\right]}{\frac{\pi}{2}\sqrt{\frac{P}{Q}}} - 1 \right\} \qquad (15)$$

$$0 \leq P \leq Q$$

This particular transcendental function occurs in various problems associated with laterally loaded columns. For example, the deflection 'w' at the center of a simply supported column with a lateral load 'N' at the midspan is

$$w = \frac{NL}{2\lambda P} \tan \frac{\lambda}{2} - \frac{NL}{4P} \tag{16}$$

where P is the compressive load applied to the column of length L, and

$$\lambda = \sqrt{\frac{PL^2}{EI}} \tag{17}$$

E and I having their usual significance. Since the critical load for a simply supported column is given by

$$Q = P_{cr} = \frac{\pi^2 EI}{L^2} \tag{18}$$

we can rewrite equation (16) as

$$w = \frac{NL}{4P} \left\{ \frac{\tan \left[\frac{\pi}{2} \sqrt{\frac{P}{Q}} \right]}{\frac{\pi}{2} \sqrt{\frac{P}{Q}}} - 1 \right\} \tag{19}$$

$$= \frac{NL}{4P} \cdot q$$

We now seek an approximate solution to the quantity q, defined by equation (15), in terms of P/Q. For the purpose of the argument we shall assume that q can be represented by the rational function - viz,

$$q = \frac{a\frac{P}{Q} + b}{c\frac{P}{Q} + 1} \tag{20}$$

We know that when P/Q = 0, q = 0, and thus we establish b = 0. Furthermore when P/Q = 1, q = ∞ and we have c = -1. The rational function can therefore be written

$$q = \frac{a\frac{P}{Q}}{1 - \frac{P}{Q}} \tag{21}$$

We then require to match at one further point to derive the value of 'a'. We shall choose, for convenience, P/Q = 1/4 as the matching condition. When this is done we have, a = 0.8197. Hence the approximation we seek is

$$q = \frac{0.8197\ (P/Q)}{1 - (P/Q)} \tag{22}$$

It should be noted that there was no particularly strong reason to choose the matching point at P/Q = 1/4. We can, for example, equally well choose P/Q = 1/9 which gives a = 0.8213, or on the other hand, the

matching condition $P/Q = 0.89$ gives $a = 0.81303$. It is clear from these calculations that the value of 'a' is virtually independent of the ordinate of the matching point. Hence, the expression

$$q = \frac{.82 \frac{P}{Q}}{1 - \frac{P}{Q}} \tag{23}$$

is an excellent approximation to the transcendental equation over the whole range of P/Q ($0 \leq P/Q \leq 1$).

Thus, the deflection function defined in equation (19) can be expressed as

$$w = \left\{ \frac{.82(P/Q)}{1 - (P/Q)} \right\} \frac{NL}{4P} \tag{24}$$

or

$$w = \frac{NL^3}{48.1\ EI} \left[\frac{1}{1 - (P/Q)} \right], \tag{25}$$

a formula which agrees well with the classic expression as, for example, derived by Salmon (86). He expanded the 'tangent' and then replaced it by geometric progression. This is an infinitely more complex procedure.

Generally speaking, however, the degree of approximation is dependent upon the matching point or points chosen. Unfortunately, the state of knowledge in the subject of rational functions and/or rational

function approximation is such that no hard and fast, infallible rules for choice of matching points can be given. To a large degree, therefore, we need to operate on a trial and error basis, choosing certain matching points, deriving an approximate expression and checking the agreement between exact and approximate values until we have achieved the desired degree of accuracy. This is elucidated by deriving an approximation for $\sec[1/2\ \pi \sqrt{P/Q}]$. Two of the three constants in this rational function approximation are obtained by matching at $P/Q = 0$ and $P/Q = 1$, the extreme points. A number of rational function expressions are obtained by choosing different third matching condition. The maximum positive and negative errors involved in these expressions against the corresponding third matching value of P/Q are plotted in Figure 22. It is seen from this plot that the rational expression corresponding to the third matching point of $P/Q = 0.81$ gives equal value of positive and negative errors. The approximate formula so determined is then the approximation to $\sec[1/2\ \pi \sqrt{P/Q}]$.

However, it is not at all certain that we shall be able to achieve the desired degree of accuracy from a rational function which has both numerator and denominator of the first degree. In fact, it is not necessary that they even be of the same degree. Of course, the higher the degree of the polynomials in the rational function the greater the number of matching points needed to evaluate the constants. We can illustrate this point readily by determining a rational function approximation for the function $\tan[1/2\ \pi \sqrt{P/Q}]$, $0 < (P/Q) < 1$. Let

The best rational function approximation for $\sec(\frac{1}{2}\pi\sqrt{P/Q})$ is obtained when the third matching condition is chosen at P/Q = 0.81.

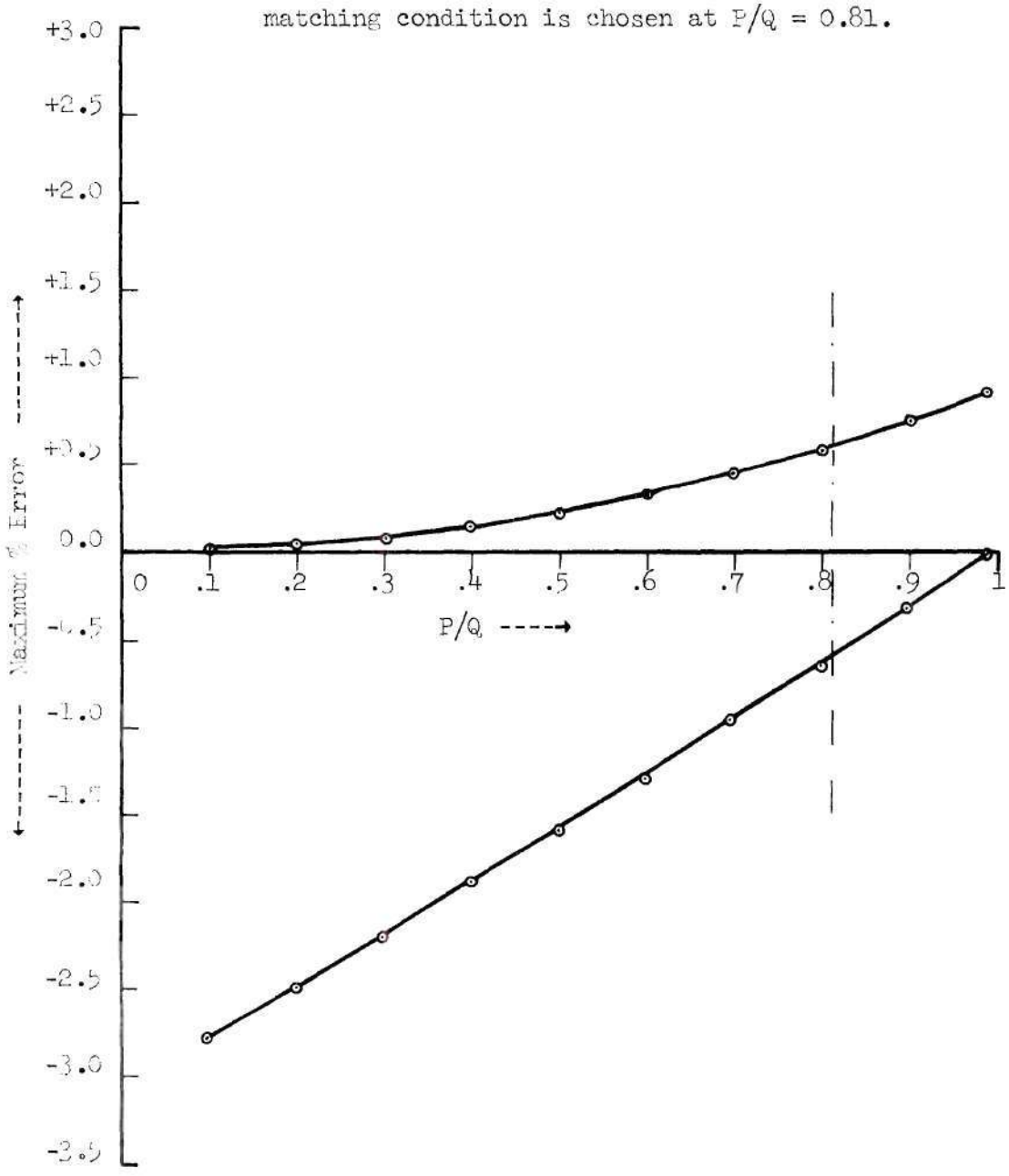

Figure 22. Maximum Percentage Error With Third Matching Point.

us suppose that

$$\tan\left[1/2\ \pi\ \sqrt{P/Q}\right] \cong \frac{a(P/Q) + b}{c(P/Q) + 1} \tag{26}$$

Now when $P/Q = 0$, $\tan[1/2\pi\ \sqrt{P/Q}] = 0$ and so $b = 0$. When $P/Q = 1$ then the function $\tan[1/2\ \pi\ \sqrt{P/Q}] = \infty$ and we establish $c = -1$. If we choose, again in this case, the third matching point at $P/Q = 1/4$ we obtain $a = 3$. Thus our linear polynomials rational function approximation becomes

$$\tan\left[1/2\pi\ \sqrt{P/Q}\right] = \frac{3(P/Q)}{1-(P/Q)} \tag{27}$$

If we had chosen instead to match at $P/Q = 1/9$ then 'a' would have the value 4.6188, which differs appreciably from that previously ascertained. It is a relatively simple numerical task to demonstrate that no matter where we choose the matching point for a linear polynomial rational function approximation, we do not get a good approximation for the function $\tan[1/2\ \pi\ \sqrt{P/Q}]$.

Turning back, however, to our previous example (equation (22)) we can find a simple, accurate approximation for $\tan\left[1/2\pi\ \sqrt{P/Q}\right]$. Hence,

$$q = \frac{\tan[1/2\ \pi\sqrt{P/Q}]}{1/2\ \pi\ \sqrt{P/Q}} - 1 \cong \frac{.8197\ (P/Q)}{1 - (P/Q)} \tag{28}$$

and so,

$$\tan[1/2\pi \sqrt{P/Q}] \simeq 1/2\pi \sqrt{P/Q} \left\{\frac{1 - .1803(P/Q)}{1 - (P/Q)}\right\} \qquad (29)$$

or

$$\tan[\pi/2 \sqrt{P/Q}] \simeq 1/2\pi \sqrt{P/Q} \left\{\frac{1 - (4/21)(P/Q)}{1 - (P/Q)}\right\} \qquad (30)$$

Here the degree of polynomial in the numerator differs from that in the denominator. The expression is an excellent approximation over the range $0 \leq (P/Q) \leq 1$. This fact is illustrated in Table 5, where the exact and approximate values are compared.

Listed in Table 6 are a number of rational function approximations for transcendental functions which frequently occur in structural analysis. The degree of error involved in each case is clearly indicated.

Stability of Columns

The critical load for a column with extreme cases of boundary conditions, i. e., pinned, fixed etc. is easily ascertained (85). This is not true for columns with boundary conditions which deviate from the ideal ones viz, columns with partial restraints at its ends. The characteristic equations which define the various eigenvalues of partially restrained columns can be readily established. However, these equations are, at best, transcendental and a closed form solution is not possible. Graphical and numerical solutions are among a few popular methods used to solve

Table 5. Accuracy of $\tan\left[\frac{\pi}{2}\sqrt{\frac{P}{Q}}\right] = \frac{\pi}{2}\sqrt{\frac{P}{Q}}\left\{\frac{1-\frac{4}{21}\frac{P}{Q}}{1-(P/Q)}\right\}$.

P/Q	$\tan\{\frac{\pi}{2}\sqrt{\frac{P}{Q}}\}$	$\frac{\pi}{2}\sqrt{\frac{P}{Q}}\ \{\frac{1-\frac{4}{21}(\frac{P}{Q})}{1-(P/Q)}\}$	% Error (ϵ)
0	0	0	0
0.005	0.111531	0.111524	-0.006
0.05	0.366435	0.366206	-0.063
0.10	0.542063	0.541408	-0.121
0.25	1.0000	0.99733	-0.267
0.5	2.01799	2.00987	-0.402
0.75	4.68141	4.66405	-0.371
0.9	12.3786	12.3472	-0.253
0.99	126.985	126.82	-0.130
1.00	∞	∞	0.000
	Maximum Error		
0.59	2.6229	2.61209	-0.412

Table 6. Transcendental Functions - Approximate Formulae.

Function	Matching Points	Approximate Formula	Maximum % Error (ε_m)
$\sin\{\frac{\pi}{2}\sqrt{\frac{P}{Q}}\}$	$P/Q = 0, .16, 1$	$\frac{\pi}{2}\sqrt{\frac{P}{Q}}\{\frac{15-4.18\frac{P}{Q}}{15+2\frac{P}{Q}}\}$	-0.0196 at $\frac{P}{Q} = .99$ $+0.0300$ at $\frac{P}{Q} = .70$
$\cos\frac{\pi}{2}\sqrt{\frac{P}{Q}}$	$P/Q = 0, .81, 1$	$\{\frac{1 - P/Q}{1 + \frac{4}{15}(\frac{P}{Q})}\}$	-0.665 at $\frac{P}{Q} = 0.41$ $+0.473$ at $\frac{P}{Q} = 0.994$
$\tan\{\frac{\pi}{2}\sqrt{\frac{P}{Q}}\}$	$P/Q = 0, .53, 1$	$\frac{\pi}{2}\sqrt{\frac{P}{Q}}\{\frac{1-\frac{4}{21}(\frac{P}{Q})}{1 - P/Q}\}$	-0.412 at $\frac{P}{Q} = .59$ $+0.000$ ---------
$\cot\{\frac{\pi}{2}\sqrt{\frac{P}{Q}}\}$	$P/Q = 0, .53, 1$	$\{\frac{1}{\frac{\pi}{2}\sqrt{\frac{P}{Q}}}\}\{\frac{1 - P/Q}{1-\frac{4}{21}(\frac{P}{Q})}\}$	-0.000 --------- $+0.414$ at $\frac{P}{Q} = .59$
$\sec\{\frac{\pi}{2}\sqrt{\frac{P}{Q}}\}$	$P/Q = 0, .81, 1$	$\{\frac{1 + \frac{4}{15}(\frac{P}{Q})}{1 - P/Q}\}$	-0.471 at $\frac{P}{Q} = .994$ $+0.670$ at $\frac{P}{Q} = .41$
$\mathrm{cosec}\{\frac{\pi}{2}\sqrt{\frac{P}{Q}}\}$	$P/Q = 0, .16, 1$	$\frac{1}{\frac{\pi}{2}\sqrt{\frac{P}{Q}}}\{\frac{15+2(\frac{P}{Q})}{15-4.18(\frac{P}{Q})}\}$	-0.0300 at $\frac{P}{Q} = .7$ $+0.0196$ at $\frac{P}{Q} = .99$

these characteristic equations for the particular values of the boundary restrain parameters. The Southwell plot (7,15) is in common use by the experimentalists to evaluate the critical load for columns. Horton, et al. (18, 87) proposed a simple, practical method for the experimental determination of the critical load of a realistic column. They discovered that the product of the critical load and the maximum value of the flexibility coefficient, determined by applying a point lateral load between 3/8 and 5/8 of the span of the column, is constant for all practical purposes and is given by $\pi^2 L/48$.

However, these methods are tedious and impractical to determine the critical loads for a family of columns for which the end restraint parameters vary over an infinite range. We can establish a very simple relationship between the critical load and the boundary fixity parameters by using the rational function method. To fix the ideas, we consider a uniform EI column of length L and with equal end rotational restraints of value $\beta EI/L$. The governing characteristic equation for the instability, derived in Appendix C, is

$$\tan \frac{\lambda}{2} + \frac{\lambda}{\beta} = 0 \qquad (31)$$

where $\lambda = \sqrt{P_{cr} L^2/EI}$, P_{cr} being the critical axial compressive force and EI having the normal significance.

If we allow β to vary between zero and infinity (i. e., we consider all columns from simply supported to clamped boundaries), we can readily compute the value of λ corresponding to any specific value

of β. Nevertheless, we certainly cannot derive a general expression for critical load in terms of the boundary restraint parameter β. We, however, can express the critical load parameter λ in terms of the boundary restraint parameter β by a rational function of the form

$$\lambda = \frac{a\,\beta + b}{c\,\beta + 1} \tag{32}$$

Here, in fact, we have an example of the second class of rational functions previously defined, namely, "... the function can remain finite when the independent variable has values extending over an infinite range." Here the eigenvalue is always finite and varies between π and 2π as the boundary restraint parameter varies between zero and infinity.

We know that when $\beta = 0$, $\lambda = \pi$ and so $b = \pi$; similarly when $\beta = \infty$, $\lambda = 2\pi$ and thus $a/c = 2\pi$. For our third matching point we choose the value of β which corresponds to a value of $\lambda = 3\pi/2$ and this is readily seen to be as $\beta = 3\pi/2$, and we determine the value $c = 2/3\pi$. Hence,

$$\lambda = \left\{ \frac{4\beta + 3\pi}{2\beta + 3\pi} \right\} \pi \tag{33}$$

Therefore, the critical load for a column which has equal rotational restraints ($\beta EI/L$) at its ends is given by

$$P_{cr} = \left\{ \frac{4\beta + 3\pi}{2\beta + 3\pi} \right\}^2 \cdot \frac{\pi^2 EI}{L^2} , \qquad (34)$$

Numerical evaluation, summarized in Table 7, shows that this is an excellent formula. It is slightly more accurate (by one percent) than the expression

$$P_{cr} = \left\{ \frac{4\beta + \pi^2}{2\beta + \pi^2} \right\}^2 \cdot \frac{\pi^2 EI}{L^2} \qquad (35)$$

which Newmark (84) obtained by other means. Table 8 lists similar simple formulae for many other cases of column stability (the corresponding characteristic equations are given in Appendix C). The errors involved in these approximations are negligible for all practical purposes. In all these formulae given, however, it is to be noted that for the sake of computational simplicity in their use, the constants have been rounded off. The errors stated are based upon these rounded off figures and not upon the exact values which are determined when the constants are computed using the matching points stated in the table.

Geometric Mean Property of Rotationally Restrained Columns

At this juncture it is expedient to point out that if P_{11} is the critical load for a column with equal end fixity parameters (β_1, β_1), P_{22} the critical load corresponding to the end fixity parameters

Table 7. Accuracy of $\frac{P_{cr}L^2}{EI} = \pi^2 \left\{\frac{4\beta+3\pi}{2\beta+3\pi}\right\}^2$

β	$\left\{\frac{P_{cr}L^2}{EI}\right\}_{exact}$	$\left\{\frac{4\beta + 3\pi}{2\beta + 3\pi}\right\}^2 \pi^2$	% Error (ϵ)
0	9.8696	9.8696	0.000
.1	10.2656	10.284	0.180
.2	10.6536	10.6896	0.338
.5	11.7719	11.8539	0.697
1	13.4924	13.6276	1.002
2	16.4634	16.6272	0.995
5	22.6699	22.6471	-0.100
10	28.1677	27.846	-1.142
20	32.7819	32.3091	-1.442
50	36.5136	36.1513	-0.992
100	37.9473	37.7217	-0.595
10000	39.4626	39.4597	-0.007
	Maximum Error		
18.2	32.2435	31.7763	-1.449
1.4	14.7509	14.9085	+1.068

Table 8. Stability of Columns - Approximate Formulae.

Case	Matching Points	Approximate Formula	Maximum % Error (ϵ_m)
One end simply supported 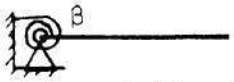	$\beta = 0, \frac{\pi}{4}, \infty$	$P_{cr} = \{\frac{\beta}{4\beta+3\pi}\}\frac{\pi^2 EI}{L^2}$	-2.904 at β=3.9* +3.826 at β=0.1
with rotational restraint (β); other end free.	β = 0, small, $\pi/6\sqrt{3}$, $\pi/\sqrt{3}$, ∞	$P_{cr} = \{\frac{\beta^2+3\beta}{4\beta^2+2\pi^2\beta+3\pi^2}\} \cdot \frac{\pi^2 EI}{L^2}$	-0.023 at β=0.8** +0.228 at β=10
Both ends simply supported 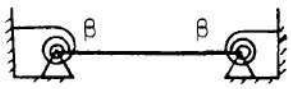	$\beta = 0, \frac{3\pi}{2}, \infty$	$P_{cr} = \{\frac{4\beta+3\pi}{2\beta+3\pi}\}\frac{\pi^2 EI}{L^2}$	-1.449 at β=18.2 +1.068 at β=1.4
with equal rotational restraints β.	β = 0, 1.5, 6, 20, ∞	$P_{cr} = \{\frac{4\beta^2+36\beta+57}{\beta^2+13\beta+57}\} \cdot \frac{\pi^2 EI}{L^2}$	-0.256 at β=10 +0.000
Both ends simply supported 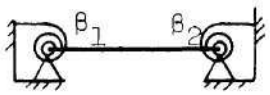	By geometric mean property	$P_{cr} = (\frac{4\beta_1+3\pi}{2\beta_1+3\pi}) \cdot (\frac{4\beta_2+3\pi}{2\beta_2+3\pi}) \frac{\pi^2 EI}{L^2}$	-3.059 at β_1=16.3, β_2=0 +1.777 at β_1=2.4, $\beta_2 = \infty$
with unequal rotational restraints β_1, β_2.	By geometric mean property	$P_{cr} = (\frac{2\beta_1^2+32\beta_1+70}{\beta_1^2+18\beta_1+70}) \cdot (\frac{2\beta_2^2+32\beta_2+70}{\beta_2^2+18\beta_2+70}) \frac{\pi^2 EI}{L^2}$	-2.581 at β_1=12, β_2=0 +1.302 at β_1=2.8, $\beta_2 = \infty$

* Error evaluated for $0.1 \leq \beta \leq \infty$, values below β=0.1 are impractical

** Error evaluated for $0 \leq \beta \leq \infty$

Table 8. Continued.

Case	Matching Points	Approximate Formula	Maximum % Error (ε_m)
One end fixed, 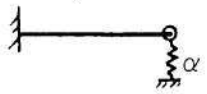 other with Lateral Restraint α.	$\alpha=0,4,15,45,\infty$	$P_{cr}=\left\{\frac{6.15\alpha^2+79\alpha+243}{3\alpha^2+33\alpha+972}\right\}\cdot\frac{\pi^2EI}{L^2}$	-2.109 at $\alpha=24.6$ +2.145 at $\alpha=8.5$
One end free, other end fixed, load applied 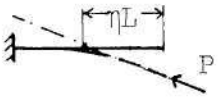 $0\le\eta\le1$ to pass through a fixed point on the column axis, between the two ends of column.	$\eta=0,.4,.75,.92,1$	$P_{cr}=\left\{\frac{80\eta^2-173\eta+96}{36\eta^2-80\eta+47}\right\}\cdot\frac{\pi^2EI}{L^2}$	-3.437 at $\eta=0.58$ +3.587 at $\eta=0.93$ -0.465 at $\eta=0.59$ +0.281 at $\eta=0.86$
One end free, other end fixed Load applied  $1\le\eta\le\infty$ to pass through a fixed point on the column axis, away from fixed end.	$\eta=1,\ \frac{4+3\pi}{3\pi},\infty$ $\eta=1,1.1,1.4,2,\infty$	$P_{cr}=\left\{\frac{5\eta+1}{20\eta-14}\right\}\frac{\pi^2EI}{L^2}$ $P_{cr}=\left\{\frac{88\eta^2-65\eta+2}{352\eta^2-544\eta+217}\right\}\cdot(\pi^2EI)/L^2$	-2.192 at $\eta=1.12$ +1.787 at $\eta=2.76$ -0.0358 at $\eta=5.1$ +0.0609 at $\eta=1.04$

Table 8. Continued.

Case	Matching Points	Approximate Formula	Maximum % Error (ϵ_m)
Both ends 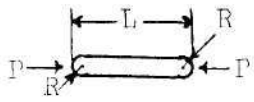 rounded $\xi=(L/2R)$.	$\xi=0,1,3,10,\infty$	$P_{cr}=\{\frac{3\xi^2+8\xi+40}{3\xi^2+3\xi+10}\}\frac{\pi^2 EI}{L^2}$	-0.953 at $\xi=1.79$ +1.886 at $\xi=0.42$
One end simply supported, other end attached to 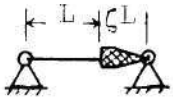 a rigid body whose far end is simply supported .	$\zeta=0,\frac{4}{3\pi},\infty$	$P_{cr}=\{\frac{5\zeta+6}{20\zeta+6}\}\frac{\pi^2 EI}{L^2}$	-2.192 at $\zeta=0.12$ +1.787 at $\zeta=1.76$
	$\zeta=0,2\sqrt{3}/5\pi$, $4/3\pi,3\sqrt{3}/2\pi$, and ∞	$P_{cr}=\{\frac{4\zeta^2+5\zeta+1}{16\zeta^2+7\zeta+1}\}\frac{\pi^2 EI}{L^2}$	-0.419 at $\zeta=0.22$ +0.020 at $\zeta=4.32$
Cantilever Tapered Column $I_x=I_1(x/a)^n$ I_1 = Moment of Inertia at the Smaller End of Column I_2 = Moment of Inertia at the Larger End of Column $\Lambda = I_1/I_2$ $\{\frac{1}{100} \le \Lambda \le 1\}$.			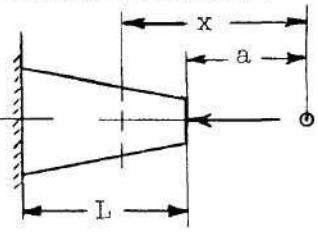
n = 2	$\Lambda=.01,.04,$ $.1,.35,1.$	$P_{cr}=\{\frac{90\Lambda^2+40\Lambda+0.7}{23\Lambda^2+29\Lambda+1}\}\cdot\frac{EI_2}{L^2}$	-0.672 at $\Lambda=.015$ +0.564 at $\Lambda=.07$
n = 4	$\Lambda=.01,.03,$ $.1,.35,1.$	$P_{cr}=\{\frac{126\Lambda^2+39\Lambda+0.31}{34\Lambda^2+32\Lambda+1}\}\cdot\frac{EI_2}{L^2}$	-0.688 at $\Lambda=.015$ +0.603 at $\Lambda=.64$

(β_2, β_2) and P_{12} is the critical load corresponding to (β_1, β_2), then P_{12} is very nearly the geometric mean of P_{11} and P_{22}, i. e.,

$$P_{12} = \sqrt{P_{11} \cdot P_{22}} \tag{36}$$

This simple, useful fact has been used to establish the formulae which involve unequal end rotational restraint parameters (83). The errors in this approximation are small and illustrated in Table 9.

Stability of Frameworks

As we have emphasized in the previous section, columns in a structural framework are never pinned at their ends, but fixed in some way to other members of the structure. Rotation of the column ends are, thus, restrained by the other members which meet at the joint. These restraints call into play end moments. Therefore, when dealing with the stability of frameworks which consists of an assemblage of members, the analysis centers around the behavior of an element with applied end moments. A detailed treatment of the subject is given in reference (73) and reference (88). It is clearly seen that there are two stability functions 'S' and 'SC' which are of significance in the stability analysis of frameworks. These functions are as follows; for compression,

$$S = \{\frac{(1-\lambda\cot\lambda)\,\lambda/2}{\tan\,\lambda/2 - \lambda/2}\} \tag{37}$$

Table 9. Accuracy of $P_{12} = \sqrt{P_{11} \cdot P_{22}}$

Errors in Percent (ε)

β_2 / β_1	0	.1	.2	.5	1	2	5	10	20	50	100	1000	10000
0	0	-0.009	-0.035	-0.176	-0.504	-1.143	-2.087	-2.359	-2.335	-2.264	-2.245	-2.235	-2.236
.1		0	-0.008	-0.104	-0.375	-0.942	-1.794	-2.012	-1.947	-1.844	-1.812	-1.791	-1.790
.2			0	-0.054	-0.273	-0.774	-1.541	-1.710	-1.608	-1.475	-1.431	-1.399	-1.396
.5				0	-0.084	-0.415	-0.971	-1.016	-0.823	-0.614	-0.539	-0.476	-0.470
1					0	-0.123	-0.431	-0.340	-0.042	0.258	0.370	0.471	0.480
2						0	-0.055	0.150	0.539	0.928	1.081	1.223	1.237
5							0	0.120	0.441	0.817	0.978	1.136	1.152
10								0	0.106	0.335	0.450	0.570	0.583
20			Symmetric						0	0.067	0.124	0.194	0.202
50										0	0.009	0.034	0.037
100											0	0.008	0.010
1000												0	0
10000													0

Maximum % Error

-2.368 when $\beta_1 = 0$, $\beta_2 = 12$

+1.369 when $\beta_1 = \infty$, $\beta_2 = 2.9$

$$C = \frac{\lambda \operatorname{cosec} \lambda - 1}{1 - \lambda \cot \lambda}$$

and for tension,

$$S = \frac{\lambda(\lambda \coth \lambda - 1)}{\lambda + 2(\operatorname{cosech} \lambda - \coth \lambda)} \tag{38}$$

$$C = \frac{1 - \lambda \operatorname{cosech} \lambda}{\lambda \coth \lambda - 1}$$

Livesley and Chandler (88) have tabulated these functions. However, they can be conveniently represented by rational function form as given in Table 10. The errors involved in various approximations are clearly indicated in this table and they are small for all practical purposes.

Instability of a Circular Plate

The closed form solution to the problem of radially symmetrical buckling of a circular plate under radial compressive forces uniformly distributed along the edge of the plate, is easily ascertained for both pinned and rigidly fixed boundary supports. There is, however, no straightforward answer for the critical stress when the circular plate is elastically restrained against rotation all along the edges. The governing characteristic equation is transcendental (89, 90) and involves Bessel functions of the first kind. As such, a closed form

Table 10. Stability of Frameworks - Approximate Formulae.

Stability Function	Matching Points	Approximate Formulae	Maximum % Error (ϵ_m)
S	P/Q = 4, 3.5, 2.045, -1, -20.	$S = \left\{\frac{260.3(P/Q)^2 - 2473(P/Q) + 3970}{9.074(P/Q)^2 - 286.3(P/Q) + 1000}\right\}$ ($4 \leq P/Q \leq -25$)	-2.116 at P/Q = 2.1 +2.613 at P/Q = -8.7
SC	P/Q = 4, 3.7, 2, -2, -30.	$SC = \left\{\frac{42.70(P/Q)^2 - 486\ (P/Q) + 2009}{39.35(P/Q)^2 - 407.4(P/Q) + 1000}\right\}$ ($4 \leq P/Q \leq -50$)	-1.153 at P/Q = -11 +1.007 at P/Q = 3.99

solution for critical radial pressure in terms of the degree of edge restraint parameter is not feasible. However, we can seek an approximate solution of the problem by the rational function method. The stability criterion (90) for the rotationally symmetric buckling mode is

$$a\sqrt{(h\sigma_r/D)}\quad J_0\left(a\sqrt{(h\sigma_r)/D}\right) + (\beta-1+\nu)\, J_1\left(a\sqrt{(h\sigma_r)/D}\right) = 0 \quad (39)$$

where a, h and D are the radius, thickness and bending rigidity of the circular plate; σ_r is the radial compressive stress and $\beta = ak/D$ the nondimensional elastic rotational restraint parameter where k being the restraining constant. The critical stress, for convenience, can be written as

$$(\sigma_r)_{cr} = K^* \cdot \frac{D}{ha^2} \quad (40)$$

where $K^* = K^*(\beta)$, i. e., the critical stress may be considered as a function of the degree of constraint along the boundary.

A simple rational function representation for K^* in terms of the boundary restraint parameter β is

$$K^* = \frac{a_1\beta + b_1}{c_1\beta + 1} \quad (41)$$

we choose the three matching conditions to be

(i) $\beta = 0$, $K^* = 4.2$,

(ii) $\beta = 2.6$, $K^* = 8.59$, and

(iii) $\beta = \infty$, $K^* = 14.68$.

The coefficients a_1, b_1, and c_1 can thus be evaluated and after a little algebraic manipulation, we obtain

$$K^* = 4.2 \left[\frac{35\beta + 36}{10\beta + 36}\right] \tag{42}$$

and the critical radial pressure, therefore, becomes

$$[\sigma_r]_{cr} = 4.2 \left\{\frac{35\beta + 36}{10\beta + 36}\right\} \frac{D}{a^2 h} \tag{43}$$

Table 11 shows a comparison between the exact and approximate values of $(\sigma_r)_{cr} \cdot ha^2/D$.

If the circular plate separates an incompressible liquid, the usually occurring rotationally symmetric first buckling mode cannot take place (90). The first buckling mode in this case will be the one corresponding to the usual second buckling mode with a diameter as nodal line. The stability criterion in this case will be

$$[2(\beta+\nu-1) + ha^2\sigma_r/D]J_1[a\sqrt{h\sigma_r/D}] - (\beta+\nu-1)a\sqrt{h\sigma_r/D}\ J_0[a\sqrt{h\sigma_r/D}] = 0 \tag{44}$$

Table 11. Accuracy of $\left\{(\sigma_r)_{cr} \frac{a^2 h}{D}\right\} = 4.2 \left\{\frac{35\beta + 36}{10\beta + 36}\right\}$

β	$\{(\sigma_r)_{cr} \frac{a^2 h}{D}\}$	$4.2\{\frac{35\beta+36}{10\beta+36}\}$	% Error (ϵ)
0	4.2	4.2	0.000
.1	4.44866	4.48378	0.790
.2	4.69097	4.75263	1.314
.5	5.36897	5.48049	2.077
1	6.35322	6.48261	2.037
2	7.88617	7.95	0.809
5	10.4617	10.3047	-1.501
10	12.1725	11.9206	-2.070
20	13.3176	13.0983	-1.647
50	14.1107	13.9948	-0.822
100	14.3923	14.3351	-0.397
∞	14.682	14.7	0.123
	Maximum Error		
9.5	12.0644	11.8145	-2.071
0.7	5.78318	5.9093	+2.181

Here again we can establish the explicit relation between critical stress and the degree of edge restraint parameter β by the rational function method. We arrive at the approximation

$$[\sigma_r]_{cr} = 13.14 \left\{ \frac{10\beta + 24}{5\beta + 24} \right\} \frac{D}{a^2 h} \qquad (45)$$

This formula was obtained by satisfying the three conditions at $\beta = 0$, 4.2 and ∞. The accuracy of this formula is extremely good. The maximum absolute error in this approximation is less than 1.5 percent.

Formulae for the critical radial stress for both cases, (i) when the plate does not separate incompressible liquid and (ii) when the plate separates incompressible liquid, are listed in Table 12.

Torsional Constants

Torsional "constants" associated with the torsion of rectangular and sectorial elements are given by equations involving complicated series summations. For example, the torque carried by a rectangular element as derived in reference (91) is given by the expression

$$M_t = \frac{1}{3} \left\{ 1 - \frac{192}{\pi^5} \cdot \frac{a}{b} \sum_{n=1,3,5,\ldots}^{\infty} \frac{1}{n^5} \tanh \frac{n\pi b}{2a} \right\} G\theta(2b)(2a)^3 \qquad (46)$$

where 2a and 2b are the smaller and larger sides of the rectangular element respectively, θ is the angular twist and M_t is the torque carried by the rectangular element. We write equation (46) in the following simple form;

Table 12. Plate Buckling - Approximate Formulae.

Case	Matching Points	Approximate Formula	Maximum % Error (ϵ_m)
Circular plate, edges S.S. and rotationally restrained (β) 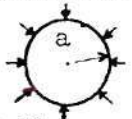 Radius = a Thickness = h $D = Eh^3/\{12(1-\nu^2)\}$	$\beta = 0, 2.6, \infty$	$[\sigma_r]_{cr} = 4.2\{\frac{35\beta+36}{10\beta+36}\}\frac{D}{a^2h}$	-2.071 at $\beta = 9.5$ +2.181 at $\beta = 0.7$
	$\beta = 0, 1.5, 4, 8, \infty$	$[\sigma_r]_{cr} = 4.2\{\frac{7\beta^2+35\beta+35}{2\beta^2+14\beta+35}\}\frac{D}{a^2h}$	-0.286 at $\beta = 4.2$ +0.122 at $\beta = 10000$
Circular plate, as described above but it separates an incompressible liquid, i.e. the first buckling mode is non symmetric	$\beta = 0, 4.2, \infty$	$[\sigma_r]_{cr} = 13.14\{\frac{10\beta+24}{5\beta+24}\}\frac{D}{a^2h}$	-1.301 at $\beta = 16$ +0.969 at $\beta = 1.1$
	$\beta = 0, 1.5, 5, 15, \infty$	$[\sigma_r]_{cr} = 13.14\{\frac{2\beta^2+16\beta+32}{\beta^2+10\beta+32}\}\frac{D}{a^2h}$	-0.386 at $\beta = 21$ +0.137 at $\beta = 1$

$$M_t = K_1 \cdot G\,\theta\,(2b)\cdot(2a)^3 \tag{47}$$

The constant K_1 for different values of b/a can be stated in the simple rational function form. We derive

$$K_1 = \{\frac{72(b/a)-35}{216(b/a)+47}\} \tag{48}$$

by using the three matching conditions at b/a = 1, 1.7, and ∞. The accuracy of this expression is excellent. The maximum absolute error is less than 1.125 percent and is negligible for all practical purposes.

The torsional constants associated with the torsion of the sectorial element involves more complicated series summation. The stress function (91) which defines the twist of a sectorial element is

$$\Phi = \frac{G\theta}{2}\{-r^2(1 - \frac{\cos 2\Psi}{\cos\alpha}) + \frac{16a^2\alpha^2}{\pi^3}\sum_{n=1,3,5\ldots}^{\infty}(-1)^{\frac{n+1}{2}} \tag{49}$$

$$\cdot\,(\frac{r}{a})^{\frac{n\pi}{\alpha}}\,\frac{\cos\,(\frac{n\pi\Psi}{\alpha})}{n(n+\frac{2\alpha}{\pi})(n-\frac{2\alpha}{\pi})}\}$$

where a and α are the radius and angle of the sectorial element respectively. Φ is the stress function and Ψ, r are the polar coordinates. The quation (49) must be substituted in the expression

$$M_t = 2 \int\int \Phi r d\Psi dr \tag{50}$$

to determine the angular twist. We can write, after carrying out the integration, the torque carried by the sectorial element as

$$M_t = K\ G\ a^4\ \theta \tag{51}$$

The infinite series which 'K' represents can be conveniently expressed by a simple formula by using the rational function technique. We do so by writing K in the rational function form as follows;

$$K = \frac{a_1\alpha^2 + b_1\alpha + c_1}{d_1\alpha^2 + f_1\alpha + 1} \tag{52}$$

where α, for convenience, will be taken in degrees. To evaluate the five constants in equation (52), we need five conditions to match. We select the five conditions to be matched at α = 30, 45, 90, 180 and 360 degrees. The values of α below 30 degrees are ignored as the sectorial element is too small to carry any appreciable torque. When this is done, we can write the expression for K, after rounding off the constants, in terms of α as following;

$$K = \left\{\frac{13 \times 10^{-5}\alpha^2 - 33 \times 10^{-4}\alpha + 35 \times 10^{-3}}{56 \times 10^{-7}\alpha^2 + 28 \times 10^{-3}\alpha + 7}\right\} \tag{53}$$

$$(30^\circ \leq \alpha \leq 360^\circ)$$

This formula is accurate within an absolute error of 3/4 percent. The approximate formulae for various torsional constants associated with the rectangular and sectorial elements are listed in Table 13.

Experimental Data

The factual information of engineering is based as frequently upon experimental observation as upon theoretical analysis. Often these experimental data are needed for design purposes. It is convenient for these purposes to have the empirical formulae which express the results of test experience. Rational function approximation can play an important role in this activity. To illustrate, we present in algebraic form the experimental data on stress concentration factors given by Timoshenko (91). The formulae given in Table 14 accurately represents Timoshenko's curves. This is clearly seen in Figures 23 and 24, which show the approximation data superposed upon the Timoshenko's experimental results.

Exponential Forms

Our approach, so far, has been to express the dependent variable in terms of the independent variable by a direct rational function of the type $y = F(x)/\Psi(x)$, where $F(x)$ and $\Psi(x)$ are the polynomials in the independent variable. There are some cases, however, where it is more convenient to adopt an indirect form viz, $y = e^{F(x)/\Psi(x)}$. The choice between a direct rational function or an indirect rational function approximation is influenced by the purpose for which the approximation is desired. For many engineering problems the direct rational function method is preferable from a calculation viewpoint. However, if the

Table 13. Torsional Constants - Approximate Formulae.

Coefficient	Matching Points	Approximate Formula	Maximum % Error (ϵ_m)
(a) Torsion of Rectangular Bars $(1 \le b/a \le \infty)$:			
$K_1 = M_t/\{G\theta(2a)^3 2b\}$	$b/a=1, 1.7, \infty$	$K_1 = \{\frac{72(b/a)-35}{216(b/a)+47}\}$	-1.125 at $b/a=3.45$ +1.051 at $b/a=1.21$
$K_2 = M_t/\{\tau_{max}(2a)^2(2b)\}$	$b/a=1, 3.8, \infty$	$K_2 = \{\frac{15(b/a)-5}{45(b/a)+51}\}$	-0.962 at $b/a=8.6$ +0.988 at $b/a=2.18$
$K = \frac{K_1}{K_2} = \frac{\tau_{max}^m}{2aG\theta}$	$b/a=1, 1.55, 3.5$	$K = \{\frac{25(b/a)-15}{23(b/a)-8}\}$ $(1 \le b/a \le 3.5)$ $= 1 \quad (3.5 \le b/a \le \infty)$	-1.280 at $b/a=1$ +0.882 at $b/a=1.23$
(b) Torsion of Sectorial Bars (α^o):			
$K = M_t/(Ga^4\theta)$ sectorial angle "α" is in degrees	$\alpha=30^o, 45^o, 90^o, 180^o,$ and 360^o	$K = \{\frac{13\times10^{-5}\alpha^2 - 33\times10^{-4}\alpha + 35\times10^{-3}}{56\times10^{-7}\alpha^2 + 28\times10^{-3}\alpha + 7}\}$ $(30^o \le \alpha \le 360^o)$	-0.654 at $\alpha=34.4^o$ +0.691 at $\alpha=270^o$

Table 14. Experimental Data (Stress Concentration Factors) - Approximate Formulae.

Loading	Matching Points	Approximate Formula	Maximum % Error (em)
Tension 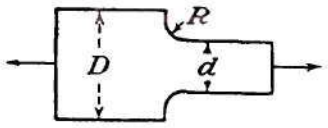	R/d=0.0336,0.2,0.5	$K_t = \{\frac{64(R/d)+12}{52(R/d)+3}\}$ $(0.0336 \leq R/d \leq 0.5)$	-0.704 at R/d=0.5 +0.905 at R/d=0.0425
Bending 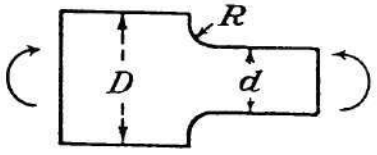	R/d=0.027,0.15,0.5	$K_b = \{\frac{81(R/d)+20}{80(R/d)+8}\}$ $(0.027 \leq R/d \leq 0.5)$	-0.738 at R/d=0.027 +0.592 at R/d=0.5

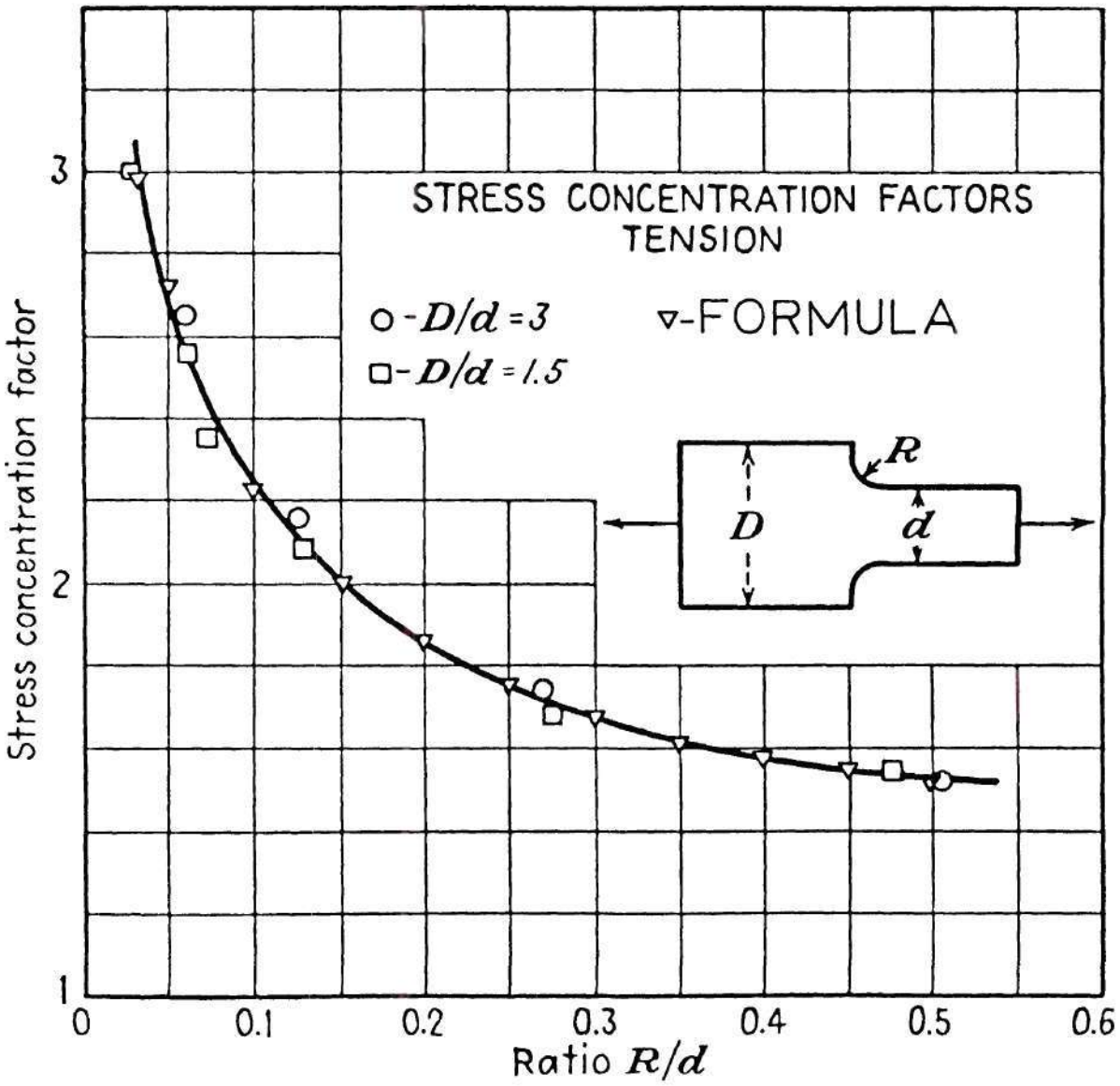

Figure 23. Stress Concentration Factors - Tension.

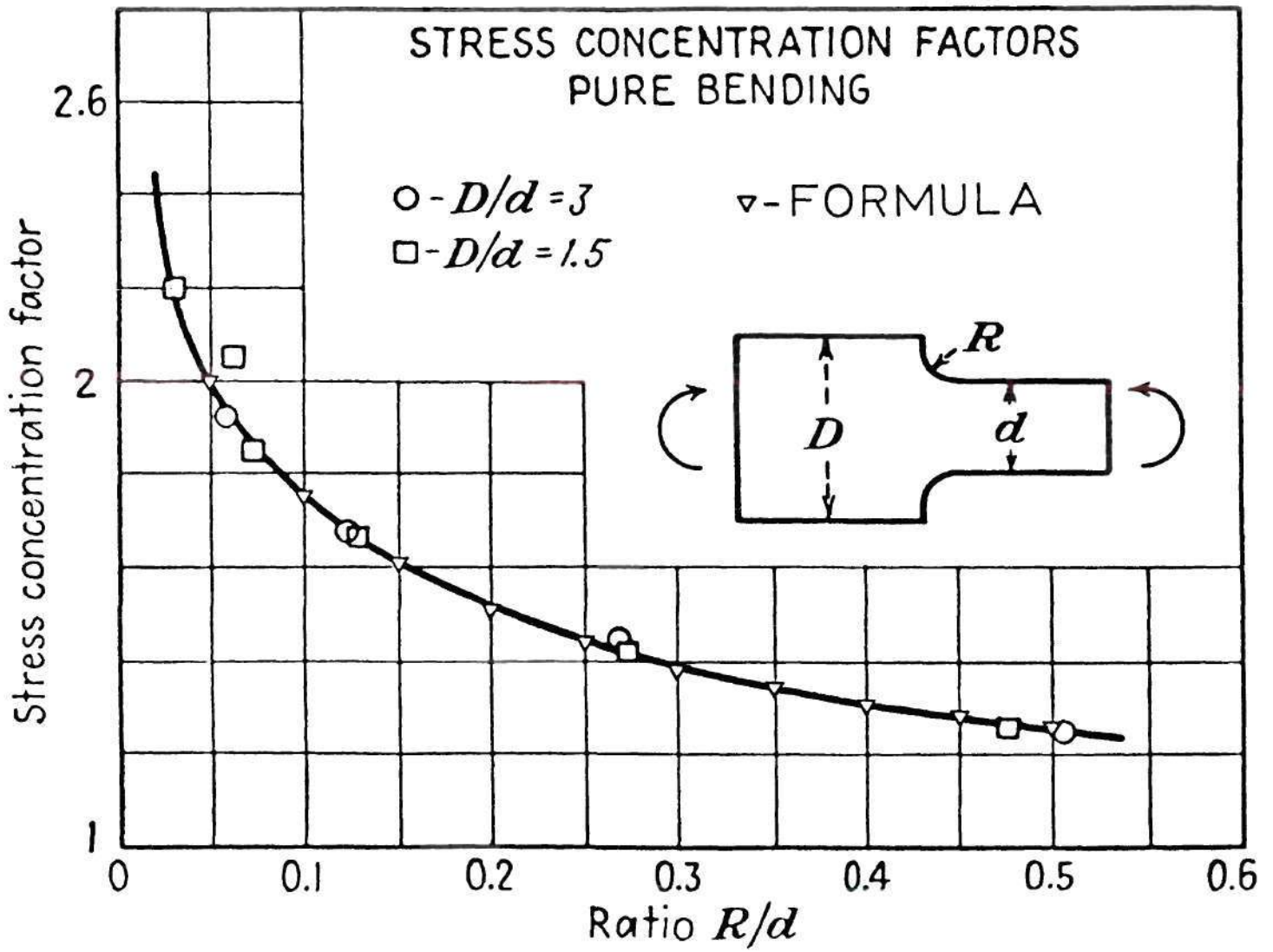

Figure 24. Stress Concentration Factors - Pure Bending.

approximation is to be used in the establishment of some relationship between two quantities which are mutually related through a third parameter, the exponential form of rational function approximation is more convenient. This is clearly shown in reference (74) by establishing a relationship between the vibrational frequency of a partially restrained beam with equal end rotational restraints, and its instability under axial loading. For the sake of completeness we give the following steps from reference (74).

If $\mu = (mL^4\omega^2/EI)^{1/4}$ is the parameter associated with vibrational frequency, ω, of the beam of mass 'm' per unit length, then

$$\mu_{\beta\beta} = \pi e^{\left\{\frac{0.409\ \beta}{\beta + 4.41}\right\}} \tag{54}$$

and the instability parameter λ, defined earlier, is

$$\lambda_{\beta\beta} = \pi e^{\left\{\frac{0.693\ \beta}{\beta + 4.41}\right\}} \tag{55}$$

Thus, from these two equations it follows that

$$\frac{\lambda_{\beta\beta}}{\pi} \cong \left(\frac{\mu_{\beta\beta}}{\pi}\right)^{1.7} \tag{56}$$

which can be generalized to

$$\frac{\lambda}{\pi} = \left(\frac{\mu}{\pi}\right)^{1.7} \tag{57}$$

since the geometric mean property applies to both λ and μ.

In Table 15, we list approximate exponential formulae for some of the problems treated earlier.

Deflection Functions

The powerful technique of rational function approximation is most effective in the simplification of complex displacement functions. Exact solutions to bending problems are obtained by this method. To exemplify this point we examine the deflection function for the symmetrical bending mode shape of a circular plate under uniform normal pressure. The plate is elastically restrained against rotation all along its boundary. The elastic restraint parameter β, defined earlier, is assumed to be uniform.

Let 'w' be the deflection function to be evaluated and 'q' be the intensity of the normal pressure applied on the plate surface. Let w_0 and w_∞ be the deflection functions of the plate corresponding to the extreme cases, $\beta = 0$ and $\beta = \infty$, of the boundary restraint, i. e., when the edges are simply supported and fixed, respectively. We suppose that w can be represented by a simple rational function in terms of the degree of edge restraint.

$$w = \frac{a_1\beta + b_1}{c_1\beta + 1} \tag{58}$$

Table 15. Exponential Formulae - Column and Plate Buckling.

Case	Matching Points	Approximate Formula	Maximum % Error (ϵ_m)
	A. Column Buckling		
Both ends simply supported 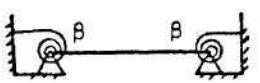 with equal rotational restraints β.	β=0,6,∞	$P_{cr} = e^{\left\{\frac{25\beta}{18\beta+60}\right\}} \frac{\pi^2 EI}{L^2}$	-0.992 at β=18.7 +0.928 at β=1.8
Both ends simply supported 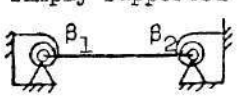 with unequal rotational restraints β_1, β_2.	By geometric mean property	$P_{cr} = e^{\left\{\frac{25\beta_1}{36\beta_1+120} + \frac{25\beta_2}{36\beta_2+120}\right\}} \frac{\pi^2 EI}{L^2}$	-2.833 at $\beta_1=0, \beta_2=16.5$ +1.908 at $\beta_1=\infty, \beta_2=2.5$
One end free, other end fixed, Load applied 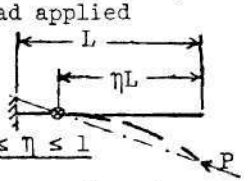 $0 \le \eta \le 1$ to pass through a fixed point on the column axis between the two ends of column.	η=0,0.8134,1	$P_{cr} = e^{\left\{\frac{37-37\eta}{51-39\eta}\right\}} \frac{\pi^2 EI}{L^2}$	-3.093 at η=0.59 +3.396 at η=0.93

Table 15. Continued.

Case	Matching Points	Approximate Formula	Maximum % Error (ϵ_m)
One end free, other end fixed, load applied 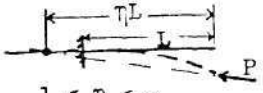 $1 \le \eta \le \infty$ to pass through a fixed point on the column axis, away from fixed end.	$\eta=1, \frac{4+3\pi}{3\pi}, \infty$	$P_{cr} = e^{\left\{\frac{7-7\eta}{5\eta-2}\right\}} \frac{\pi^2 EI}{L^2}$	-1.423 at η=1.12 +0.----------
One end simply supported, other end attached to 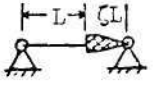 a rigid body whose far end is simply supported.	$\zeta=0, 4/3\pi, \infty$	$P_{cr} = e^{\left\{\frac{-7\zeta}{5\zeta+3}\right\}} \frac{\pi^2 EI}{L^2}$	-1.423 at ζ=0.12 +0.000----------
		B. Plate Buckling	
Circular plate, edges s.s. and rotationally restrained (β) 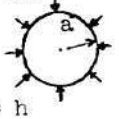 radius = a thickness = h $D = Eh^3 / \{12(1-\nu^2)\}$	$\beta=0, 3, \infty$	$[\sigma_r]_{cr} = 4.2\, e^{\left\{\frac{20\beta}{16\beta+31}\right\}} \frac{D}{a^2 h}$	-1.685 at β = 10.3 +1.207 at β = 0.8

Table 15. Continued.

Case	Matching Points	Approximate Formula	Maximum % Error(ϵ_m)
Circular plate as described above but it seperates an incompressible liquid, i.e. the first buckling mode is nonsymmetric	$\beta = 0, 4.3, \infty$	$[\sigma_r]_{cr} = 13.14 \; e^{\left\{\frac{7\beta}{10\beta+34}\right\}} \frac{D}{h \cdot a^2}$	-0.633 at $\beta = 15$ +0.996 at $\beta = 1.3$

Now, when $\beta = 0$, we have the simply supported plate and so $w = w_0$, which establishes $b_1 = w_0$. Similarly when $\beta = \infty$, the deflection function becomes $w = w_\infty$ and hence, $a_1/c_1 = w_\infty$. Therefore,

$$w = \frac{c_1 \beta w_\infty + w_0}{c_1 \beta + 1} \tag{59}$$

The well known expressions for deflection shape of the simply supported and clamped circular plate (92) are,

$$w_0 = \frac{q}{64\ D} \cdot (a^2 - r^2)^2 \tag{60}$$

and

$$w_\infty = \frac{q}{64D} \cdot (a^2 - r^2) \cdot \left(\frac{5+\nu}{1+\nu}\ a^2 - r^2\right) \tag{61}$$

To evaluate the remaining third constant c_1, we make use of the slope-moment relation at the boundary of the circular plate, i. e., at $r = a$. Using the simplifying notations w' and w", respectively, for the first and second derivative of w with respect to r, we can write the boundary condition in the following simple form;

$$(w')_{r\,=\,a} = -a\beta\left(w'' + w'\frac{\nu}{r}\right)_{r\,=\,a} \tag{62}$$

substituting the value of w from equation (59) into the equation (62) and simplifying for c_1, we obtain

$$c_1 = -\frac{1}{\beta}\left\{\frac{a\beta w_0'' + (1+\nu\beta)w_0'}{a\beta w_\infty'' + (1+\nu\beta)w_\infty'}\right\}_{r=a} \tag{63}$$

The deflection function, therefore, becomes

$$w = \frac{qr^4}{64D} - \frac{qa^2r^2}{64D}\left\{1 + \frac{1+(5+\nu)\beta}{1+(1+\nu)\beta}\right\} + \frac{qa^4}{64D}\left\{\frac{1 + (5+\nu)\beta}{1 + (1+\nu)\beta}\right\} \tag{64}$$

which is exactly the same expression Lakshmi Kantham (92) obtained by solving the exact governing differential equation. Nassar (93) has shown this "exactness" of rational function technique for a wide variety of beam bending problems.

This exactness of rational function method is, however, not true for the buckling mode shape of column instability. Nevertheless, for all practical purposes, the process gives sufficiently accurate functional forms which have considerable significance in energy solutions (94). We exemplify by deriving an approximation for the deflection curve for a rotationally restrained compressed column. The expression for the exact deflection function, derived in Appendix C, for equal end restraint parameter β is,

$$w = A\{\sin \lambda x + \frac{\beta}{\lambda}(1 - \cos \lambda x)\} \tag{65}$$

where λ, defined earlier, is the critical load parameter. We suppose that the deflection function, w, can be represented by a simple rational function. If this is so, then, it would seem reasonable to suggest that it might be either of the form

$$w = \frac{a\beta + b}{c\beta + 1} \tag{66}$$

where a, b and c may be functions of x; or of the form

$$w = \frac{a_1 x + b_1}{c_1 x + 1} \tag{67}$$

where a_1, b_1, and c_1 may be functions of β. Since we know explicitly the functions of x which corresponds to the extreme cases of $\beta = 0$ and ∞, we choose the first form, viz

$$w = \frac{a\beta + b}{c\beta + 1} \tag{68}$$

when $\beta = 0$, $w = A \sin(\pi x)$ and thus $b = A \sin(\pi x)$. Further, when $\beta = \infty$, $w = B(1-\cos 2\pi x)$ and hence, $a/c = B(1 - \cos 2\pi x)$. Therefore, we can write

$$w = \frac{Bc\beta(1-\cos 2\pi x) + A\sin\pi x}{c\beta + 1} \tag{69}$$

If we choose, now, to satisfy the moment slope boundary conditions $w'' = \beta w'$ at $x = 0$, then we arrive at the value of $A = 4\pi \cdot Bc$ and our first approximation becomes

$$w = \frac{Bc}{c\beta+1} \{4\pi \sin\pi x + \beta(1-\cos 2\pi x)\} \tag{70}$$

which for computational simplicity can be written as

$$w = A \{ \frac{4\pi}{\beta+1} \sin\pi x + \frac{\beta}{\beta+1}(1-\cos 2\pi x) \} \tag{71}$$

since 'A' is an undetermined multiplier and we wish each term inside the brackets of our approximation to have finite multipliers under all circumstances. The accuracy of this simple expression is illustrated in Table 16. It is only fair to note that as we approach the support points the error rises sharply. This, however, is unlikely to give much difficulty in the normal applications of the expression. The treatment of the error, in detail, is given in reference (94). Approximate instability mode shapes for various partially restrained columns are listed in Table 17. The degree of error in each case is clearly shown.

In the foregoing sections rational function technique has been used to derive useful approximations to many structural problems. Such applications of the rational functions is not mentioned in any textbook of engineering science. Treatises on pure mathematics (95, 96) also

Table 16. Accuracy of $w = A\left\{\frac{4\pi}{\beta+1}\sin\pi x + \frac{\beta}{\beta+1}(1-\cos 2\pi x)\right\}$.

% Error (ϵ)

x \ β	0	.1	.2	.5	1	2	5	10	20	50	100	1000	∞
0	0.000	0.000	0.000	0.000	0.000	0.000	0.000	0.000	0.000	0.000	0.000	0.000	0.000
.1	0.000	-0.371	-0.723	-1.679	-2.982	-4.782	-6.799	-6.630	-4.966	-2.530	-1.354	-0.142	0.000
.2	0.000	-0.253	-0.492	-1.139	-2.001	-3.178	-4.363	-4.080	-2.920	-1.427	-0.753	-0.078	0.000
.3	0.000	-0.127	-0.247	-0.568	-0.997	-1.559	-2.085	-1.895	-1.320	-0.632	-0.331	-0.034	0.000
.4	0.000	-0.034	-0.066	-0.151	-0.265	-0.411	-0.541	-0.484	-0.333	-0.157	-0.082	-0.009	0.000
.5	0.000	0.000	0.000	0.000	0.000	0.000	0.000	0.000	0.000	0.000	0.000	0.000	0.000
.6	--------- S												
.7			Y										
.8				M	M	E	T	R					
.9									I				
1										C	----------		

Table 17. Approximate Formulae for the Buckling Shapes of Partially Restrained Columns.

Case	Approximate Formula	Maximum % Error (ϵ_m)
	$w = A\left\{\frac{4\pi}{\beta+1}\sin\pi x + \frac{\beta}{\beta+1}(1-\cos 2\pi x)\right\}$	-6.952* at x = .1 and β = 7
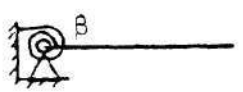	$w = A\left\{\frac{\pi^2/4}{\beta+1}x + \frac{\beta}{\beta+1}(1-\cos\frac{\pi x}{2})\right\}$	-4.602** at x = .1 and β = 3

* Error evaluated for $.1 \le x \le .9$

** Error evaluated for $.1 \le x \le 1$

give little guidance on their practical use. Although no specific rules can be given with regards to the most suitable points from which to evaluate the constants in the approximations yet, it can be stated that in the absence of an adequate computing facility the matching at the two extremes is an essential beginning. The third matching point, in case of the first order rational function, should be chosen approximately midway between the limits of the finite variable.

CHAPTER VI

CONCLUSIONS AND RECOMMENDATIONS

The concept that the normal stiffness of a compression member tends to zero as the axial load tends to the critical value has been shown to be of as great value to test engineers as it is to theoreticians. It has been demonstrated that the critical load for any strut can be ascertained from the knowledge of its lateral stiffness as the stiffness-axial load plots for all boundary conditions of a column are parallel lines.

The loss of stiffness concept has been used to establish a simple, accurate nondestructive method of evaluating shell bodies liable to instability. Not only the method predicts the critical load but it generates useful data on the strength distribution of the shell body also. The compressive load level used for the generation of the pertinent data is very small, 40 percent or less of the actual buckling load. This is far lower than the lowest load level employed in any previous known nondestructive method of shell testing. Due to the simplicity of the instrumentation employed and elimination of complex analysis of the data, this method has obvious advantages in parametric studies. The broadness of the method is demonstrated by its successful application to a noncircular shell. However, the method appears to work only for the cases where the shape of the imperfection caused by the side force and the buckle pattern formed

under axial load are similar. This has been demonstrated by tests made on a spirally stiffened shell. Nonetheless, we feel that a detailed investigation is needed to resolve this issue. We suggest that a compressed shell subjected to internal and external pressure would be an ideal model for such a study.

The study reported in Chapter V has shown the merit of rational function approximations in a wide variety of structural problems. In particular, it shows the power of this method with reference to deriving critical instability conditions for various structural members, e. g., columns and plates. It is clear from the investigation made in this area that some of the approximations derived therein would be of great assistance in parametric studies and most helpful in reducing the program sizes for many computer design problems. The practical engineers could certainly use these simple formulae for a quick and good approximate answer.

APPENDIX A

DATA ACQUISITION PROGRAM AND FLOW DIAGRAM

The data acquisition consisted of a teletype input of side force used to determine the shell wall stiffness, reading the output from the stiffness probe and the end shortening LVDTs. An operating program, for the acquisition and analysis of this data, written in BASIC is given below. The data acquisition system flow diagram is given in Figure 25.

```
1       REM: CALL CALL CALIBRATION WITH INCREMENT OF
11      DIM D[4]
12        T  =16
13      LET J=1
14      LET T=0
15      LET C1=.85
16      FOR I=1 TO 4
17      READ D[I]
18      NEXT I
19      DATA 60.6,70,70,80.6
20      PRINT "CALL =";
21      INPUT Z[1]
22      PRINT "NO OF CYCLE LOOP = ";
23      INPUT N
24      PRINT "STATIC OR CALIBRATION CALL IF = ";
25      INPUT Z[4]
26      PRINT
27      CLS
28      PRINT "CYCLE",,"CALL DISP ... IN"
29      PRINT
30      LET J=1
31      CALL (4,5)
32      IF S>4 THEN 30
33      CALL (1,V[1],J,T,4)
34      CALL (1,D[1],J,T,1)
35      FOR I=1 TO 4
36      LET V[I]=(V[I]-D[I])*1000/D[I]
37      NEXT I
```

```
700   LET P[I]=INT(1000*P[I]/C0+.5)
730   LET I[J,J]=V[4]
750   LET V[4]=INT(100*V[4]/3+.5)/100
760   FOR I=1 TO 3
770   LET V[I]=INT(V[I]+.5)
776   NEXT I
780   PRINT P[J],V[4];V[1];V[2];V[3]
810   IF J=W THEN 900
820   LET J=J+1
830   GOTO 630
900   PRINT
1000  COSTI 5000
1500  COSTI 5400
1900  END
5000  PRINT " DESIRED LOAD (LB CIS ONLY) = ";
5010  INPUT C
5020  LET C1=C/453.6
5030  PRINT
5090  PRINT "INITIAL PLOT"
5100  CALL (4,S)
5110  CALL (4,S)
5120  IF S>0 THEN 5110
5200  CALL (1,S[1],J,5,4)
5260  PRINT " APPLY LATERAL LOAD "
5300  PRINT
5390  END
5400  PRINT "AXIAL COMP","DISP...I","(E-I0)","STIFFNESS"
5410  PRINT
5420  LET J=1
5450  CALL (4,S)
5460  IF S>0 THEN 5450
5470  CALL (1,V[1],J,5,4)
5480  CALL (1,P[1],J,5,1)
5490  FOR I=1 TO 4
5500  LET V[I]=1000*(V[I]-S[I])/V[I]
5510  NEXT I
5520  LET P[J]=INT(1000*P[J]/C0+.5)
5650  LET I0=V[4]-P[J]
5700  LET S1=1000*C1/L0
5710  LET S1=INT(100*S1+.5)/100
5730  LET I0=INT(100*I0+.5)/100
5740  LET V[4]=INT(100*V[4]+.5)/100
5830  PRINT P[J],V[4],I0,S1
5840  IF J=W THEN 5890
5850  LET J=J+1
5860  GOTO 5450
5890  PRINT
9999  END
```

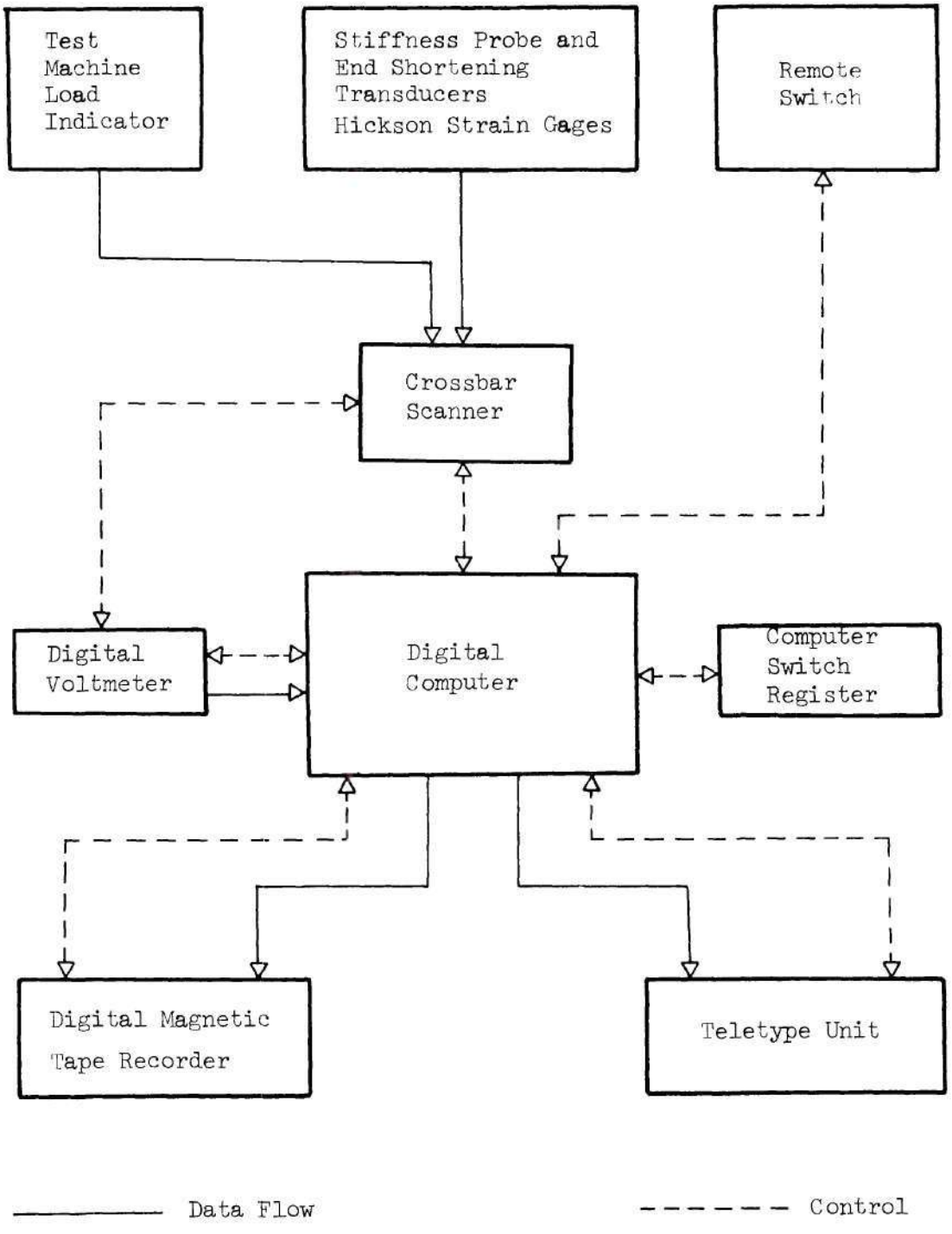

Figure 25. Data Acquisition System Flow Diagram.

APPENDIX B

ANALYSIS OF A SPIRAL STIFFENED SHELL

The following constants appearing in Soong's (80) analysis were found to be in error. The correct expressions for these constants are given below.

$$c_1 = \left(\frac{E_x}{1 - \mu_x' \mu_y'} + \frac{2E_r A_r}{l_p} \cos^4\theta\right)/E_0 t_0$$

$$c_7 = \left(\frac{t_0}{R}\right)^2 \left(\frac{D_x}{1 - \mu_x \mu_y} + \frac{G_r J_r}{2l_p} \sin^2 2\theta + \frac{2E_r I_{0r}}{l_p} \cos^4\theta\right)/E_0 t_0^3$$

$$c_8 = \left(\frac{t_0}{R}\right)^2 \left(2D_{xy} + \frac{2G_r J_r}{l_p} \cos^2 2\theta + \frac{2E_r I_{0r}}{l_p} \sin^2 2\theta\right)/E_0 t_0^3$$

$$c_9 = \left(\frac{t_0}{R}\right)^2 \left(\frac{D_y}{1-\mu_x \mu_y} + \frac{G_r J_r}{2l_p} \sin^2 2\theta + \frac{2E_r I_{0r}}{l_p} \sin^4\theta\right)/E_0 t_0^3$$

$$c_{13} = \frac{t_0}{R} \left(\frac{4E_r A_r \bar{z}_r}{l_p} \cos^4\theta\right)/E_0 t_0^2$$

$$c_{10} \left[-(G_r J_r/l_p) \cos 2\theta + (2E_r I_{0r}/l_p) \cos^2\theta\right]/E_0 t_0 R^2$$

$$c_{12} = [(G_r J_r/\ell_p)\cos 2\theta + (2E_r I_{0r}/\ell_p)\sin^2\theta]/E_0 t_0 R^2$$

$$C_{81} = c_7 d_{11} - \tfrac{1}{2} c_{13} d_{21} - \phi^2 \tfrac{1}{4} c_{15} d_{31}$$

$$C_{82} = c_7 d_{13} + (c_8 + c_{11}) d_{11} - \tfrac{1}{2} c_{13} d_{23} - \tfrac{3}{2} c_{16}(d_{21} + d_{32})$$

$$+ \phi^2(c_{10} d_{12} - \tfrac{3}{4} c_{15} d_{22} - \tfrac{1}{4} c_{15} d_{33} - \tfrac{3}{2} c_{17} d_{31})$$

$$C_{83} = c_7 d_{15} + (c_8 + c_{11}) d_{13} + c_9 d_{11} - \tfrac{1}{2} c_{13} d_{25} - \tfrac{1}{2} c_{18} d_{32} -$$

$$\tfrac{3}{2} c_{16} d_{23} - \tfrac{3}{2} c_{16} d_{34} + \phi^2(c_{10} d_{14} + c_{12} d_{12} -$$

$$\tfrac{1}{2} c_{17} d_{22} - \tfrac{3}{4} c_{15} d_{24} - \tfrac{1}{4} c_{15} d_{35} - \tfrac{3}{2} c_{17} d_{33})$$

$$C_{61} = c_{16} d_{11} - \tfrac{1}{2} c_{13} d_{27} - \tfrac{1}{2} c_5 d_{21} + \phi^2(-\tfrac{1}{4} c_{15} d_{37} - \tfrac{1}{2} c_6 d_{31})$$

$$C_{63} = c_{16} d_{13} + c_{18} d_{11} + \tfrac{1}{2} c_{13} d_{15} - \tfrac{3}{2} c_{16} d_{27} - \tfrac{1}{2} c_5 d_{23} -$$

$$\frac{3}{2} c_{16}d_{38} - c_3d_{32} + \phi^2(2c_{17}d_{12} - \frac{1}{4}c_{15}d_{28} -$$

$$\frac{1}{2} c_6d_{22} - \frac{3}{2} c_{17}d_{37} - \frac{1}{2} c_6d_{33})$$

$$C_{67} = 0$$

$$E_{81} = c_7d_{12} + c_{10}d_{11} - \frac{1}{2} c_{13}d_{22} - \frac{3}{4} c_{15}d_{21} - \frac{3}{2} c_{16}d_{31} - \frac{1}{4}c_{15}d_{32}$$

$$E_{82} = c_7d_{14} + (c_8 + c_{11})d_{12} + c_{10}d_{13} + c_{12}d_{11} -$$

$$\frac{1}{2} c_{13}d_{24} - \frac{3}{2} c_{16}d_{22} - \frac{1}{2} c_{17}d_{21} - \frac{3}{4} c_{15}d_{23} -$$

$$\frac{3}{2} c_{16}d_{33} - \frac{1}{2} c_{18}d_{31} - \frac{1}{4} c_{15}d_{34} - \frac{3}{2} c_{17}d_{32}$$

$$E_{83} = (c_8 + c_{11})d_{14} + c_9d_{12} + c_{10}d_{15} + c_{12}d_{13} -$$

$$\frac{1}{2} c_{13}d_{26} - \frac{3}{2} c_{16}d_{24} - \frac{1}{2} c_{17}d_{23} - \frac{3}{4} c_{15}d_{25} -$$

$$\frac{3}{2} c_{16}d_{35} - \frac{1}{2} c_{18}d_{33} - \frac{1}{4} c_{15}d_{36} - \frac{3}{2} c_{17}d_{34}$$

$$E_{61} = c_{16}d_{12} + 2c_{17}d_{11} - \frac{1}{2}c_{13}d_{28} - \frac{1}{2}c_{5}d_{22} - \frac{3}{4}c_{15}d_{27} -$$

$$\frac{1}{2}c_{6}d_{21} - \frac{3}{2}c_{16}d_{37} - c_{3}d_{31} - \frac{1}{4}c_{15}d_{38} - \frac{1}{2}c_{6}d_{32}$$

$$E_{62} = \frac{1}{4}c_{16}d_{14} + c_{18}d_{12} + 2c_{17}d_{13} - \frac{1}{2}c_{17}d_{27} - \frac{1}{2}c_{5}d_{24} -$$

$$\frac{1}{2}c_{6}d_{23} - \frac{1}{2}c_{18}d_{37} - c_{3}d_{33} + \frac{1}{2}c_{15}d_{15} -$$

$$\frac{3}{2}c_{17}d_{38} - \frac{1}{2}c_{6}d_{34}$$

$$E_{63} = \frac{1}{2}c_{18}d_{14} - \frac{1}{2}c_{5}d_{26} - \frac{1}{2}c_{6}d_{25} - c_{3}d_{35} - \frac{1}{2}c_{6}d_{36} + c_{17}d_{15}$$

APPENDIX C

COLUMN INSTABILITY

Consider a column of uniform EI and length L subjected to an axial compression P.

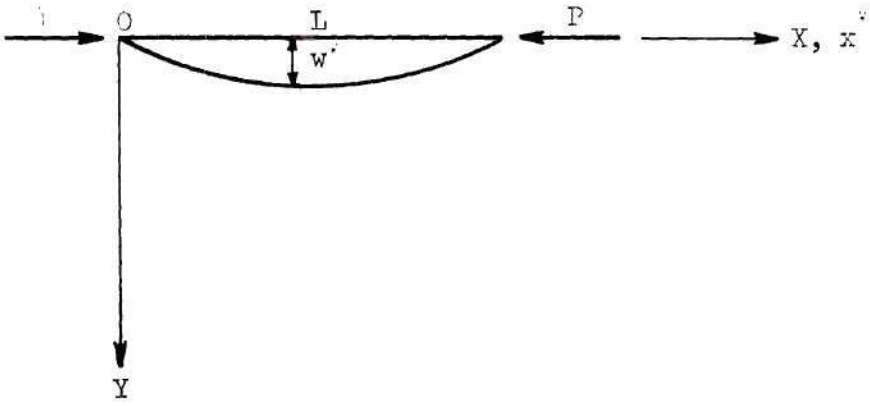

We define, for simplicity sake, the following nondimensional parameters;

$$x = x^*/L \tag{C-1}$$

$$w = w^*/L \tag{C-2}$$

$$\lambda^2 = PL^2/EI \tag{C-3}$$

The nondimensionalized differential equation governing the instability of a column is, therefore,

$$w^{iv} + \lambda^2 w'' = 0 \tag{C-4}$$

The general solution to the above stability equation is

$$w = C_1 + C_2x + C_3\sin(\lambda x) + C_4\cos(\lambda x) \qquad (C\text{-}5)$$

where C_1, C_2, C_3 and C_4 are constants.

Characteristic Equation

Four homogeneous equations are obtained by substituting the general solution for 'w', given by equation (C-5), into the proper set of four boundary conditions of the column. For a nontrivial solution the determinant of the coefficients C_1, C_2, C_3 and C_4 must vanish. The characteristic equation is obtained by expanding the determinant.

Given below are the parameters associated with the partial restraints at the ends of the column.

k = lateral spring stiffness

ϕ = rotational restraint stiffness constant

$\alpha = kL^3/EI$

$\beta = \phi L/EI$

The characteristic equations for various cases of column instability are given in Table 18.

Mode Shape

The buckling mode shape for a column is obtained by establishing a ratio between the four constanta C_1, C_2, C_3 and C_4 of the general

Table 18. Characteristic Equations for Column Instability.

Case	Boundary Conditions at x=0	Boundary Conditions at x=1	Characteristic Equation
One end simply supported 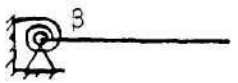 with rotational restraint (β); other end free.	$w = 0$	$w'' = 0$	
	$w'' = \beta w'$	$w''' = -\lambda^2 w'$	$\tan \lambda = \frac{\beta}{\lambda}$

	x = 0	x = 1/2	x = 1	
Both ends simply supported 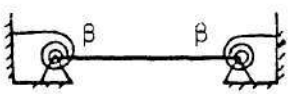 with equal rotational restraints β.	$w = 0$	$w' = 0$	$w = 0$	
	$w'' = \beta w'$			$\tan \frac{\lambda}{2} + \frac{\lambda}{\beta} = 0$

	x = 0	x = 1	
Both ends simply supported 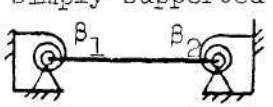 with unequal rotational restraints β_1, β_2.	$w = 0$	$w = 0$	$[\lambda^3 + (\beta_1+\beta_2)\lambda - \beta_1\beta_2\lambda\ ]\sin\lambda$
	$w'' = \beta_1 w'$	$w'' = -\beta_2 w'$	$-[(\beta_1+\beta_2)\lambda^2 + 2\beta_1\beta_2]\cos\lambda$
			$+ 2\beta_1\beta_2 = 0$

Table 18. Continued.

Case	Boundary Conditions at x = 0	Boundary Conditions at x = 1	Characteristic Equation
One end fixed, 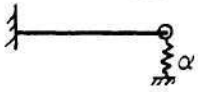 other with lateral restraint α.	$w = 0$ $w' = 0$	$w'' = 0$ $w''' + \lambda^2 w' = \alpha w$	$\tan \lambda = \lambda - \frac{\lambda^3}{\alpha}$
One end fixed, other end free, load applied 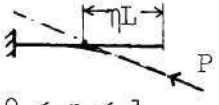 $0 \leq \eta \leq 1$ to pass through a fixed point on the column axis.	$w = 0$ $w' = 0$	$w'' = 0$ $w''' + \lambda^2 w' = \lambda^2 \frac{w}{\eta}$	$\tan \lambda = \lambda(1-\eta)$
One end simply supported, other end attached to 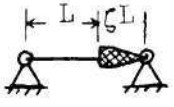 a rigid body whose far end is simply supported.	$w = 0$ $w'' = 0$	$w = -\zeta w'$ $w'' = -\zeta w'''$	$\tan \lambda = -\zeta\lambda$

Table 18. Continued.

Case	Characteristic Equation
Both ends 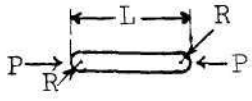 rounded $\xi = (L/2R)$.	$\frac{\lambda}{2} \tan \frac{\lambda}{2} = -\xi$
Cantilever tapered column 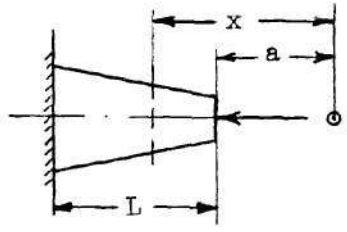 $I_x = I_1(x/a)^n$ I_1 = Moment of Inertia at the smaller end of column. I_2 = Moment of Inertia at the larger end of column.	$n = 2$ $\tan [\rho \ln\sqrt{I_2/I_1}] + 2\rho = 0$ where $\rho = \{ \frac{Pa^2}{EI_1} - \frac{1}{4} \}^{1/2}$ $n = 4$ $\frac{\tan \gamma}{\gamma} = -a/L$ where $\gamma = (\frac{L}{a+L}) \cdot \sqrt{\frac{Pa^2}{EI_1}}$

solution. Three of these four constants are expressed in terms of the fourth constant by using the homogeneous equations obtained in the previous section. The mode shape is, therefore, established but for an undetermined multiplier. The mode shapes for two cases of rotationally restrained column are given below.

(1) One end simply supported with

rotational restraint (β); other end free.

$$w = C_1 \left[\sin\lambda x + \frac{\beta}{\lambda}(1-\cos\lambda x)\right].$$

(2) Both ends simply supported with

equal rotational restraints β.

$$w = C_1 \left[\sin\lambda x + \frac{\beta}{\lambda}(1-\cos\lambda x)\right].$$

REFERENCES

1. Todhunter, Isaac and Pearson, Karl, A History of the Theory of Elasticity and of the Strength of Materials, Dover Publications, Inc., New York, 1960.

2. Euler, Leonhard, "Methodus Inveniendi Lineas Curvas Maximi Minimive Proprietate gaudentes, Sive Solutio Problematis Isoperimentrici Latissimo Sensu Accepti, "Additamentum 1, De Curvis Elastics, Marcus-Michaelus Bousquet, Lausanne and Geneva, 1744.

3. Hodgkinson, Eaton, "Experimental Researches on the Strength of Pillars of Cast Iron and Other Materials," Phil. Trans. Roy. Soc., Pt. II, 1840, pp. 385.

4. Ayrton, W. E., and Perry, John, "On Struts," The Engineer, 62, 1886, pp. 464-465, 513-515.

5. Young, T., A Course of Lectures on Natural Philosophy and the Mechanical Arts, 1st edition, Vol. II, Sect. IX, London, 1807, p. 47.

6. Smith, R. H., Wheatley and Wood, "Stiffness of Struts," The Engineer, Vol. LXV, January 6, 1888, p. 1.

7. Southwell, R. V., "On the Analysis of Experimental Observations in Problems of Elastic Stability," Proceedings of the Royal Society London, Ser. A.,135, 1932, pp. 601-616.

8. von Kármán, Theodore, "Unter Suchunger Uber Knick Fest Ig Keit," Mitteil Unger Uber Forschungsarbeiten Auf Dem Gebeite Des Ingenieurwesens, Vol. 81, 1910.

9. Gough, H. J. and Cox, H. L., "Some Tests on the Stability of Thin Strip Material Under Shearing Forces," Proceedings of the Royal Society, A, Vol. 137, 1932, p. 145-157.

10. Bridget, F. J., Jerome, C. C. and Vosseller, A. B., "Some New Experiments on the Buckling of Thin Wall Construction," Transactions of the American Society of Mechanical Engineers, Vol.56, 1934.

11. Fisher, H. R., "An Extension of Southwell's Method of Analyzing Experimental Observations in Problems of Elastic Stability," Proc. R. Soc., A, Vol. 144, 1934, pp. 609-630.

12. Westergaard, H. M., "Buckling of Elastic Structures," Transactions of the American Society of Civil Engineers, Vol. 85, 1922, pp. 576-654.

13. Fairthorne, R. A., "The Small Displacements and Stability of Elastic Systems Under Static Load," RAE Report MT-5575, March 1934.

14. Donnell, L. H., "On the Application of Southwell's Method for the Analysis of Buckling Tests," Stephen Timoshenko 60th Anniversary Volume, MacMillan Book Company, 1938, pp. 27-38.

15. Horton, W. H., Cundari, F. L., and Johnson, R. W., "Applicability of the Southwell Plot to the Interpretation of Test Data Obtained from Stability Studies of Elastic Column and Plate Structures," USAAVLABS Technical Report 69-32, November 1971.

16. Struble, D. E., "Boundary Effects in Structural Stability: A New Approach," Ph.D. Thesis, 1970, Georgia Institute of Technology, Atlanta, Georgia.

17. Salmon, E. H., "Columns, a Treatise on the Strength and Design of Compressive Members," Henry Frowde and Hodder and Stoughton, London, 1921.

18. Horton, W. H., Craig, J. I., and Struble, D. E., "A Simple, Practical Method for the Experimental Determination of the End Fixity of a Column," Proceedings of the Eithth International Symposium on Space Technology and Science, Tokyo, 1969.

19. Iwamoto, Takaya, "The Effect of End Fixity on the Stability of Structures," Ph.D. Thesis, 1970, Georgia Institute of Technology, Atlanta, Georgia.

20. Baruch, Menahem, "Undestructive Determination of the Buckling Load of an Elastic Bar," AIAA Journal, December 1970, pp. 2274-2276.

21. Dunn, L. G., "An Investigation of Sheet-Stiffener Panels Subjected to Compression Loads with Particular Reference to Torsionally Weak Stiffeners," NACA TN 752, 1940.

22. Farrar,D. J., "Investigations of Skin Buckling," ARC R & M 2652, 1947.

23. Yoshiki, Masao and Fujita, Yuzuru, "Determination of Plastic Buckling Load for Axially Compressed Plates From Experimental Data," Test Methods for Compression Members, ASTM STP 419, Am. Soc. Testing Mats., 1967, pp. 47-59.

24. Fairbairn, W., "On the Resistance of Tubes to Collapse," Philosophical Transactions on the Royal Society, London, Vol. 148, p. 389, 1859.

25. Timoshenko, S. P., History of Strength of Materials, McGraw-Hill Book Company, Inc., 1953.

26. Bryan, G. H., "On the Stability of Elastic Systems," Proceedings Cambridge, Philosophical Society, Vol. 6, p. 199, 1888.

27. Lorenz, R., "Achsensymmetrische Verzerrungen in Dunnwandigen Hohlzylindern," Zeitschrift des Vereins Dautscher Ingenieure, Vol. 52, No. 43, October 1908, p. 1706.

28. Timoshenko, S. P., "Einige Stabilitatsprobleme der Elastizitastsstheorie," Zeitschrift fur Mathematick und Physik, Vol. 58, No. 4, June 1910, p. 337.

29. Lorenz, R., "Die Nicht Achsensymmetrische Knickung Dunnwandiger Hohlzylindern,"Physikalische Zerischrift, Vol. 12, 1911, p. 241.

30. Timoshenko, S., Bulletin, Electrotechnical Institute, St. Petersburg, Vol. 11, 1914.

31. Southwell, R. V., "On the General Theory of Elastic Stability," Philosophical Transactions of the Royal Society, London, Series A, Vol. 213, No. A501, p. 187, August 1913.

32. Flugge, W., "Die Stabilitat ket Kreiszylinderschale," Ingenieur-Archiv, Vol. 3, No. 5, p. 463, December 1932.

33. Robertson, Andrew, "The Strength of Tubular Struts," Proceedings of the Royal Society, London, Series A, Vol. 121, No. 788, p. 558, December 1, 1928.

34. Robertson, Andrew, "The Strengths of Tubular Struts," Reports and Memoranda of the Aeronatuical Research Council, No. 1185, 1929.

35. Wilson, W. M., and Newmark, N. M., "The Strength of Thin Cylindrical Shells as Columns," University of Illinois, Engineering Experiment Station Bulletin No. 255, February 1933.

36. Lundquist, E., "Strength Tests of Thin-Walled Duralumis Cylinders in Compression," NACA Report 473, 1933.

37. Donnell, L. H., "A New Theory for the Buckling of the Cylinders Under Axial Compression and Bending," Trans. ASME, Vol. 56, pp. 795-806, 1934.

38. Harris, L. A., Suer, H. S., Skene, W. T. and Benjamin, R. J., "The Stability of Thin-Walled Unstiffened Circular Cylinders Under Axial Compression Including the Effects of Internal Pressure," Journal of Aeronautical Science, Vol. 24, no. 8, p. 587, 1957.

39. Ballerstedt, W., and Wagner, H., Versuche über die Festigken dünner Unversteifter Zylinder unter Schub-und Längskräften, Luft-fahrtforschung, Vol. 18, pp. 309-312, 1936.

40. Clark, J. W., and Holt, M., Discussion of the Paper Effect of Imperfections on Buckling of Thin Cylinders and Columns Under Axial Compression, by L. H. Donnel and C. S. Wan. Journal of Applied Mechanics, Trans. ASME, Vol. 72, pp. 340-342, 1950.

41. Fung, Y. C., and Sechler, E. E., Instability of Thin Elastic Shells, Structural Mechanics, Proceedings of the First Symposium on Naval Structural Mechanics, Stanford University, edited by J. N. Goodier and N. J. Hoff, Pergamon Press, p. 115, 1958.

42. Kanemitsu, S., and Nojima, N. M.,"Axial Compression Tests of Thin Circular Cylinders," M. S. Thesis, Department of Aeronautical Engineering, California Institute of Technology, 1939.

43. Lo, H., Crate, H., and Schwartz, E. B.,"Buckling of Thin-Walled Cylinders Under Axial Compression and Internal Pressure," NACA Report 1027 (1951).

44. von Kármán, T., and Tsien, H. S., "The Buckling of Thin Cylindrical Shells Under Axial Compression," Journal of the Aeronautical Sciences, Vol. 8, No. 8, p. 302, 1941.

45. Yoshimura, Y., "On the Mechanism of Buckling of a Circular Cylindrical Shell Under Axial Compression," National Advisory Committee for Aeronautics, Technical Memorandum 1390, Washington, D. C., July 1955.

46. Hoff, N. J., and Rehfield, L. W., "Buckling of Axially Compressed Circular Cylindrical Shells at Stresses Smaller Than the Classical Critical Value," SUDAER No. 191, Stanford University, May 1961.

47. Nachbar, W., and Hoff, N. J., "On Edge Buckling of Axially Compressed Circular Cylindrival Shells," Quarterly of Applied Mathematics, Vol. XX, No. 3, p. 267, October 1962.

48. Stein, M., "The Effect on the Buckling of Perfect Cylinders of Prebuckling Deformations and Stresses," Collected Papers on Instability of Shell Structures, National Aeronautics and Space Administration, Technical Note D-1510, p. 217, 1962.

49. Mayers, J., and Rehfield, L. W., "Further Nonlinear Considerations in the Postbuckling of Axially-Compressed Circular Cylindrical Shells," SUDAER No. 197, Stanford University, June 1964.

50. Horton, W. H., Bailey, S. C., "Structural Instability," Final Report AFOSR 68-1194, June 1968.

51. Koiter, W. T., "The Effect of Axisymmetric Imperfections on the Buckling of Cylindrical Shells Under Axial Compression," Lockheed Missiles and Space Company, 6-90-63-86, Sunnyvale, Calif., August 1963.

52. Budiansky, Bernard and Hutchinson, J. W., "A Survey of Some Buckling Problems," AIAA Journal, Vol. 4, No. 9, September, 1966, pp. 1505-1510.

53. Arbocz, Johann and Babcock, C. D., "The Effect of General Imperfections on the Buckling of Cylindrical Shells," Transactions of the ASME, March 1969, pp. 28-38.

54. Baker, E. H., Kovalevsky, L. and Rish, F. L., Structural Analysis of Shells, McGraw-Hill Book Company, New York, 1972.

55. Nash, W. A., "Bibliography on Shells and Shell-like Structures," TMB Report 863, David Taylor Model Basin, U. S. Navy Department, Washington, D. C., 1954.

56. Nash, W. A., "Bibliography on Shells and Shell-like Structures (1954-1956)," University of Florida, Contract DA-01009-ORD-404, Office of Ordnance Research, U. S. Army, Washington, D. C., 1957.

57. Flügge, W., Stresses in Shells, Springer-Verlag, Berlin, 1960, p. 466.

58. Galletly, G. D., Slankard, R. C. and Wenk, E., "General Instability of Ring-Stiffened Cylindrical Shells Subject to External Hydrostatic Pressure - A Comparison of Theory and Experiment," Journal of Applied Mechanics, June 1958, pp. 259-266.

59. Galletly, G. D., Reynolds, T. E., "A Simple Extension of Southwell's Method for Determining the Elastic General Instability of Ring Reinforced Cylinders Subjected to External Pressure," Proceeding of SESA, XIII, No. 2, 1956, pp. 141-151.

60. Sturm, R. G., "A Study of the Collapse Pressure of Thin-Walled Cylinders," Engineering Experiment Station Bulletin, No. 329, University of Illinois, Urbana, Illinois, November 1941.

61. Bank, M. H., "The Effect of Fiber Direction on the Instability of Single-layer Resin Impregnated Glass Cloth Cylinders Under Torsion," Engineers Thesis, Stanford University, September 1966.

62. Tenerelli, D. J., Horton, W. H., "An Experimental Study of the Local Buckling of Ring Stiffened Cylinders Subject to Axial Compression," Israel Journal of Technology, Vol. 7, No. 1-2, 1969, pp. 181-194.

63. Craig, J. I., "An Experimental Study of Wall Motions in Circular Cylindrical Shells Under Combined Loadings," Ph.D. Thesis, 1968, Stanford University, Stanford, California.

64. Horton, W. H. and Craig, J. I., "The Nondestructive Evaluation of Shell Bodies Liable to Instability," unpublished, Georgia Institute of Technology, Atlanta, Georgia, 1973.

65. Tuckerman, L. B., "Heterostatic Loading and Critical Astatic Loads," National Bureau of Standards Research Paper RP 1163, Journal of Research, N. B. S. 22, 1939, pp. 27-38.

66. Ford, J. S., "Parametric Studies on the Stability of Stringer and Ring Reinforced Circular Shells," Ph.D. Thesis, 1970, Georgia Institute of Technology, Atlanta, Georgia.

67. Almroth, B. O., Holmes, A. M. C., and Brush, D. O., "An Experimental Study of the Buckling of Cylinders Under Axial Compression," Experimental Mechanics, p. 263-270, September 1964.

68. Horton, W. H., and Durham, S. C., "Imperfections, A Main Contributor to Scatter in Experimental Values of Buckling Load," International Journal of Solids and Structures, Vol. 1, pp. 59-72, 1965.

69. Horton, W. H., and Bailey, S. C., "Influence of Test Machine Rigidity on the Buckling Load of Shells," Test Methods for Compression Members, ASTM STP 419, Am. Soc. Testing Mats., 1967, p. 183.

70. Hu, P. C., Lundquist, E. E., and Batdorff, S. B., "Effect of Small Deviations From Flatness on Effective Width and Buckling of Plates in Compression," NACA TN 1124, National Advisory Committee for Aeronautics, 1946.

71. Peterson, J. P., and Dow, M. B., "Structural Behavior of Pressurized, Ring Stiffened, Thin-Wall Cylinders Subjected to Axial Compression," NASA TN D-506, National Aeronautics and Space Administration, 1960.

72. Peterson, J. P., and Anderson, J. K., "Bending Tests of Large-Diameter Ring Stiffened Corrugated Cylinders," NASA TN D-3336, National Aeronautics and Space Administration, 1966.

73. Gregory, Malcolm, Elastic Instability, E. & F. N. Spon Limited, London, 1967.

74. Bank, M. H., "Some Discussions on the Stability of Structural and Mechanical Systems," Ph.D. Thesis, 1971, Georgia Institute of Technology, Atlanta, Georgia.

75. Khilnani, V. V., M. S. Thesis in Course of preparation, Georgia Institute of Technology, Atlanta, Georgia.

76. Horton, W. H. and Durham, S. C., "Variation in Buckle Shape in Cylindrical Shells Under External Pressure and Axial Load," AIAA Journal, Vol. 2, No. 5, May 1964, pp. 943-944.

77. Horton, W. H., Singhal, M. K., and Haack, T. A., "The Use of Models in Structural Testing," Proceedings entitled Instrumentation in the Aerospace Industry - Volume 18, Instrument Society of America, Pittsburgh, Pennsylvania 15222.

78. Haack, T. A., "The Development of New Techniques for the Manufacture and Testing of Cylindrical Shells," M. S. Thesis, 1973, Georgia Institute of Technology, Atlanta, Georgia.

79. Giesecke, F. E., Mitchell, Alva, Spencer, H. C., and Hill, I. L., Technical Drawing, The MacMillan Company, New York, 1967, p. 116.

80. Soong, T. C., "Buckling of Cylindrical Shells with Eccentric Spiral-Type Stiffeners, AIAA Journal, Vol. 7, No. 1, January, 1969, pp. 65-72.

81. Baruch, M. and Singer, J., "Effect of Eccentricity of Stiffeners on the General Instability of Stiffened Cylindrical Shells Under Hydrostatic Pressure," Journal of Mechanical Engineering Sciences, Vol. 5, No. 1, March 1963, pp. 23-27.

82. Meyer, R. R., "Buckling of 45° Eccentric-Stiffened Waffle Cylinders," Journal of the Royal Aeronautical Society, Vol. 71, July, 1967, pp. 516-520.

83. Horton, W. H., "The Use of Rational Functions in Approximating Relationships of Significance in the Buckling and Vibration of Partially Restrained Columns," Lecture Notes, School of Aerospace Engineering, Georgia Institute of Technology, Atlanta, Georgia.

84. Newmark, N. M., "A Simple Approximate Formula for Effective End-Fixity of Columns," Journal of the Aeronautical Sciences, Vol. 16, February 1949, p. 116.

85. Timoshenko, S. P., Gere, J. M., Theory of Elastic Stability, 2nd Edition, McGraw-Hill Book Company, New York.

86. Salmon, E. H., Materials and Structures, Vol. 1, Longmans, Green and Company, London.

87. Horton, W. H., Ford, J. S., "Some Experimental Studies on the Relationship Between End Fixity and Critical Load Level for Struts," USAAVLABS Technical Report 70-21, August 1970.

88. Livesley, R. K., Chandler, D. B., Stability Functions for Structural Frameworks, Manchester University Press, 1956.

89. Reismann, H., "Bending and Buckling of an Elastically Restrained Circular Plate," Journal of Applied Mechanics, June 1952, pp. 167-172.

90. Kerr, A. D., "On the Instability of Circular Plates," Journal of the Aerospace Sciences, April 1962, pp. 486-487.

91. Timoshenko, S. P., Goodier, J. N., Theory of Elasticity, 3rd Edition, McGraw-Hill Book Company, New York.

92. Lakshmi Kantham, C., "Bending and Vibration of Elastically Restrained Circular Plates," Journal of the Franklin Institute, Vol. 265, No. 6, June 1958, pp. 483-491.

93. Nassar, E. M., "On the Dynamic Characteristic of Beams, Plates and Shells," Ph.D. Thesis, Georgia Institute of Technology, Atlanta, Georgia, 1973.

94. Horton, W. H., Singhal, M. K., and Nassar, E. M., "The Application of Rational Functions to Produce Simple Approximation of Significance in Structural Analysis," unpublished, Georgia Institute of Technology, Atlanta, Georgia.

95. Hardy, G. H., A Course of Pure Mathematics, 10th Edition, Cambridge University Press, 1960.

96. Cody, W. J., "A Survey of Practical Rational and Polynomial Approximation of Functions," SIAM Review, Vol. 12, No. 3, July 1970, pp. 400-423.

VITA

Mahender Kumar Singhal was born September 8, 1942 in New Delhi, the son of Hans Raj and Rukmani Devi Singhal. He attended high school in Rewari, Haryana (India), graduating in June 1959. In July 1959 he entered the Hans Raj college, University of Delhi for an one year pre-university course. Subsequently he attended D. A. V. College, Ambala City and passed the intermediate examination of April 1961, held by Panjab University.

In August of 1962, he entered the M. B. M. Engineering College, Jodhpur, Rajasthan (India) and in June 1966, graduated with a honors degree of Bachelor of Engineering in Mechanical Engineering. Upon graduation he joined the Fort William Wire Ropes, Konnagar, Calcutta as a mechanical engineer. He entered the Indian Institute of Science, Bangalore in August 1967, and completed the requirements for the degree of Master of Engineering in Aircraft Structures in July 1969. In the fall of that year he entered the Georgia Institute of Technology as a graduate student and research assistant in Aerospace Structures.